Matsubara Dynamics and its Practical Implementation

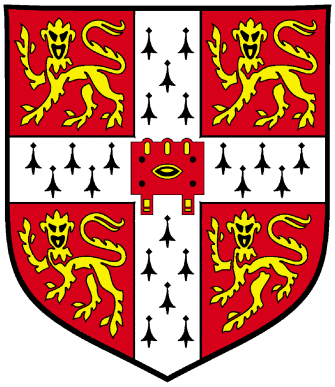

Michael John Willatt

St. John's College

University of Cambridge

A thesis submitted for the degree of Doctor of Philosophy

August, 2017

Matsubara Dynamics and its Practical Implementation

Michael John Willatt

This thesis develops a theory for approximate quantum time-correlation functions, Matsubara dynamics, that rigorously describes how to combine quantum statistics with classical dynamics. Matsubara dynamics is based on Feynman's path integral formulation of quantum mechanics and is expected to describe the physics of any system that satisfies quantum Boltzmann statistics and exhibits rapid quantum decoherence, e.g. liquid water at room temperature.

Having derived the Matsubara dynamics theory and explored the symmetry properties that it shares with the quantum Kubo time-correlation function, we demonstrate that two heuristic computational methods, Centroid Molecular Dynamics and Ring Polymer Molecular Dynamics, are based on quantifiable approximations to the Matsubara dynamics time-correlation function. This provides these methods with a stronger theoretical foundation and helps to explain their strengths and shortcomings. We then apply the Matsubara dynamics theory to a recently developed computational method of Poulsen *et al.* called the planetary model. We show that the planetary model is based on a harmonic approximation to Matsubara dynamics that is engineered to maintain the conservation of the quantum Boltzmann distribution, so quantum statistics and classical dynamics remain harmonised.

By making practical modifications to the planetary model, we were able to calculate infrared absorption spectra for a point charge model of condensed-phase water over a range of thermodynamic conditions. We find that this harmonic approximation to Matsubara dynamics provides a good description of bending and vibrational motions and is expected to be a useful tool for future spectroscopic studies of more complex, polarisable models of water.

Declaration

This thesis is the result of my own work and includes nothing which is the outcome of work done in collaboration except where specifically indicated in the text. Some of the work described in this thesis has been published in

- T.J.H. Hele, M.J. Willatt, A. Muolo, and S.C. Althorpe, J. Chem. Phys. **142**, 134103 (2015)
- T.J.H. Hele, M.J. Willatt, A. Muolo, and S.C. Althorpe, J. Chem. Phys. **142**, 191101 (2015).

The number of words in this thesis does not exceed the limit set by the Degree Committee. It is not substantially the same as any that I have submitted, or, is being concurrently submitted for a degree or diploma or other qualification at the University of Cambridge or any other university or similar institution.

Acknowledgements

I owe a debt of gratitude to my supervisor, Stuart Althorpe, for guidance and encouragement throughout the PhD. I could not have asked for a better supervisor. I am also very grateful to the other members of the Althorpe group. In particular, Tim Hele kept me on my toes and helped to bring me up to speed with much of the relevant theory. David Manolopoulos suggested the use of ring polymers to calculate an alternative to the Feynman-Kleinert frequency and the use of TRPMD for the centroid dynamics in the planetary model. Michele Ceriotti suggested the form of the path integral frequency and took time out of his busy schedule to help me integrate the planetary model into i-PI. I am very grateful to them both.

Contents

1 Introduction **1**

2 Background Theory **7**

2.1 Thermal expectation values and time-correlation functions 7
2.2 The centroid potential of mean force 11
2.3 The Feynman-Kleinert approximation 12
2.4 Centroid Molecular Dynamics (CMD) 14
2.5 Feynman-Kleinert CMD 15
2.6 Ring Polymer Molecular Dynamics (RPMD) 16
2.7 Thermostatted Ring Polymer Molecular Dynamics (TRPMD) 18
2.8 The Wigner phase space representation 19
2.9 The quantum Louvillian 21
2.10 The Linearised Semiclassical Initial Value Representation (LSC-IVR) 22

3 Matsubara Dynamics **25**

3.1 Introduction 25
3.2 Derivation 26
3.2.1 The quantum Kubo time-correlation function 26
3.2.2 The Wigner phase space representation 27
3.2.3 The quantum Liouvillian 28
3.2.4 Normal mode coordinates and Matsubara modes 29
3.2.5 The Matsubara dynamics approximation 33
3.2.6 The Matsubara dynamics time-correlation function 34
3.2.7 The continuum picture 36
3.3 Symmetries 36
3.3.1 Time translation symmetries 37
3.3.2 Time reversal symmetries 42
3.4 Relation to CMD and RPMD 45
3.4.1 CMD 46

3.4.2 RPMD . . . 48
3.5 Limits . . . 51
3.5.1 The classical limit . . . 51
3.5.2 The harmonic limit . . . 52
3.6 Numerical results for one-dimensional systems . . . 54

4 The Planetary Model 59
4.1 Introduction . . . 59
4.2 Matsubara dynamics for two-point correlation . . . 62
4.3 The Feynman-Kleinert approximation . . . 63
4.4 An approximate dynamics . . . 65
4.5 Integrating out the Matsubara phase . . . 68
4.6 Recovering conservation of energy . . . 73
4.7 Limits and momentum-dependent observables . . . 74
4.7.1 The zero-time limit . . . 74
4.7.2 The harmonic limit . . . 75
4.7.3 Momentum-dependent observables . . . 75
4.8 Multidimensional generalisation . . . 76
4.9 Practicalities . . . 78
4.9.1 Imaginary frequencies . . . 78
4.9.2 Two practical modifications . . . 78

5 Infrared Absorption Spectroscopy of Water 85
5.1 Simulation of infrared absorption spectra . . . 85
5.2 The q-TIP4P/F model of water . . . 86
5.3 The single molecule . . . 88
5.3.1 Computational details . . . 89
5.3.2 Infrared absorption spectra . . . 90
5.4 The condensed phase . . . 93
5.4.1 Computational details . . . 93
5.4.2 Infrared absorption spectra . . . 95
5.5 Motional narrowing and lineshapes . . . 98

6 Conclusions 103

A Background Theory Appendix 107
A.1 The classical propagator . . . 107
A.2 Trajectories in LSC-IVR . . . 108

B Matsubara Dynamics Appendix **109**
B.1 Exactness of the generalised quantum Kubo time-correlation function 109
B.2 Derivation of the Matsubara dynamics time-correlation function . . . 111
B.3 The error Liouvillian and the harmonic limit 114
B.4 The Matsubara limit for polynomial potentials 114
B.5 Noether's theorem and Matsubara phase conservation 115
B.6 The thermal kinetic energy 116

C The Planetary Model Appendix **119**
C.1 Identities involving sums of Matsubara frequencies 119
C.2 The Matsubara dynamics two-point time-correlation function distribution 120
C.3 Convergence of the path integral frequency estimator 123
C.4 The path integral frequency in the $T \to 0$ limit 123

D Infrared Absorption Spectroscopy of Water Appendix **127**
D.1 The effect of modifying the planetary model on the infrared absorption spectrum of the q-TIP4P/F water molecule 127
D.2 Spectroscopic data for the condensed-phase q-TIP4P/F water simulations 131

References **133**

Chapter 1

Introduction

Computational chemists routinely simulate molecular systems comprising thousands of atoms.[1] The aim of such simulations is ordinarily to calculate static and dynamical properties, e.g. radial distribution functions, chemical reaction rates, infrared absorption spectra etc., for the discovery of new phenomena and comparison with experiment.

Often classical molecular dynamics or classical Monte Carlo simulations of molecular systems are capable of reproducing experimental results. However, for systems containing light atoms or stiff degrees of freedom, or those at low temperature, it is usually necessary to include nuclear quantum effects (NQEs) like zero-point energy and tunnelling.[2,3] For example, since a classical simulation will not account for the significant zero-point energy of the stiff OH covalent bond in water (even with a highly accurate *ab initio* nuclear potential energy surface), a classical simulation of room-temperature liquid water will underestimate the acid dissociation constant of each water molecule by at least an order of magnitude.[4]

To include NQEs in statistical mechanics simulations, we could solve the time-independent Schrödinger equation for the nuclear degrees of freedom to construct the density matrix for the system. For systems where nuclear exchange effects are unimportant, the appropriate density matrix is the Boltzmann operator. By representing the Hamiltonian operator in an appropriate basis, e.g. a Discrete Variable Representation (DVR),[5,6] exploiting the sparsity of the Hamiltonian matrix and focusing only on the lowest-lying eigenstates (with the Lanczos algorithm,[7] for example), it is feasible to calculate the quantum Boltzmann statistics of small systems. Nevertheless, such a calculation scales exponentially with the number of nuclear degrees of freedom and is therefore prohibitively expensive for systems of moderate size.

However, it is a remarkable fact that the quantum Boltzmann statistics of any

system is equivalent to the classical Boltzmann statistics of N replicas of the same system connected by harmonic springs in the $N \to \infty$ limit.[8] This fact is based on Feynman's path integral formulation of quantum mechanics in imaginary time and was first used to calculate quantum-statistical properties of molecular systems in the 1980s.[9,10] Since classical simulations scale linearly with the number of nuclear degrees of freedom, this makes the inclusion of NQEs astronomically more affordable.

While the scaling with the number of nuclear degrees of freedom is linear, the computational expense of such a simulation is clearly dependent on the number of replicas that are required to converge the quantum Boltzmann statistics as well. In practice, for systems like liquid water at room temperature, the number of required replicas is of the order of tens to hundreds.[11,4] This makes the inclusion of NQEs in a statistical mechanics simulation only one to two orders of magnitude more computationally expensive than a traditional classical simulation. Moreover, various improvements have been made to statistical mechanics methods like Path Integral Monte Carlo (PIMC) and Path Integral Molecular Dynamics (PIMD) that exploit this isomorphism between the quantum and classical Boltzmann distributions. These include the ring-polymer contraction technique[12,13] and time-evolution algorithms based on the generalised Langevin equation.[14,15,16] Such advances have made statistical mechanics simulations of molecular systems that include NQEs almost as cheap as traditional classical simulations, and computational chemists now routinely include NQEs to study the statistical mechanics of complex molecular systems.

To simulate the quantum-dynamical properties of molecular systems is significantly more challenging than statistical properties, even if the nuclei are restricted to remain on the potential energy surface associated with the electronic ground state. The quantum-dynamical properties of systems governed by quantum Boltzmann statistics are encapsulated in quantum time-correlation functions (TCFs). TCFs measure the correlation of a pair of observables at two moments in time within the quantum canonical ensemble. Of course, the observables depend on the application; for instance, the infrared absorption and Raman spectra are related to the Fourier transform of the dipole moment and polarisability tensor autocorrelation functions respectively.[17] Likewise, transport coefficients (diffusion constant, shear viscosity etc.) are related to the zero-frequency components of autocorrelation functions through what are known as the Green-Kubo relations.[18,19]

In principle, to reproduce experimental results like the Raman spectrum for systems where quantum coherence effects are important, e.g. an isolated water molecule in the gas phase, we must resort to finding approximate solutions to the

time-dependent Schrödinger equation for the nuclear degrees of freedom. Popular approaches to this end include the use of a DVR to construct time-dependent solutions from stationary states,[5,20,6] or the use of wavepackets, e.g. the Multiconfiguration Time-dependent Hartree method (MCTDH)[21,22] and Gaussian wavepacket methods.[23,24,25,26,27] There are also a variety of methods based on semiclassical approximations to the exact quantum propagator, e.g. the Semiclassical Initial Value Representation (SC-IVR) and the Forward Backward Initial Value Representation (FB-IVR) etc.[28,29,2] However, owing to their computational expense, these approaches usually focus on relatively small systems, e.g. the nuclear dynamics of a single pyrazine molecule.[30,22,31]

Fortunately, for most large condensed-phase chemical systems at room temperature, we expect quantum coherence effects to be unimportant because the vast number of thermally-accessible degrees of freedom lead to rapid decoherence.[2,28,4] This suggests that, while a quantum description of the thermal statistics is necessary, the appropriate level of theory for such systems is a classical one for the dynamics. Of course, this then raises the question of how to combine quantum statistics and classical dynamics rigorously in approximate quantum TCFs.

To explore the link between quantum and classical mechanics, Wigner reformulated quantum statistical mechanics in a phase space akin to the classical phase space.[32] The cornerstone of this formulation is an integral transform that takes his name.[33] In the 1940s, Moyal discovered the Moyal series, the quantum analogue of the Poisson bracket, which governs the time-evolution of observables in the Wigner phase space.[34] The Moyal series is equivalent to what we call the quantum Liouvillian in this thesis, which is the Wigner phase space analogue of the classical Liouvillian.

As is well known, if we formulate the quantum TCF in the Wigner phase space and make a semiclassical approximation for the quantum Liouvillian, we reach the Linearised Semiclassical Initial Value Representation (LSC-IVR).[35,36] LSC-IVR has been regarded as the pre-eminent theory for combining quantum statistics with classical dynamics in approximate quantum TCFs that exclude quantum coherence effects. The classical dynamics in LSC-IVR is, however, inconsistent with the quantum statistics since it does not conserve the quantum Boltzmann distribution. This inconsistency leads to spurious predictions related to the erroneous redistribution of energy over time. For example, the significant zero-point energy in the intramolecular degrees of freedom in an LSC-IVR description of liquid water can leak into the intermolecular degrees of freedom.[37] In principle, this could predict the spontaneous boiling of the liquid at room temperature.[2]

Despite this shortcoming of LSC-IVR, various approximate dynamical methods

have been heuristically developed since the end of the last century that successfully combine quantum statistics and classical mechanics in the sense that they conserve the quantum Boltzmann distribution. The most popular methods are Centroid Molecular Dynamics (CMD) and Ring Polymer Molecular Dynamics (RPMD), both of which are based on the path-integral isomorphism between the quantum and classical Boltzmann distributions.[38,39] While approximate, these methods allow the computational chemist to include NQEs in dynamical simulations of large molecular systems without needing to worry about spurious results related to the non-conservation of the quantum Boltzmann distribution. However, it has been unclear how each of these methods relates to LSC-IVR, and thus how they relate to the quantum TCFs that they approximate at finite time.[40,41]

Furthermore, CMD and RPMD are known to poorly describe TCFs involving observables that are non-linear in position (often called the 'non-linear operator problem').[42,39] They also possess well-known shortcomings for the calculation of infrared absorption spectra for systems like room-temperature liquid water. In CMD, the OH stretch band exhibits a spurious, temperature-dependent redshift (the 'curvature problem'). In RPMD, the temperature-dependent coupling between the internal modes of the ring polymer can lead to the presence of spurious peaks and splitting of the genuine bands (the 'spurious resonance problem').

In this work we develop Matsubara dynamics, a theory that rigorously combines quantum Boltzmann statistics with classical dynamics in approximate quantum TCFs. Matsubara dynamics derives from the Wigner phase space representation of the quantum TCF through an approximation to the quantum Liouvillian that, unlike LSC-IVR, maintains the conservation of the quantum Boltzmann distribution.[43] Matsubara dynamics suffers from the sign problem so the Matsubara dynamics TCF is in general just as difficult to compute as an exact solution to the time-dependent Schrödinger equation.

However, using the content of the Matsubara dynamics theory, we are able to demonstrate that CMD and RPMD are related to Matsubara dynamics via quantifiable approximations.[44] This provides the missing theoretical link to exact quantum dynamics for these popular methods and helps to explain the origin of the non-linear operator, curvature and spurious resonance problems. We are also able to demonstrate that a more recently-developed approximate method that conserves the quantum Boltzmann distribution, the planetary model of Poulsen *et al.*, is related to Matsubara dynamics via several quantifiable approximations that do not lead to the non-linear operator problem.[45,46]

The thesis culminates in a spectroscopic study of condensed-phase water over

a range of thermodynamic conditions. We develop a more practical version of the planetary model and compare with CMD and a thermostatted version of RPMD (TRPMD) which was developed to remedy the spurious resonance problem.[47] We find that the planetary model provides a faithful representation of the high-frequency portion of the water infrared absorption spectra, which for hexagonal ice at 150K is undoubtedly more realistic than the CMD and TRPMD results. Using a stochastic theory of lineshape that was developed by Kubo, we are able to rationalise the success of the planetary model for the condensed-phase simulations on the basis of a motional narrowing argument.[48]

We are ultimately led to speculate that the planetary model is likely to be a useful computational tool for future spectroscopic studies of condensed-phase systems and also a useful theoretical tool to assess the validity of centroid-based approximate methods (namely CMD and RPMD) for the calculation of non-linear quantum TCFs. We also expect that the theoretical framework that Matsubara dynamics provides will lead to the development of new, approximate quantum dynamics methods to complement CMD, RPMD and the planetary model in the future.

Chapter 2

Background Theory

2.1 Thermal expectation values and time-correlation functions

In classical statistical mechanics, the canonical partition function is given by a phase space integral over the Boltzmann factor,

$$Z = \frac{1}{2\pi\hbar} \int \mathrm{d}q \int \mathrm{d}p \; e^{-\beta H(q,p)}, \tag{2.1}$$

where $\beta = 1/kT$ is the inverse temperature, $H(q,p) = \frac{p^2}{2m} + V(q)$ is the classical Hamiltonian and the integrals are taken over the entire real line. We assume the system is one-dimensional in this and the following sections but the multidimensional generalisation is straightforward in every case. For the partition function written in Cartesian coordinates (2.1), the momentum may be integrated out at once to give

$$Z = \sqrt{\frac{m}{2\pi\beta\hbar^2}} \int \mathrm{d}q \; e^{-\beta V(q)}, \tag{2.2}$$

which is often called the configuration integral.[1] The thermal expectation value of an observable $A(q,p)$ is given by a phase space integral over the normalised probability distribution $e^{-\beta H(q,p)}/Z$ (the classical Boltzmann distribution),

$$\langle A \rangle = \frac{1}{Z} \frac{1}{2\pi\hbar} \int \mathrm{d}q \int \mathrm{d}p \; e^{-\beta H(q,p)} \, A(q,p). \tag{2.3}$$

It is these expectation values that provide the link between the statistical mechanics theory and static equilibrium properties. For example, the constant-volume heat capacity is related to the variance of the total energy,[49]

$$C_V(T) = \frac{\langle H^2 \rangle - \langle H \rangle^2}{kT^2}. \tag{2.4}$$

For dynamical properties, it is time-correlation functions (TCFs) that provide the link between theory and experiment. The classical TCF for two observables $A(q,p)$ and $B(q,p)$ is defined by

$$C_{AB}(t) = \frac{1}{2\pi\hbar} \int \mathrm{d}q \int \mathrm{d}p \; e^{-\beta H(q,p)} \, A(q,p) e^{\mathcal{L}_0 t} B(q,p) \tag{2.5}$$

$$= \frac{1}{2\pi\hbar} \int \mathrm{d}q \int \mathrm{d}p \; e^{-\beta H(q,p)} \, A(q,p) B(q_t, p_t), \tag{2.6}$$

where $\mathcal{L}_0$ is the classical Liouvillian,

$$\mathcal{L}_0 = \frac{p}{m}\frac{\partial}{\partial q} - V'(q)\frac{\partial}{\partial p}, \tag{2.7}$$

and the coordinates (q_t, p_t) result from (q,p) after classical evolution for time t. For example, for $A(q,p) = B(q,p) = \mu(q)$ where $\mu(q)$ is the dipole moment of the system, the Fourier transform of the dipole moment autocorrelation function,

$$C_{\mu\mu}(t) = \frac{1}{2\pi\hbar} \int \mathrm{d}q \int \mathrm{d}p \; e^{-\beta H(q,p)} \, \mu(q)\mu(q_t), \tag{2.8}$$

has a simple relationship with the infrared absorption spectrum.[17] By expanding the classical propagator $e^{\mathcal{L}_0 t}$ as a Taylor series in t and repeatedly applying integration by parts in the position and momentum coordinates, it is straightforward to show that the classical TCF satisfies the important detailed balance relation,

$$C_{AB}(t) = \frac{1}{2\pi\hbar} \int \mathrm{d}q \int \mathrm{d}p \; e^{-\beta H(q,p)} \, B(q,p) \, A(q_{-t}, p_{-t}) \tag{2.9}$$

$$= C_{BA}(-t), \tag{2.10}$$

where we have exploited conservation of the classical Boltzmann distribution,

$$\mathcal{L}_0 \, \frac{e^{-\beta H(q,p)}}{Z} = 0, \tag{2.11}$$

which results from conservation of energy $H(q,p)$. For the special case of $A(q,p) = 1$, the detailed balance relation implies

$$\frac{C_{1B}(t)}{Z} = \langle B \rangle \,, \tag{2.12}$$

which provides the link between classical TCFs and thermal expectation values.

In quantum statistical mechanics, the canonical partition function is given by the trace of the Boltzmann operator,

$$Z = \mathrm{Tr}\left[e^{-\beta\hat{H}}\right], \tag{2.13}$$

where $\hat{H} = \hat{T} + \hat{V}$ is the Hamiltonian operator. The quantum counterpart to the classical Boltzmann distribution is the following normalised density matrix,

$$\hat{\rho} = \frac{e^{-\beta\hat{H}}}{Z}, \tag{2.14}$$

with which we can neatly write the thermal expectation value of an operator $\hat{A}$ as

$$\langle A \rangle = \mathrm{Tr}\left[\hat{\rho}\hat{A}\right]. \tag{2.15}$$

Ostensibly this expectation value has a fundamentally different form to its classical counterpart (2.3). However, by using the Trotter factorisation[50] of an exponentiated operator, the quantum thermal expectation value can be brought into a form that resembles the classical one. Without approximation, the Boltzmann operator can be written as follows for any positive integer N,

$$e^{-\beta\hat{H}} = \prod_{l=1}^{N} e^{-\beta_N\hat{H}}, \tag{2.16}$$

where $\beta_N = \beta/N$. Now, in the $N \to \infty$ limit we have

$$e^{-\beta\hat{H}} = \lim_{N\to\infty} \prod_{l=1}^{N} e^{-\beta_N\hat{V}/2} e^{-\beta_N\hat{T}} e^{-\beta_N\hat{V}/2}, \tag{2.17}$$

owing to the Trotter factorisation of each $e^{-\beta_N\hat{H}}$ in the product. If we insert this form into the definition of the quantum canonical partition function, expand the trace in position states and insert $N-1$ copies of the identity operator,

$$\hat{I} = \int_{-\infty}^{\infty} \mathrm{d}x \; |x\rangle \langle x|, \tag{2.18}$$

we find[8]

$$Z = \lim_{N\to\infty} \left(\frac{m}{2\pi\beta_N\hbar^2}\right)^{N/2} \int \mathrm{d}\mathbf{q} \; \exp\left[-\beta_N \sum_{l=1}^{N} V(q_l) + \frac{1}{2} m \frac{(q_l - q_{l-1})^2}{(\beta_N\hbar)^2}\right], \tag{2.19}$$

where $\int \mathrm{d}\mathbf{q}$ is shorthand for $\prod_{l=1}^{N} \int_{-\infty}^{\infty} \mathrm{d}q_l$ and the coordinates are cyclic (so $q_0 = q_N$ etc.). It is clear that for a given N, the right-hand side of (2.19) has the same form as the classical configuration integral (2.2) but at a temperature that is elevated by a factor of N in a configuration space that has N-fold as many dimensions. If we interpret the content of the right-hand side of (2.19) from a classical point of view, the system in this extended configuration space is a 'ring polymer' composed of N 'beads' (each coordinate q_l represents the position of a bead). Each bead experiences the external potential $V(q_l)$ as well as harmonic forces from each of its two neighbours in the ring polymer.

By inserting N copies of the following identity,[10]

$$1 = \sqrt{\frac{\beta_N}{2\pi m}} \int_{-\infty}^{\infty} \mathrm{d}p \; e^{-\beta_N \frac{p^2}{2m}}, \tag{2.20}$$

we may rewrite the quantum canonical partition function (2.19) as a phase space integral over the unnormalised ring-polymer representation of the quantum Boltzmann distribution $e^{-\beta_N R(\mathbf{q},\mathbf{p})}$,

$$Z = \lim_{N\to\infty} \frac{1}{(2\pi\hbar)^N} \int \mathrm{d}\mathbf{q} \int \mathrm{d}\mathbf{p} \; e^{-\beta_N R(\mathbf{q},\mathbf{p})}, \tag{2.21}$$

where we have defined the ring-polymer Hamiltonian,

$$R(\mathbf{q},\mathbf{p}) = \sum_{l=1}^{N} \frac{p_l^2}{2m} + V(q_l) + \frac{1}{2} m \frac{(q_l - q_{l-1})^2}{(\beta_N \hbar)^2}. \tag{2.22}$$

Quantum thermal expectation values can be evaluated in this extended ring-polymer phase space. For an operator $\hat{A} = A(\hat{q})$ we have

$$\langle A \rangle = \lim_{N\to\infty} \frac{1}{Z} \frac{1}{(2\pi\hbar)^N} \int \mathrm{d}\mathbf{q} \int \mathrm{d}\mathbf{p} \; e^{-\beta_N R(\mathbf{q},\mathbf{p})} A(\mathbf{q}), \tag{2.23}$$

where

$$A(\mathbf{q}) = \frac{1}{N} \sum_{l=1}^{N} A(q_l). \tag{2.24}$$

This isomorphism between the quantum and classical Boltzmann distributions is used to calculate thermal expectation values according to (2.23) in Path Integral Monte Carlo (PIMC) and Path Integral Molecular Dynamics (PIMD). In PIMC, Monte Carlo sampling is used to generate ring-polymer configurations that are consistent with the quantum Boltzmann distribution. In PIMD, the classical dynamics

of the ring polymer, as governed by the Hamiltonian in (2.22), is used to generate the configurations instead.[9,51,52,53]

As for the classical theory, it is quantum TCFs that provide the link between theory and experiment for dynamical properties. The standard quantum TCF for two operators $\hat{A}$ and $\hat{B}$ is defined by

$$C_{AB}(t) = \mathrm{Tr}\left[e^{-\beta\hat{H}}\hat{A}\hat{B}(t)\right], \tag{2.25}$$

where $\hat{B}(t)$ is the operator $\hat{B}$ at time t in the Heisenberg picture,

$$\hat{B}(t) = e^{+i\hat{H}t/\hbar}\hat{B}e^{-i\hat{H}t/\hbar}. \tag{2.26}$$

Many practical methods approximate the quantum Kubo TCF (also known as the quantum canonical TCF[54]) instead. This is defined by[19]

$$C_{AB}(t) = \frac{1}{\beta}\int_0^\beta \mathrm{d}\lambda\ \mathrm{Tr}\left[e^{-(\beta-\lambda)\hat{H}}\hat{A}e^{-\lambda\hat{H}}\hat{B}(t)\right]. \tag{2.27}$$

In common with the classical TCF (2.5), the quantum Kubo TCF satisfies the detailed balance relation (2.10) while the standard quantum TCF (2.25) does not. However, it is straightforward to show by writing the quantum Kubo TCF as $\frac{1}{\beta}\int_0^\beta \mathrm{d}\lambda\ C_{AB}\left(t + i\lambda\hbar\right)$ (i.e. analytic continuation of the standard quantum TCF) that the Fourier transforms of these two quantum TCFs are in the ratio

$$f(\omega) = \frac{\beta\hbar\omega}{1 - e^{-\beta\hbar\omega}}, \tag{2.28}$$

so each can be inferred from the other. This function of the frequency is often called the harmonic correction factor. In the harmonic limit, the Fourier transforms of the classical position autocorrelation function ($A(q,p) = B(q,p) = q$) and the standard quantum position autocorrelation function are in the ratio (2.28).[55]

2.2 The centroid potential of mean force

The canonical partition function is related to the Helmholtz free energy as follows,[1]

$$Z = e^{-\beta F}, \tag{2.29}$$

which is of course related to the internal energy $\langle H\rangle$ and entropy S through

$$F = \langle H\rangle - TS. \tag{2.30}$$

By introducing the definition of the centroid of the bead positions $\{q_l\}$ (note that since all the beads have the same mass, this is the same as the ring-polymer centre of mass),

$$Q_0 = \frac{1}{N}\sum_{l=1}^{N} q_l, \tag{2.31}$$

and by associating a free energy with a given centroid configuration space point (c.f. the global free energy in (2.29)), we may write the quantum canonical partition function as an integral over the centroid position and momentum,

$$Z = \frac{1}{2\pi\hbar}\int \mathrm{d}Q_0 \int \mathrm{d}P_0 \; e^{-\beta H(Q_0,P_0)}, \tag{2.32}$$

where $H(Q_0, P_0) = \frac{P_0^2}{2m} + F(Q_0)$ and the centroid free energy $F(Q_0)$, or centroid potential of mean force (so named for reasons to become clear shortly), is defined implicitly by

$$\begin{aligned} e^{-\beta H(Q_0,P_0)} = \lim_{N\to\infty} \frac{1}{(2\pi\hbar)^{N-1}} \int \mathrm{d}\mathbf{q} \int \mathrm{d}\mathbf{p} \; e^{-\beta_N R(\mathbf{q},\mathbf{p})} \\ \times \delta\left(Q_0 - \frac{1}{N}\sum_{l=1}^{N} q_l\right) \delta\left(P_0 - \frac{1}{N}\sum_{l=1}^{N} p_l\right). \end{aligned} \tag{2.33}$$

With this representation we may evaluate the quantum thermal expectation value of a position-dependent operator $\hat{A} = A(\hat{q})$ as follows,

$$\langle A \rangle = \frac{1}{Z}\frac{1}{2\pi\hbar}\int \mathrm{d}Q_0 \int \mathrm{d}P_0 \; e^{-\beta H(Q_0,P_0)} \, A(Q_0), \tag{2.34}$$

which is exact for $\hat{A}$ linear in $\hat{q}$. Note that such an operator is often called a linear operator in this context and we follow this convention throughout the thesis. The equality (2.34) does not hold if $\hat{A}$ is a non-linear operator since $A(Q_0) \neq \frac{1}{N}\sum_{l=1}^{N} A(q_l)$ in that case (c.f. (2.23)).

2.3 The Feynman-Kleinert approximation

It follows from the Gibbs-Bogoliubov inequality that the centroid potential of mean force $F(Q_0)$ is bounded from above by[56]

$$F(Q_0) \leq W(Q_0), \tag{2.35}$$

where

$$W(Q_0) = \frac{1}{\beta} \ln \left(\frac{\sinh(\beta\hbar\Omega/2)}{\beta\hbar\Omega/2} \right) - \frac{1}{2} m\Omega^2 a^2 + V_{a^2}(Q_0), \tag{2.36}$$

and $V_{a^2}(Q_0)$ is the convolution of a Gaussian of width a with the external potential,

$$V_{a^2}(Q_0) = \frac{1}{\sqrt{2\pi}a} \int \mathrm{d}q \; e^{-\frac{q^2}{2a^2}} \, V(Q_0 + q). \tag{2.37}$$

Note that the Gibbs-Bogoliubov inequality is a simple application of Jensen's inequality from probability theory: $\left\langle e^X \right\rangle \geq e^{\langle X \rangle}$ for any random variable X.[8] The function $W(Q_0)$ is the Feynman-Kleinert approximation[56] to the exact centroid potential of mean force. (While this approximation carries Feynman and Kleinert's names, it was also developed independently by Giachetti and Tognetti.[57,58]) For the right-hand side of the inequality (2.35) to be a minimum, it must be independently minimised with respect to a^2 and Ω^2. This leads to the following pair of simultaneous equations that define $a^2 = a^2(Q_0)$ and $\Omega^2 = \Omega^2(Q_0)$ as functions of the centroid position (though we suppress this explicit dependence in what follows to maintain a clear notation),

$$a^2 = \frac{\beta\hbar\Omega \coth\left(\frac{\beta\hbar\Omega}{2}\right) - 2}{2\beta m\Omega^2}, \tag{2.38}$$

and

$$m\Omega^2 = \frac{1}{\sqrt{2\pi}a} \int \mathrm{d}q \; e^{-\frac{q^2}{2a^2}} \, V''(Q_0 + q). \tag{2.39}$$

In other words, for the trial centroid potential of mean force (2.36) to be a minimum with respect to the parameters a^2 and Ω^2, the squared frequency Ω^2 must be the convolution of the mass-weighted Hessian with a Gaussian whose width is dictated by (2.38). It is important to note that a^2 must be positive for (2.39) to be well defined. From (2.38), a^2 is positive for $\Omega^2 > -(2\pi/\beta\hbar)^2$ and for any bound system this inequality is guaranteed.[56] Therefore, for any bound system there is always a solution to the simultaneous equations (2.38) and (2.39). In practice, the equations are solved by fixed-point iteration.

These considerations allow us to approximate the quantum thermal expectation value of an operator $\hat{A} = A(\hat{q})$ as follows (c.f. (2.34)),

$$\langle A \rangle \approx \frac{1}{Z_0} \frac{1}{2\pi\hbar} \int \mathrm{d}Q_0 \int \mathrm{d}P_0 \; e^{-\beta H_0(Q_0, P_0)} \, A(Q_0), \tag{2.40}$$

where $H_0(Q_0, P_0) = \frac{P_0^2}{2m} + W(Q_0)$ and

$$Z_0 = \frac{1}{2\pi\hbar} \int \mathrm{d}Q_0 \int \mathrm{d}P_0 \; e^{-\beta H_0(Q_0,P_0)}. \tag{2.41}$$

Equality holds in (2.40) in the harmonic limit provided $\hat{A}$ is a linear operator.

2.4 Centroid Molecular Dynamics (CMD)

Returning to (2.34), for two operators $\hat{A} = A(\hat{q})$ and $\hat{B} = B(\hat{q})$ it is straightforward to show that

$$C_{AB}(0) = \frac{1}{2\pi\hbar} \int \mathrm{d}Q_0 \int \mathrm{d}P_0 \; e^{-\beta H(Q_0,P_0)} \, A(Q_0)B(Q_0), \tag{2.42}$$

where $C_{AB}(0)$ is the zero-time value of the quantum Kubo TCF,

$$C_{AB}(0) = \frac{1}{\beta} \int_0^\beta \mathrm{d}\lambda \; \mathrm{Tr} \left[e^{-(\beta-\lambda)\hat{H}} \hat{A} e^{-\lambda\hat{H}} \hat{B} \right], \tag{2.43}$$

and equality holds provided $\hat{A}$ and $\hat{B}$ are linear in $\hat{q}$. Note that $\frac{C_{AB}(0)}{Z} \neq \langle AB \rangle$ unless $A(\hat{q})$ commutes with the Boltzmann operator.

In the Centroid Molecular Dynamics method (CMD), this observation (2.42) is used to approximate the quantum Kubo TCF for operators $\hat{A} = A(\hat{q})$ and $\hat{B} = B(\hat{q})$ at $t \geq 0$. The CMD TCF is defined by[38]

$$C_{AB}(t) = \frac{1}{2\pi\hbar} \int \mathrm{d}Q_0 \int \mathrm{d}P_0 \; e^{-\beta H(Q_0,P_0)} \, A(Q_0) \, e^{\mathcal{L}_0 t} \, B(Q_0), \tag{2.44}$$

where the CMD Hamiltonian is $H(Q_0, P_0) = \frac{P_0^2}{2m} + F(Q_0)$, as defined before, and its corresponding classical Liouvillian is the CMD Liouvillian,

$$\mathcal{L}_0 = \frac{P_0}{m} \frac{\partial}{\partial Q_0} - F'(Q_0) \frac{\partial}{\partial P_0}. \tag{2.45}$$

It is straightforward to show by differentiation of (2.33) that the centroid force is given by

$$\begin{aligned} -F'(Q_0) = \; e^{\beta H(Q_0,P_0)} \lim_{N\to\infty} \frac{1}{(2\pi\hbar)^{N-1}} \int \mathrm{d}\mathbf{q} \int \mathrm{d}\mathbf{p} \; e^{-\beta_N R(\mathbf{q},\mathbf{p})} \, \frac{1}{N} \sum_{l=1}^{N} -V'(q_l) \\ \times \, \delta \left(Q_0 - \frac{1}{N} \sum_{l=1}^{N} q_l \right) \delta \left(P_0 - \frac{1}{N} \sum_{l=1}^{N} p_l \right). \end{aligned} \tag{2.46}$$

In other words, it is a centroid-constrained ring-polymer average over the force on each ring-polymer bead, hence the name 'potential of mean force' for $F(Q_0)$. Note that the factor $e^{\beta H(Q_0,P_0)}$ normalises the integral. Of course, action of the CMD Liouvillian on the CMD Hamiltonian gives zero, $\mathcal{L}_0 H(Q_0, P_0) = 0$, so the distribution is conserved. This ensures that CMD satisfies the detailed balance relation (2.10) in accordance with the quantum Kubo TCF that it approximates.

In practice, CMD TCFs are calculated using the classical dynamics of ring polymers. The mass of the ring-polymer centroid is fixed at the physical mass, while the other masses are decreased so the fluctuation modes (the non-centroid internal ring-polymer modes) become adiabatically separated from the centroid. This means that the centroid-constrained ring-polymer average (2.46) can be calculated on the fly. To aid the sampling of this integral, the fluctuation modes are usually thermostatted with Nosé-Hoover chains. Such an implementation of CMD is called Partially Adiabatic CMD (PA-CMD).[59]

CMD has been successfully applied to many condensed phase systems for the calculation of, for example: reaction rates, diffusion constants, infrared absorption and Raman spectra.[60,61,62,63] However, CMD is known to suffer from the 'curvature problem' in some multidimensional systems, as first described by Marx *et al.*[64,65] This problem is characterised by a temperature-dependent redshift of high frequency vibrations in infrared absorption spectra, which is particularly troublesome for molecular systems with stiff vibrations (e.g. water). The temperature-dependent redshift is ultimately caused by the breakdown of the mean-field approximation at low temperatures for these systems.

For some one-dimensional systems where quantum coherence effects are important (e.g. the quartic oscillator), CMD is known to become increasingly accurate in the $T \to 0$ limit. This is because in the $T \to 0$ limit, the thermally-accessible portion of the centroid potential of mean force becomes increasingly harmonic with a frequency $\omega \approx (E_1 - E_0)/\hbar$ that captures the coherent dynamics of the cold quantum system. We direct the reader to a series of papers concerning this theory presented by Ramirez and López-Ciudad[66] and other theory concerning CMD, including its practical implementation and its multidimensional generalisation.[67,38]

2.5 Feynman-Kleinert CMD

The Feynman-Kleinert approximation was developed for the approximation of static properties. However, since the approximation amounts to a particular form for the centroid potential of mean force, the methodology is immediately applicable to CMD

for dynamical properties as well. The CMD TCF within the Feynman-Kleinert approximation is (c.f. (2.44))

$$C_{AB}(t) = \frac{1}{2\pi\hbar}\int \mathrm{d}Q_0 \int \mathrm{d}P_0 \; e^{-\beta H_0(Q_0,P_0)} A(Q_0)\, e^{\mathcal{L}_0 t}\, B(Q_0), \tag{2.47}$$

where

$$\mathcal{L}_0 = \frac{P_0}{m}\frac{\partial}{\partial Q_0} - W'(Q_0)\frac{\partial}{\partial P_0}. \tag{2.48}$$

Given that the Feynman-Kleinert centroid potential of mean force is minimised with respect to a^2 and Ω^2, it is clear that the centroid force is given by

$$-W'(Q_0) = -\frac{1}{\sqrt{2\pi}a}\int \mathrm{d}q \; e^{-\frac{q^2}{2a^2}}\, V'(Q_0+q), \tag{2.49}$$

i.e. it is the convolution of a Gaussian of width a with the external force.[67]

2.6 Ring Polymer Molecular Dynamics (RPMD)

In Section 2.1, we demonstrated that the quantum thermal expectation value of an operator $\hat{A} = A(\hat{q})$ can be calculated as the $N \to \infty$ limit of a ring-polymer average,

$$\langle A \rangle = \lim_{N\to\infty} \frac{1}{Z}\frac{1}{(2\pi\hbar)^N}\int \mathrm{d}\mathbf{q}\int \mathrm{d}\mathbf{p} \; e^{-\beta_N R(\mathbf{q},\mathbf{p})} A(\mathbf{q}). \tag{2.50}$$

For two operators $\hat{A} = A(\hat{q})$ and $\hat{B} = B(\hat{q})$ it is straightforward to show that

$$C_{AB}(0) = \lim_{N\to\infty} \frac{1}{(2\pi\hbar)^N}\int \mathrm{d}\mathbf{q}\int \mathrm{d}\mathbf{p} \; e^{-\beta_N R(\mathbf{q},\mathbf{p})} A(\mathbf{q})B(\mathbf{q}), \tag{2.51}$$

where $C_{AB}(0)$ is the zero-time value of the quantum Kubo TCF, as defined before (2.43), and the equality holds for any $\hat{A}$ and $\hat{B}$ dependent on the position operator only. In the same spirit as CMD, this last observation is used in the Ring Polymer Molecular Dynamics method (RPMD) to approximate the quantum Kubo TCF for $t \geq 0$. The RPMD TCF for two observables $A(\mathbf{q})$ and $B(\mathbf{q})$ is[55]

$$C_{AB}^{[N]}(t) = \frac{1}{(2\pi\hbar)^N}\int \mathrm{d}\mathbf{q}\int \mathrm{d}\mathbf{p} \; e^{-\beta_N R(\mathbf{q},\mathbf{p})}\, A(\mathbf{q})\, e^{\mathcal{L}^{[\mathrm{RP}]}t}\, B(\mathbf{q}), \tag{2.52}$$

where $A(\mathbf{q})$ is as defined before (2.24) and $B(\mathbf{q})$ is defined equivalently. The RPMD Liouvillian is the classical Liouvillian for the ring-polymer Hamiltonian,

$$\mathcal{L}^{[\mathrm{RP}]} = \sum_{l=1}^{N} \frac{p_l}{m}\frac{\partial}{\partial q_l} - \left[V'(q_l) + m\frac{2q_l - q_{l+1} - q_{l-1}}{(\beta_N\hbar)^2}\right]\frac{\partial}{\partial p_l}. \tag{2.53}$$

Of course, from the definition of the RPMD Liouvillian we have $\mathcal{L}^{[\mathrm{RP}]}R(\mathbf{q},\mathbf{p}) = 0$, so the distribution is conserved. This ensures that, in common with CMD, RPMD also satisfies the detailed balance relation (2.10). As highlighted previously for the classical TCF (see (2.12)), for the special case of $\hat{A} = \hat{I}$ the detailed balance relation implies

$$\frac{C_{IB}(t)}{Z} = \langle B \rangle \,. \tag{2.54}$$

In other words, thermal expectation values are time-independent in the RPMD framework. It is precisely this quality that is exploited in PIMD to calculate a phase space average as a time average instead (provided the system is ergodic).

Like CMD, RPMD has been successfully applied to many condensed phase systems for the calculation of reaction rates, diffusion constants, infrared absorption spectra, among other dynamical properties.[68,69,70,71,72,73] RPMD has found most success in the calculation of reaction rate constants through the flux-side TCF.[74,75] This success has been explained by recent theoretical developments. Firstly, Richardson and Althorpe established the theoretical connection between RPMD rate theory and semiclassical instanton (Im F) rate theory.[76] Their analysis shows that in the deep tunnelling regime (temperatures satisfying $T \leq \hbar\omega_b/2\pi$ where ω_b is the harmonic frequency at the top of the reaction barrier), RPMD will slightly underestimate the rate of a reaction with a symmetric barrier and slightly overestimate with an asymmetric barrier. More recently, Hele and Althorpe proved that RPMD Transition State Theory (RPMD-TST), which is the $t \to 0^+$ limit of RPMD rate theory, is identical to Quantum Transition State Theory (QTST).[77,78,79,80] This means that in the absence of quantum-dynamical recrossing of the transition state dividing surface, RPMD-TST will give the exact quantum reaction rate.

Despite the special success of RPMD for reaction rate calculation, it is known to suffer from the 'spurious resonance problem', as first described by Habershon *et al.* and developed further by Marx *et al.*[69,64,65] As for the curvature problem in CMD, this phenomenon is particularly pronounced for the infrared absorption spectroscopy of water. Its origin is the temperature-dependent coupling of the internal modes of the ring polymer. At certain temperatures, the fluctuation modes come into resonance with the centroid mode which leads to spurious resonances and splittings in infrared absorption spectra.

We direct the reader to a comprehensive review of RPMD by Habershon *et al.*[39] which describes, among other developments, its practical implementation (including the powerful ring-polymer contraction technique[12]), rate theory,[74,75] the spurious resonance problem and its multidimensional generalisation. The non-adiabatic extension of RPMD is discussed in a variety of articles,[81,82] and its non-equilibrium extension is discussed in Ref. 83.

2.7 Thermostatted Ring Polymer Molecular Dynamics (TRPMD)

Thermostatted Ring Polymer Molecular Dynamics (TRPMD) is an extension of RPMD that was developed heuristically to mitigate the spurious resonance problem. The equations of motion that correspond to the RPMD Liouvillian are

$$\dot{\mathbf{q}} = \frac{\mathbf{p}}{m} \tag{2.55}$$

$$\dot{\mathbf{p}} = \boldsymbol{F}(\mathbf{q}), \tag{2.56}$$

where the elements of the force vector $\boldsymbol{F}(\mathbf{q})$ are given by

$$F_l(\mathbf{q}) = -V'(q_l) - m\frac{2q_l - q_{l+1} - q_{l-1}}{(\beta_N\hbar)^2}. \tag{2.57}$$

In TRPMD, the ring-polymer beads are subjected to a Langevin thermostat,[47]

$$\dot{\mathbf{q}} = \frac{\mathbf{p}}{m} \tag{2.58}$$

$$\dot{\mathbf{p}} = \boldsymbol{F}(\mathbf{q}) - \gamma\mathbf{p} - \sqrt{\frac{2m}{\beta_N}}\gamma^{1/2}\boldsymbol{\xi}(t), \tag{2.59}$$

where γ is a real, symmetric, positive semi-definite $N \times N$ friction matrix and $\boldsymbol{\xi}(t)$ is a vector of uncorrelated normal deviates with unit variance and zero mean: $\langle\xi_l(t)\rangle = 0$ and $\langle\xi_l\xi_j(t)\rangle = \delta_{lj}\delta(t)$. This is the same scheme that is used in stochastic implementations of PIMD.[51,14] The friction matrix is chosen to satisfy the following relation,

$$\sum_{l=1}^{N}\gamma_{jl} = 0, \tag{2.60}$$

which ensures that the centroid is not coupled to the thermostat.

In practice, the friction matrix is constructed from

$$\left(T^T \gamma T\right)_{lk} = \delta_{lk} \left|\omega_k\right|, \tag{2.61}$$

where $\omega_k = 2\sin(\pi k/N)/\beta_N\hbar$ are the free ring-polymer normal mode frequencies and the matrix of orthonormal vectors,

$$T_{lk} = \begin{cases} \sqrt{\frac{1}{N}} & k = 0 \\ \sqrt{\frac{2}{N}}\sin(2\pi lk/N) & 0 < k \leq \overline{N} \\ \sqrt{\frac{2}{N}}\cos(2\pi lk/N) & -\overline{N} \leq k < 0, \end{cases} \tag{2.62}$$

where $\overline{N} = (N-1)/2$ and N is odd, corresponds to the N-dimensional real discrete Fourier transform.[84] In the free-particle limit, this choice of the friction matrix (2.61) corresponds to underdamping of all the fluctuation modes of the ring polymer. Nevertheless, it has been found strong enough to remove spurious resonances from infrared absorption spectra in simulations of liquid water, albeit with a slight broadening of the lineshapes at room temperature.[47] More rigorously, this choice of the friction matrix can be justified with arguments concerning optimal sampling of the ring-polymer space[47] and the best approximation to the non-linear position ($\hat{A} = \hat{B} = \hat{q}^2$) quantum Kubo autocorrelation function in the harmonic limit.[85]

2.8 The Wigner phase space representation

By inserting the following identity operator,

$$\hat{I} = \int_{-\infty}^{\infty} \mathrm{d}y \; \left|y\right\rangle \left\langle y\right|, \tag{2.63}$$

the standard quantum TCF for two operators $\hat{A}$ and $\hat{B}$ (2.25) may be written in the basis of position states as

$$C_{AB}(t) = \int \mathrm{d}x \int \mathrm{d}y \;\; \left\langle x\right| e^{-\beta\hat{H}} \hat{A} \left|y\right\rangle \left\langle y\right| \hat{B}(t) \left|x\right\rangle. \tag{2.64}$$

Making the following change of variables,

$$q + \Delta/2 = \; x \tag{2.65}$$

$$q - \Delta/2 = \; y, \tag{2.66}$$

gives the following for the TCF,

$$C_{AB}(t) = \int \mathrm{d}q \int \mathrm{d}\Delta \ \langle q + \Delta/2| \, e^{-\beta \hat{H}} \hat{A} \, |q - \Delta/2\rangle \\ \times \langle q - \Delta/2| \, \hat{B}(t) \, |q + \Delta/2\rangle \, , \tag{2.67}$$

where we have recognised the Jacobian of the transformation as unity,

$$\mathrm{d}x \, \mathrm{d}y = \mathrm{d}q \, \mathrm{d}\Delta. \tag{2.68}$$

By using the following identity for the Dirac delta function,

$$\delta(\Delta + \Delta') = \frac{1}{2\pi\hbar} \int_{-\infty}^{\infty} \mathrm{d}p \ e^{ip(\Delta+\Delta')/\hbar}, \tag{2.69}$$

we may rewrite (2.67) as

$$C_{AB}(t) = \frac{1}{2\pi\hbar} \int \mathrm{d}q \int \mathrm{d}p \ \left[e^{-\beta \hat{H}} \hat{A}\right](q,p) \left[\hat{B}(t)\right](q,p), \tag{2.70}$$

where the Wigner transform of any operator $\hat{\mathcal{A}}$ is defined to be[33]

$$\left[\hat{\mathcal{A}}\right](q,p) = \int \mathrm{d}\Delta \ \langle q + \Delta/2| \, \hat{\mathcal{A}} \, |q - \Delta/2\rangle \ e^{ip\Delta/\hbar}. \tag{2.71}$$

The TCF in (2.70) is the Wigner phase space representation of the standard quantum TCF, which was first presented in the 1930s.[32]

There are two special types of operator for which the Wigner transform is trivial to evaluate. For $\hat{B} = B(\hat{q})$ we have

$$\left[\hat{B}\right](q,p) = B(q), \tag{2.72}$$

and for $\hat{B} = B(\hat{p})$,

$$\left[\hat{B}\right](q,p) = B(p). \tag{2.73}$$

Of course, since the Wigner transform is a linear transform, the same relations also hold for any linear combination $\hat{B} = f(\hat{q}) + g(\hat{p})$,

$$\left[\hat{B}\right](q,p) = f(q) + g(p). \tag{2.74}$$

However, for any operator involving products of $\hat{q}$ and $\hat{p}$ (e.g. $e^{-\beta \hat{H}}$ or $\hat{q}(t)$ for $t > 0$),

the Wigner transform is more difficult to evaluate in general.

2.9 The quantum Louvillian

It is straightforward to show that the k^{th} time derivative of the Wigner phase space representation of $C_{AB}(t)$ is[34,36]

$$\frac{\mathrm{d}^k C_{AB}(t)}{\mathrm{d}t^k} = \frac{1}{2\pi\hbar}\int \mathrm{d}q \int \mathrm{d}p \left[e^{-\beta\hat{H}}\hat{A}\right](q,p)\hat{L}^k\left[\hat{B}(t)\right](q,p), \tag{2.75}$$

where $\hat{L}$ is the quantum Liouvillian (also known as the Moyal series),

$$\hat{L} = \frac{p}{m}\frac{\partial}{\partial q} - V(q)\frac{2}{\hbar}\sin\left(\frac{\hbar}{2}\frac{\overleftarrow{\partial}}{\partial q}\frac{\overrightarrow{\partial}}{\partial p}\right), \tag{2.76}$$

and the arrows over the partial derivatives describe the direction in which the derivatives are to be taken. Formally, we can express $C_{AB}(t)$ as an infinite Taylor series in t,

$$C_{AB}(t) = \sum_{k=0}^{\infty} \left.\frac{\mathrm{d}^k C_{AB}(t)}{\mathrm{d}t^k}\right|_{t=0} \frac{t^k}{k!} \tag{2.77}$$

$$= \frac{1}{2\pi\hbar}\int \mathrm{d}q \int \mathrm{d}p \left[e^{-\beta\hat{H}}\hat{A}\right](q,p)\, e^{\hat{L}t}\left[\hat{B}(0)\right](q,p), \tag{2.78}$$

which leads to the appearance of the quantum propagator $e^{\hat{L}t}$ for the Wigner phase space. The Wigner phase space representation of the quantum TCF (2.78) is an exact rewriting of the quantum TCF but resembles its classical counterpart (2.5). However, there are important differences between the two. Firstly, we cannot associate the time-evolved Wigner transform with its $t = 0$ value at some other point in the phase space,

$$e^{\hat{L}t}\left[\hat{B}(0)\right](q,p) \neq \left[\hat{B}(0)\right](e^{\hat{L}t}q, e^{\hat{L}t}p), \tag{2.79}$$

(see Appendix A.1). This is in contrast to the classical TCF, where the observable $B(q,p)$ at time t is simply $e^{\mathcal{L}_0 t}B(q,p) = B(q_t,p_t)$. Secondly, the Wigner transform of the Boltzmann operator (commonly called the Wigner function),

$$\left[e^{-\beta\hat{H}}\right](q,p) = \int \mathrm{d}\Delta\ \langle q+\Delta/2|\, e^{-\beta\hat{H}}\, |q-\Delta/2\rangle\ e^{ip\Delta/\hbar}, \tag{2.80}$$

whose classical analogue is the Boltzmann factor $e^{-\beta H(q,p)}$, is not positive definite.[86,33] It is therefore difficult to interpret it as a regular probability distribution.

2.10 The Linearised Semiclassical Initial Value Representation (LSC-IVR)

In the Linearised Semiclassical Initial Value Representation (LSC-IVR), also known as the classical Wigner approximation, the quantum Liouvillian (2.76) is truncated to zeroth order in powers of $\hbar^2$ to give the classical Liouvillian,

$$\hat{L} \approx \frac{p}{m}\frac{\partial}{\partial q} - V'(q)\frac{\partial}{\partial p} \tag{2.81}$$

$$= \mathcal{L}_0. \tag{2.82}$$

As for any semiclassical approximation, this truncation can be justified by appealing to arguments concerning the relative smallness of $\hbar$ as the classical limit is approached (i.e. as the mass or temperature is increased). However, such arguments are known to be problematic in LSC-IVR since at least one of the Wigner transforms contains derivatives that scale as $\hbar^{-1}$.[87] Nevertheless, this approximation gives the following for the LSC-IVR TCF,

$$C_{AB}(t) \approx \frac{1}{2\pi\hbar}\int \mathrm{d}q \int \mathrm{d}p \, \left[e^{-\beta\hat{H}}\hat{A}\right](q,p)\, e^{\mathcal{L}_0 t} \, \left[\hat{B}(0)\right](q,p) \tag{2.83}$$

$$= \frac{1}{2\pi\hbar}\int \mathrm{d}q \int \mathrm{d}p \, \left[e^{-\beta\hat{H}}\hat{A}\right](q,p) \, \left[\hat{B}(0)\right](q_t,p_t), \tag{2.84}$$

where (q_t, p_t) is the phase space point (q, p) after classical evolution for time t.

For the Kubo TCF (2.27), the LSC-IVR approximation is

$$C_{AB}(t) = \frac{1}{2\pi\hbar}\int \mathrm{d}q \int \mathrm{d}p \, \left[\hat{A}_K(\beta)\right](q,p) \, \left[\hat{B}(0)\right](q_t,p_t), \tag{2.85}$$

where $\hat{A}_K(\beta)$ is the Kubo transform of the operator $\hat{A}$,

$$\hat{A}_K(\beta) = \frac{1}{\beta}\int_0^\beta \mathrm{d}\lambda \; e^{-(\beta-\lambda)\hat{H}}\hat{A}\, e^{-\lambda\hat{H}}. \tag{2.86}$$

By expanding the classical propagator $e^{\mathcal{L}_0 t}$ as a Taylor series in t and repeatedly applying integration by parts in the position and momentum coordinates, we find

$$C_{AB}(t) = \frac{1}{2\pi\hbar}\int \mathrm{d}q \int \mathrm{d}p \, \left[\hat{A}_K(\beta)\right](q_{-t},p_{-t}) \, \left[\hat{B}(0)\right](q,p). \tag{2.87}$$

However,

$$C_{AB}(t) \neq \frac{1}{2\pi\hbar}\int \mathrm{d}q \int \mathrm{d}p \, \left[\hat{B}_K(\beta)\right](q,p) \, \left[\hat{A}(0)\right](q_{-t},p_{-t}), \tag{2.88}$$

so, unlike CMD and RPMD, the LSC-IVR Kubo TCF fails to satisfy the detailed balance relation (2.10). For the special case of $\hat{A} = \hat{I}$, this implies

$$\frac{C_{IB}(t)}{Z} \neq \langle B \rangle \,. \tag{2.89}$$

In other words, thermal expectation values are generally time-dependent in LSC-IVR.

The Wigner phase space and the truncation of the quantum Liouvillian in LSC-IVR provide a theory for how quantum statistics and classical dynamics can be combined in approximate quantum TCFs. This theory has led to many practical methods that rely on some approximation to the Wigner transform involving $\hat{A}$ and the Boltzmann operator. As stated earlier, for $\hat{B} = B(\hat{q})$ the Wigner transform of $\hat{B}$ is trivial to evaluate and the LSC-IVR Kubo TCF adopts the following form,

$$C_{AB}(t) = \frac{1}{2\pi\hbar} \int \mathrm{d}q \int \mathrm{d}p \, \left[\hat{A}_K(\beta)\right](q,p)\, B(q_t). \tag{2.90}$$

The only remaining difficulty is the evaluation of $\left[\hat{A}_K(\beta)\right](q,p)$, for which a variety of computational schemes have been developed.[88,89,90,91,92] These methods have been applied to many condensed-phase systems to calculate dynamical properties including diffusion constants, the dynamic structure factor and infrared absorption spectra.[93,94,91,95]

Of course, the non-conservation of the quantum Boltzmann distribution (2.89) has important ramifications for quantities like the diffusion constant that are dependent on the long-time behaviour of the TCF. Habershon and Manolopoulos found that the LSC-IVR diffusion constant for a model of liquid water gave a value in error with other methods by a factor of three at room temperature.[37] This error is the result of the degradation of the velocity autocorrelation function at long time, owing to the leakage of intramolecular zero-point energy into the intermolecular modes of the liquid.

While this shortcoming in the LSC-IVR theory gives rise to unphysical predictions, the LSC-IVR TCF (for any partitioning of the Boltzmann operator about $\hat{A}$) is exact in the important harmonic limit. Without approximation, the quantum Liouvillian (2.76) in the harmonic limit is the classical (LSC-IVR) Liouvillian. This exactness in the harmonic limit is in contrast to the CMD and RPMD methods, both of which are inexact for non-linear $\hat{A}$ and $\hat{B}$, even for a harmonic system.

An interesting recent development for LSC-IVR has been presented by Liu and Miller to address the non-conservation of the quantum Boltzmann distribu-

tion.[96,97,98] Their approach is to propagate the phase space points (q, p) not according to the classical Liouvillian, but rather along the level sets of the Wigner function $\left[e^{-\beta\hat{H}}\right](q, p)$. The effective force in this dynamics is given by the ratio of partial derivatives of the Wigner function, and generally depends on both the position and momentum. We direct the reader to a recent review by Liu[35] which describes this and other developments in LSC-IVR.

Note that the derivation of LSC-IVR presented here is but one of many derivations. The LSC-IVR TCF is perhaps most naturally derived from the Van-Vleck SC-IVR approximation to the real-time propagator.[99] Linearisation of the difference in forwards and backwards paths in the SC-IVR TCF gives LSC-IVR as first described by Miller *et al.*[100] We have focused on the quantum Liouvillian derivation of LSC-IVR since this route is traced in the Matsubara dynamics derivation in the following chapter. We direct the reader to a comprehensive review of SC-IVR (including LSC-IVR) by Miller.[28] We also direct the reader to Appendix A.2 for another perspective on the LSC-IVR approximation.

Chapter 3

Matsubara Dynamics

3.1 Introduction

In the previous chapter we presented CMD and RPMD, two practical methods for calculating approximate quantum Kubo TCFs. We also presented LSC-IVR, a theory for combining quantum statistics and classical dynamics in approximate quantum TCFs. As stressed before, the classical dynamics in LSC-IVR does not conserve the quantum Boltzmann distribution which renders the theory inadequate for describing any method that does, e.g. CMD and RPMD. Before our development of Matsubara dynamics in Ref. 43 and Ref. 44, the relation between CMD, RPMD and the quantum Kubo TCF for $t > 0$ was unknown, since a classical approximation to the quantum Liouvillian that conserves the quantum Boltzmann distribution was not forthcoming. As a result, these methods were generally considered to be *ad hoc* approximations to the quantum Kubo TCF.

In this chapter we develop Matsubara dynamics, a theory for combining quantum statistics and classical dynamics that does conserve the quantum Boltzmann distribution. The starting point is a rewriting of the quantum Kubo TCF as a discretised imaginary-time path integral. We consider the behaviour of the TCF if the imaginary-time paths remain smooth functions of imaginary time for all $t \geq 0$. We find that in this limit the quantum Liouvillian reduces to the classical Liouvillian associated with a set of 'Matsubara modes', the Fourier coefficients of the smooth imaginary-time paths. The quantum Boltzmann distribution adopts the classical Boltzmann distribution of the Matsubara modes with a complex phase factor that couples positions and momenta. The resulting classical (Matsubara) dynamics conserves the quantum Boltzmann distribution.

The Matsubara dynamics TCF suffers from the sign problem and is thus prohibitively difficult to calculate for all but simple one-dimensional systems. However,

we are able to use its content as a rigorous theory for combining quantum statistics and classical dynamics to derive the CMD and RPMD methods as approximations to it. This gives a stronger theoretical justification for these methods and helps to explain their successes and shortcomings too.

3.2 Derivation

3.2.1 The quantum Kubo time-correlation function

The generalised quantum Kubo TCF for two operators $\hat{A} = A(\hat{q})$ and $\hat{B} = B(\hat{q})$ is

$$\begin{aligned} C_{AB}^{[N]}(t) = &\int \mathrm{d}\mathbf{q} \int \mathrm{d}\boldsymbol{\Delta} \int \mathrm{d}\mathbf{z}\ A(\mathbf{q})B(\mathbf{z}) \\ &\times \prod_{l=1}^{N} \langle q_{l-1} - \Delta_{l-1}/2|\, e^{-\beta_N \hat{H}}\, |q_l + \Delta_l/2\rangle \\ &\times \langle q_l + \Delta_l/2|\, e^{i\hat{H}t/\hbar}\, |z_l\rangle \, \langle z_l|\, e^{-i\hat{H}t/\hbar}\, |q_l - \Delta_l/2\rangle\,, \end{aligned} \tag{3.1}$$

where $\beta_N = \beta/N$, the indices are cyclic (so $q_0 = q_N$ etc.), $\int \mathrm{d}\mathbf{q}$ is shorthand for $\prod_{k=1}^{N} \int_{-\infty}^{\infty} \mathrm{d}q_k$ and likewise for the variables $\boldsymbol{\Delta}$ and $\mathbf{z}$. The function $A(\mathbf{q})$ is defined by

$$A(\mathbf{q}) = \frac{1}{N} \sum_{l=1}^{N} A(q_l), \tag{3.2}$$

with $B(\mathbf{z})$ defined equivalently. We assume the operators have this form, but the following derivation also holds for operators that are dependent on $\hat{p}$ only as well.[43] Likewise, we present a derivation for the one-dimensional case for the sake of clarity but the multidimensional generalisation is straightforward. It is straightforward to show that[77] (see Appendix B.1)

$$C_{AB}(t) = \lim_{N\to\infty} C_{AB}^{[N]}(t), \tag{3.3}$$

where $C_{AB}(t)$ is the conventional form of the quantum Kubo TCF,

$$C_{AB}(t) = \frac{1}{\beta} \int_0^{\beta} \mathrm{d}\lambda\ \mathrm{Tr}\left[e^{-(\beta-\lambda)\hat{H}} \hat{A} e^{-\lambda\hat{H}} \hat{B}(t)\right]. \tag{3.4}$$

In other words, the generalised quantum Kubo TCF is, in the $N \to \infty$ limit, just an alternative way of writing the quantum Kubo TCF. A schematic representation of the generalised quantum Kubo TCF is shown in Figure 3.1 for $N = 5$. Note that

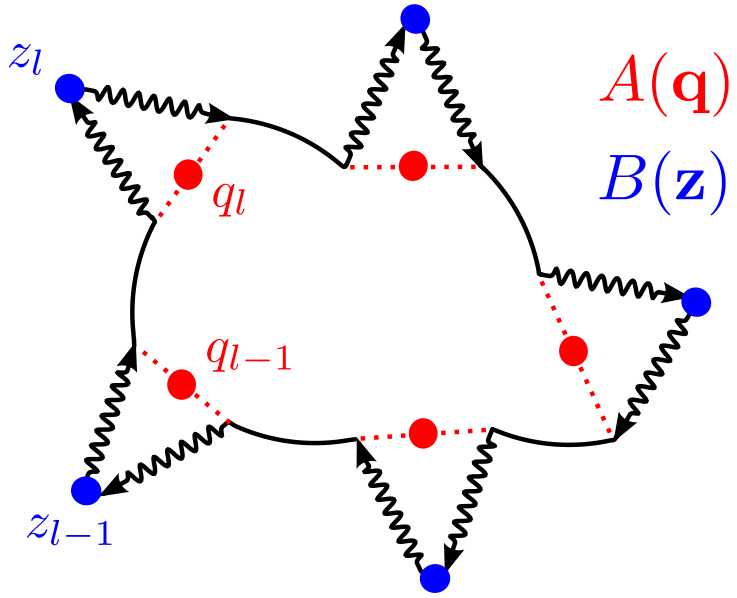

Figure 3.1: The generalised quantum Kubo TCF for $N = 5$. The wavy arrows represent real-time propagation and the curved lines represent imaginary-time propagation. The circles show the points where $A(\mathbf{q})$ and $B(\mathbf{z})$ are evaluated.

the generalised quantum Kubo TCF is not new, having been used to derive QTST by Hele and Althorpe[77,78,79] and in a slightly different form by Shi and Geva.[101]

3.2.2 The Wigner phase space representation

Following the procedure presented in Section 2.10 to rewrite the standard quantum TCF in the Wigner phase space representation, we insert the following identity for each $l = 1, 2, \ldots, N$,

$$\delta(\Delta_l + \Delta_l') = \frac{1}{2\pi\hbar} \int_{-\infty}^{\infty} \mathrm{d}p_l \; e^{ip_l(\Delta_l + \Delta_l')/\hbar}, \tag{3.5}$$

into the generalised quantum Kubo TCF (3.1). This gives

$$C_{AB}^{[N]}(t) = \frac{1}{(2\pi\hbar)^N} \int \mathrm{d}\mathbf{q} \int \mathrm{d}\mathbf{p} \left[e^{-\beta\hat{H}}\hat{A}\right]_{\overline{N}}(\mathbf{q},\mathbf{p}) \left[\hat{B}(t)\right]_N(\mathbf{q},\mathbf{p}), \tag{3.6}$$

where we have defined two generalised Wigner transforms,

$$\begin{aligned} &\left[e^{-\beta\hat{H}}\hat{A}\right]_{\overline{N}}(\mathbf{q},\mathbf{p}) \\ &= \int \mathrm{d}\boldsymbol{\Delta} \; A(\mathbf{q}) \prod_{l=1}^{N} \langle q_{l-1} - \Delta_{l-1}/2 | \, e^{-\beta_N \hat{H}} \, | q_l + \Delta_l/2 \rangle \;\; e^{ip_l\Delta_l/\hbar}, \end{aligned} \tag{3.7}$$

and

$$\left[\hat{B}(t)\right]_N(\mathbf{q},\mathbf{p}) = \int \mathrm{d}\mathbf{\Delta} \int \mathrm{d}\mathbf{z}\; B(\mathbf{z}) \prod_{l=1}^{N} \langle q_l - \Delta_l/2|\, e^{i\hat{H}t/\hbar}\, |z_l\rangle \langle z_l|\, e^{-i\hat{H}t/\hbar}\, |q_l + \Delta_l/2\rangle\; e^{ip_l\Delta_l/\hbar}. \quad (3.8)$$

Note that $[\cdot]_N$ and $[\cdot]_{\overline{N}}$ have different forms. $[\cdot]_N$ is a sum of products of one-dimensional Wigner transforms (see (2.71)), whereas $[\cdot]_{\overline{N}}$ is more complicated, with each product coupling variables in l and $l-1$. Note also that since $\left[\hat{B}(t)\right]_N(\mathbf{q},\mathbf{p})$ is simply a sum of one-dimensional Wigner transforms, it follows immediately from (2.72) that

$$\left[\hat{B}(0)\right]_N(\mathbf{q},\mathbf{p}) = B(\mathbf{q}), \quad (3.9)$$

for $\hat{B} = B(\hat{q})$, as we have assumed. (For $\hat{B} = B(\hat{p})$ we have $\left[\hat{B}(0)\right]_N(\mathbf{q},\mathbf{p}) = B(\mathbf{p})$ instead.) The TCF in (3.6) is an exact rewriting of the generalised quantum Kubo TCF in the Wigner phase space. The advantage of this representation is that it allows us to study the time-dependence of the TCF in terms of the quantum Liouvillian, as detailed in the following section.

3.2.3 The quantum Liouvillian

The k^{th} derivative of (3.6) with respect to time is

$$\frac{\mathrm{d}^k C_{AB}^{[N]}(t)}{\mathrm{d}t^k} = \frac{1}{(2\pi\hbar)^N} \int \mathrm{d}\mathbf{q} \int \mathrm{d}\mathbf{p} \left[e^{-\beta\hat{H}}\hat{A}\right]_{\overline{N}}(\mathbf{q},\mathbf{p}) \hat{L}_N^k \left[\hat{B}(t)\right]_N(\mathbf{q},\mathbf{p}), \quad (3.10)$$

where the quantum Liouvillian is given by

$$\hat{L}_N = \sum_{l=1}^{N} \frac{p_l}{m}\frac{\partial}{\partial q_l} - V(q_l)\frac{2}{\hbar}\sin\left(\frac{\hbar}{2}\frac{\overleftarrow{\partial}}{\partial q_l}\frac{\overrightarrow{\partial}}{\partial p_l}\right), \quad (3.11)$$

m is the physical mass, and the arrows above each partial derivative describe the direction in which the derivatives are to be taken. This can be written more compactly in terms of $U_N(\mathbf{q}) = \sum_{l=1}^{N} V(q_l)$ as

$$\hat{L}_N = \frac{1}{m}\mathbf{p}\cdot\nabla_q - U_N(\mathbf{q})\frac{2}{\hbar}\sin\left(\frac{\hbar}{2}\overleftarrow{\nabla}_q \cdot \overrightarrow{\nabla}_p\right), \quad (3.12)$$

where $\nabla_q^T = \left(\frac{\partial}{\partial q_1}, \frac{\partial}{\partial q_2}, \cdots, \frac{\partial}{\partial q_N}\right)$ etc. Formally we can write the Wigner phase space

representation of the TCF (3.6) as an infinite Taylor series in t,

$$C_{AB}^{[N]}(t) = \sum_{k=0}^{\infty} \left.\frac{\mathrm{d}^k C_{AB}^{[N]}(t)}{\mathrm{d}t^k}\right|_{t=0} \frac{t^k}{k!} \tag{3.13}$$

$$= \frac{1}{(2\pi\hbar)^N} \int \mathrm{d}\mathbf{q} \int \mathrm{d}\mathbf{p} \left[e^{-\beta\hat{H}}\hat{A}\right]_{\overline{N}}(\mathbf{q},\mathbf{p})\, e^{\hat{L}_N t}\, B(\mathbf{q}). \tag{3.14}$$

This is a formal rewriting of (3.6) since, as discussed in the derivation of LSC-IVR, the quantum Liouvillian contains derivatives higher than first order.

We shall not do so in the following derivation, but note that if we truncate the quantum Liouvillian to zeroth order in its expansion in powers of $\hbar^2$,

$$\hat{L}_N \approx \sum_{l=1}^{N} \frac{p_l}{m}\frac{\partial}{\partial q_l} - V'(q_l)\frac{\partial}{\partial p_l} \tag{3.15}$$

$$= \mathcal{L}_0, \tag{3.16}$$

then we recover the classical Liouvillian for N independent particles. The TCF reduces to

$$C_{AB}^{[N]}(t) \approx \frac{1}{(2\pi\hbar)^N} \int \mathrm{d}\mathbf{q} \int \mathrm{d}\mathbf{p} \left[e^{-\beta\hat{H}}\hat{A}\right]_{\overline{N}}(\mathbf{q},\mathbf{p})\, e^{\mathcal{L}_0 t}\, B(\mathbf{q}) \tag{3.17}$$

$$= \frac{1}{(2\pi\hbar)^N} \int \mathrm{d}\mathbf{q} \int \mathrm{d}\mathbf{p} \left[e^{-\beta\hat{H}}\hat{A}\right]_{\overline{N}}(\mathbf{q},\mathbf{p})\, B(\mathbf{q}_t), \tag{3.18}$$

which is equivalent to the LSC-IVR Kubo TCF in the $N \to \infty$ limit. Note that the propagator $e^{\mathcal{L}_0 t}$ has been subsumed by $B(\mathbf{q})$ since the Liouvillian now involves only first derivatives. Note also that in general,

$$\frac{1}{(2\pi\hbar)^N} \int \mathrm{d}\mathbf{q} \int \mathrm{d}\mathbf{p} \left[e^{-\beta\hat{H}}\hat{A}\right]_{\overline{N}}(\mathbf{q},\mathbf{p})\, B(\mathbf{q}_t)$$

$$= \frac{1}{(2\pi\hbar)^N} \int \mathrm{d}\mathbf{q} \int \mathrm{d}\mathbf{p}\; B(\mathbf{q}) \left[e^{-\beta\hat{H}}\hat{A}\right]_{\overline{N}}(\mathbf{q}_{-t},\mathbf{p}_{-t}) \tag{3.19}$$

$$\neq \frac{1}{(2\pi\hbar)^N} \int \mathrm{d}\mathbf{q} \int \mathrm{d}\mathbf{p} \left[e^{-\beta\hat{H}}\hat{B}\right]_{\overline{N}}(\mathbf{q},\mathbf{p})\, A(\mathbf{q}_{-t}), \tag{3.20}$$

which shows that LSC-IVR does not satisfy the detailed balance relation, as demonstrated previously (see Section 2.10).

3.2.4 Normal mode coordinates and Matsubara modes

In the following development of the Matsubara dynamics derivation, we will find it convenient to use the normal modes of a free ring polymer composed of N beads,

defined by the following matrix of orthonormal vectors,

$$T_{lk} = \begin{cases} \sqrt{\frac{1}{N}} & k = 0 \\ \sqrt{\frac{2}{N}} \sin(2\pi lk/N) & 0 < k \leq \overline{N} \\ \sqrt{\frac{2}{N}} \cos(2\pi lk/N) & -\overline{N} \leq k < 0, \end{cases} \tag{3.21}$$

where $\overline{N} = (N-1)/2$ and N is odd. As previously noted, this transformation matrix corresponds to the N-dimensional real discrete Fourier transform.[84] The orthonormal vectors are the eigenvectors of the free ring-polymer mass-weighted Hessian,

$$\overline{H}_{lk} = \frac{2\delta_{lk} - \delta_{lk+1} - \delta_{lk-1}}{(\beta_N \hbar)^2}, \tag{3.22}$$

and the square roots of the eigenvalues are $\omega_k = 2\sin(k\pi/N)/\beta_N\hbar$. In these coordinates the quantum Liouvillian is

$$\hat{L}_N = \frac{1}{m}\mathbf{P}\cdot\nabla_Q - U_N(\mathbf{Q})\frac{2}{\hbar}\sin\left(\frac{\hbar}{2}\overleftarrow{\nabla}_Q \cdot \overrightarrow{\nabla}_P\right). \tag{3.23}$$

The Wigner phase space representation of the TCF is

$$C_{AB}^{[N]}(t) = \frac{1}{(2\pi\hbar)^N}\int \mathrm{d}\mathbf{Q}\int \mathrm{d}\mathbf{P}\left[e^{-\beta\hat{H}}\hat{A}\right]_{\overline{N}}(\mathbf{Q},\mathbf{P})\, e^{\hat{L}_N t}\, B(\mathbf{Q}), \tag{3.24}$$

where by $B(\mathbf{Q})$ we mean $B(T\mathbf{Q})$ etc. and we have recognised the Jacobian of this transformation as unity, since the matrix of eigenvectors (3.21) is an orthogonal matrix. This is, of course, an exact rewriting of the TCF in (3.14).

In the following sections, we will refer to the transformation corresponding to the matrix of orthonormal vectors (3.21) as the 'normal mode transformation'. These orthonormal vectors are only the normal modes of a ring polymer in the harmonic limit (with the free ring polymer as a special case). For any anharmonicity, they no longer constitute the normal modes of the ring polymer, but we will nevertheless refer to them as the 'normal modes'.

Consider the M lowest-frequency normal modes in the limit $N \to \infty$, with $M \ll N$. The frequencies tend to the values

$$\lim_{N\to\infty}\omega_k = \frac{2\pi k}{\beta\hbar}, \tag{3.25}$$

which are the Matsubara frequencies.[102] In studying the behaviour of the lowest M

normal mode positions and momenta in the same limit, it is necessary to scale them as $Q_k/\sqrt{N} \to Q_k$. Having done so, we find for the $k > 0$ normal modes,

$$Q_k = \lim_{N\to\infty} \frac{1}{\sqrt{N}} \sum_{l=1}^{N} \sqrt{\frac{2}{N}} \sin(2\pi lk/N) q_l \tag{3.26}$$

$$= \frac{\sqrt{2}}{\beta\hbar} \int_0^{\beta\hbar} \mathrm{d}\tau \ \sin(\omega_k \tau) q(\tau), \tag{3.27}$$

where we have identified $\Delta\tau = \beta\hbar/N$, $\tau_l = l\Delta\tau$ and taken the set of coordinates $\{q_l\}$ to a function of imaginary time $q(\tau)$ which is periodic over $\beta\hbar$ (in accordance with the cyclic nature of the coordinates $\{q_l\}$). The replacement of the Riemann sum with its corresponding integral over $0 \leq \tau \leq \beta\hbar$ is valid since for all k satisfying $-(M-1)/2 \leq k \leq (M-1)/2$ we have $\omega_k \Delta\tau \to 0$ in the $N \to \infty$ limit. Similarly, for the other normal modes we find

$$Q_{-k} = \frac{\sqrt{2}}{\beta\hbar} \int_0^{\beta\hbar} \mathrm{d}\tau \ \cos(\omega_k \tau) q(\tau), \tag{3.28}$$

and the zeroth normal mode becomes the centroid of $q(\tau)$,

$$Q_0 = \frac{1}{\beta\hbar} \int_0^{\beta\hbar} \mathrm{d}\tau \ q(\tau). \tag{3.29}$$

Clearly then, in this limit the M lowest-frequency normal modes are the Fourier coefficients of the imaginary-time path $q(\tau)$. This is unsurprising since, as recognised earlier, the transformation matrix (3.21) corresponds to the real discrete Fourier transform. We call these lowest M normal modes the 'Matsubara modes',

$$Q_k = \begin{cases} \frac{\sqrt{2}}{\beta\hbar} \int_0^{\beta\hbar} \mathrm{d}\tau \ \cos(\omega_k \tau) q(\tau) & -\overline{M} \leq k < 0 \\ \frac{\sqrt{2}}{\beta\hbar} \int_0^{\beta\hbar} \mathrm{d}\tau \ \sin(\omega_k \tau) q(\tau) & 0 < k \leq \overline{M} \\ \frac{1}{\beta\hbar} \int_0^{\beta\hbar} \mathrm{d}\tau \ q(\tau) & k = 0, \end{cases} \tag{3.30}$$

where $\overline{M} = (M-1)/2$. Conversely, we may construct the imaginary-time path $q(\tau)$ from the Matsubara modes,

$$q(\tau) = Q_0 + \sqrt{2} \sum_{k=1}^{\overline{M}} \sin(\omega_k \tau) Q_k + \cos(\omega_k \tau) Q_{-k}. \tag{3.31}$$

However, it is clear from this construction that something has been lost in taking this limit, for the Fourier decomposition of the function $q(\tau)$ over the interval $0 \leq \tau \leq \beta\hbar$

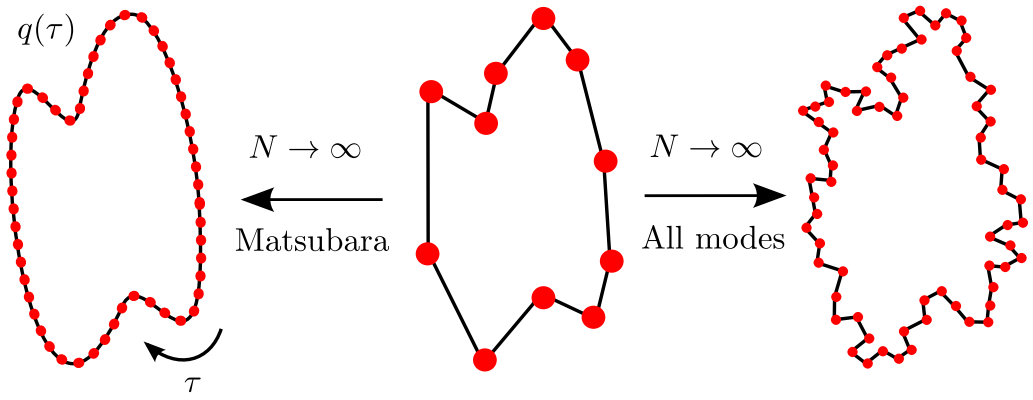

Figure 3.2: Schematic diagram showing that superpositions of Matsubara modes give imaginary-time paths $q(\tau)$ that are smooth and differentiable functions of imaginary time τ. An arbitrary collection of points $\{q_l\}$ in the $N \to \infty$ limit is not necessarily smooth or differentiable.

is necessarily smooth and differentiable, whereas a general function $f(\tau)$ as we have from an arbitrary collection of points, $\{q_l\}$ in the $N \to \infty$ limit, is not guaranteed to be so (see Figure 3.2). The question is, how important are jagged, discontinuous imaginary-time paths (that cannot be constructed by (3.31)) for describing static and dynamical properties?

In the context of static properties, this is a well-studied problem.[103,104,a] It is well known that the Matsubara modes give rise to an alternative ring-polymer expression for the zero-time value of the quantum Kubo TCF $C_{AB}(0)$. We define

$$C_{AB}^{[M]}(0) = \frac{\alpha_M}{2\pi\hbar} \int \mathrm{d}\mathbf{Q} \int \mathrm{d}\mathbf{P}\; e^{-\beta R(\mathbf{Q},\mathbf{P})}\; A(\mathbf{Q})B(\mathbf{Q}), \tag{3.32}$$

where the prefactor is $\alpha_M = \hbar^{1-M}\overline{M}!^2$, the ring-polymer Hamiltonian in terms of the imaginary-time paths $q(\tau)$ and $p(\tau)$ is

$$R(\mathbf{Q},\mathbf{P}) = \frac{1}{\beta\hbar} \int_0^{\beta\hbar} \mathrm{d}\tau\; \frac{p(\tau)^2}{2m} + \frac{1}{2} m q'(\tau)^2 + V(q(\tau)), \tag{3.33}$$

and in the space of M Matsubara modes this becomes

$$R(\mathbf{Q},\mathbf{P}) = \sum_{k=-\overline{M}}^{\overline{M}} \frac{P_k^2}{2m} + \frac{1}{2} m\omega_k^2 Q_k^2 + U_M(\mathbf{Q}). \tag{3.34}$$

The Matsubara potential $U_M(\mathbf{Q})$ in the same space is

[a] The concept of path smoothness also appears in the context of coherent-state path integrals.[105]

$$U_M(\mathbf{Q}) = \frac{1}{\beta\hbar}\int_0^{\beta\hbar} \mathrm{d}\tau\ V\left[Q_0 + \sqrt{2}\sum_{k=1}^{\overline{M}} \sin(\omega_k\tau)Q_k + \cos(\omega_k\tau)Q_{-k}\right], \tag{3.35}$$

with $A(\mathbf{Q})$ and $B(\mathbf{Q})$ defined equivalently. Then

$$C_{AB}(0) = \lim_{N\to\infty} \frac{1}{(2\pi\hbar)^N}\int \mathrm{d}\mathbf{q}\int \mathrm{d}\mathbf{p}\ e^{-\beta R(\mathbf{q},\mathbf{p})}A(\mathbf{q})B(\mathbf{q}) \tag{3.36}$$

$$= \lim_{M\to\infty} C_{AB}^{[M]}(0), \tag{3.37}$$

where $R(\mathbf{q},\mathbf{p})$ is the ring-polymer Hamiltonian in the space of N beads (2.22) and $A(\mathbf{q})$ is as defined before (3.2), with $B(\mathbf{q})$ defined equivalently. In practice a good approximation to the exact result is reached once $\omega_{\overline{M}}$ exceeds the highest frequency in the external potential $V(q)$.

The Matsubara modes expression (3.32) is less often used nowadays to compute static properties, because the convergence with respect to M is typically slower than the convergence of the right-hand side of (3.36) with respect to N.[106] However, the equivalence of the two expressions tells us something interesting: the Boltzmann factor ensures that only smooth distributions of $\{q_l\}$ and $\{p_l\}$ survive in $C_{AB}(t)$ at $t = 0$. The question of what happens for $t > 0$ if the structure of the imaginary-time path is restricted in this way lies at the heart of Matsubara dynamics.

3.2.5 The Matsubara dynamics approximation

As discussed earlier, the LSC-IVR Kubo TCF can be recovered from the Wigner phase space representation of the generalised quantum Kubo TCF by truncating the quantum Liouvillian to zeroth order in $\hbar^2$. In Matsubara dynamics, instead of truncating the quantum Liouvillian at zeroth order in $\hbar^2$, we retain all powers of $\hbar^2$ when taking the $N \to \infty$ limit, but we split the quantum Liouvillian (3.23) into

$$\hat{L}_N = \overline{\mathcal{L}}_M + \hat{L}_{\mathrm{error}}(N, M), \tag{3.38}$$

where the nascent Matsubara Liouvillian is

$$\overline{\mathcal{L}}_M = \sum_{k=-\overline{M}}^{\overline{M}} \frac{P_k}{m}\frac{\partial}{\partial Q_k} - U_N(\mathbf{Q})\frac{2}{\hbar}\sin\left(\sum_{k=-\overline{M}}^{\overline{M}} \frac{\hbar}{2}\frac{\overleftarrow{\partial}}{\partial Q_k}\frac{\overrightarrow{\partial}}{\partial P_k}\right), \tag{3.39}$$

and the error Liouvillian is

$$\hat{L}_{\mathrm{error}}(N, M) = \hat{L}_N - \overline{\mathcal{L}}_M. \tag{3.40}$$

In preparation for taking the 'Matsubara limit' ($N \to \infty$ and $M \ll N$) we scale the position and momentum normal modes, $Q_k/\sqrt{N} \to Q_k$ and $P_k/\sqrt{N} \to P_k$, as discussed earlier. We also scale the potential, $U_N(\mathbf{Q})/N \to U_N(\mathbf{Q})$. This gives the following for the nascent Matsubara Liouvillian,

$$\overline{\mathcal{L}}_M = \sum_{k=-\overline{M}}^{\overline{M}} \frac{P_k}{m}\frac{\partial}{\partial Q_k} - U_N(\mathbf{Q})\frac{2N}{\hbar}\sin\left(\sum_{k=-\overline{M}}^{\overline{M}} \frac{\hbar}{2N}\frac{\overleftarrow{\partial}}{\partial Q_k}\frac{\overrightarrow{\partial}}{\partial P_k}\right). \tag{3.41}$$

Now, taking the Taylor expansion of the sine term we find,

$$\frac{2N}{\hbar}\sin\left(\sum_{k=-\overline{M}}^{\overline{M}} \frac{\hbar}{2N}\frac{\overleftarrow{\partial}}{\partial Q_k}\frac{\overrightarrow{\partial}}{\partial P_k}\right) = \sum_{k=-\overline{M}}^{\overline{M}} \frac{\overleftarrow{\partial}}{\partial Q_k}\frac{\overrightarrow{\partial}}{\partial P_k} + \mathcal{O}\left(\frac{M^3\hbar^2}{N^2}\right). \tag{3.42}$$

Therefore, if we now take the Matsubara limit then only the classical part of the Liouvillian survives and we are left with

$$\lim_{N\to\infty} \overline{\mathcal{L}}_M = \sum_{k=-\overline{M}}^{\overline{M}} \frac{P_k}{m}\frac{\partial}{\partial Q_k} - \frac{\partial U_N(\mathbf{Q})}{\partial Q_k}\frac{\partial}{\partial P_k}, \tag{3.43}$$

where,[b]

$$U_N(\mathbf{Q}) = \lim_{N\to\infty} \frac{1}{N}\sum_{l=1}^{N} V\left(\sum_{k=-\overline{N}}^{\overline{N}} T_{lk}\sqrt{N}Q_k\right). \tag{3.44}$$

In the context of LSC-IVR, the reduction of the quantum Liouvillian to the classical one is often justified by appealing to the relative smallness of $\hbar$. However, it is clear from (3.42) that for the Matsubara dynamics approximation, there is no need to appeal to the relative smallness of $\hbar$ since the effective reduced Planck's constant in the space of M Matsubara modes is not $\hbar$ but rather $\hbar\sqrt{M^3/N^2}$, which can be made as small as desired by increasing N. We direct the reader to Appendix B.3 for a discussion of the error Liouvillian.

3.2.6 The Matsubara dynamics time-correlation function

The approximation described in the previous section for the quantum Liouvillian is the only approximation in Matsubara dynamics. Having made this approximation, it is straightforward to evaluate the Wigner phase space representation of the

[b]Note that this is not the same as $U_M(\mathbf{Q})$ (3.35) because the non-Matsubara position modes still feature in the potential.

generalised quantum Kubo TCF in the Matsubara limit. The preliminary result is

$$C_{AB}^{[M]}(t) = \lim_{N\to\infty} \frac{1}{(2\pi\hbar)^N} \int \mathrm{d}\mathbf{Q} \int \mathrm{d}\mathbf{P} \left[e^{-\beta\hat{H}}\hat{A}\right]_{\overline{N}} (\mathbf{Q},\mathbf{P})\, e^{\overline{\mathcal{L}}_M t}\, B(\mathbf{Q}). \tag{3.45}$$

where the superscript $[M]$ reminds us that this expression is dependent on the number of Matsubara modes. In Appendix B.2 we demonstrate that this expression reduces to

$$C_{AB}^{[M]}(t) = \frac{\alpha_M}{2\pi\hbar} \int \mathrm{d}\mathbf{Q} \int \mathrm{d}\mathbf{P}\; e^{-\beta H(\mathbf{Q},\mathbf{P})} e^{i\beta\theta(\mathbf{Q},\mathbf{P})}\, A(\mathbf{Q})\, e^{\mathcal{L}_M t}\, B(\mathbf{Q}), \tag{3.46}$$

where the α_M prefactor is

$$\alpha_M = \left(\int \mathrm{d}\mathbf{Q}' \int \mathrm{d}\mathbf{P}'\; e^{-\beta \sum_{k\neq 0} \frac{P_k^2}{2m} + \frac{1}{2} m\omega_k^2 Q_k^2} \right)^{-1} \tag{3.47}$$

$$= \hbar^{1-M} \overline{M}!^2, \tag{3.48}$$

the primes denote all Matsubara modes besides the centroid, the Matsubara Hamiltonian $H(\mathbf{Q},\mathbf{P})$ is

$$H(\mathbf{Q},\mathbf{P}) = \sum_{k=-\overline{M}}^{\overline{M}} \frac{P_k^2}{m} + U_M(\mathbf{Q}), \tag{3.49}$$

and the Matsubara potential $U_M(\mathbf{Q})$ is

$$U_M(\mathbf{Q}) = \lim_{N\to\infty} \frac{1}{N} \sum_{l=1}^{N} V\left(\sum_{k=-\overline{M}}^{\overline{M}} T_{lk} \sqrt{N} Q_k \right), \tag{3.50}$$

with $A(\mathbf{Q})$ and $B(\mathbf{Q})$ defined equivalently. The Matsubara phase couples pairs of non-centroid positions and momenta,

$$\theta(\mathbf{Q},\mathbf{P}) = \sum_{k=-\overline{M}}^{\overline{M}} \omega_k Q_{-k} P_k, \tag{3.51}$$

and the Matsubara Liouvillian $\mathcal{L}_M$ is

$$\mathcal{L}_M = \sum_{k=-\overline{M}}^{\overline{M}} \frac{P_k}{m} \frac{\partial}{\partial Q_k} - \frac{\partial U_M(\mathbf{Q})}{\partial Q_k} \frac{\partial}{\partial P_k}, \tag{3.52}$$

which is the classical Liouvillian that corresponds to the Hamiltonian (3.49).

3.2.7 The continuum picture

In Section 3.2.4, we constructed the imaginary-time path $q(\tau)$ from the definition of the Matsubara modes as Fourier coefficients (3.31). This continuous representation of the imaginary-time path is not required to derive the Matsubara dynamics TCF. However, having derived the TCF we may interpret various quantities in terms of continuous imaginary-time paths $q(\tau)$. This 'continuum picture' will prove helpful in the following section concerning the symmetry properties of the Matsubara dynamics TCF. We restate the imaginary-time position and momentum paths as superpositions of the Matsubara modes,

$$q(\tau) = Q_0 + \sqrt{2}\sum_{k=1}^{\overline{M}} \sin(\omega_k\tau)Q_k + \cos(\omega_k\tau)Q_{-k} \tag{3.53}$$

$$p(\tau) = P_0 + \sqrt{2}\sum_{k=1}^{\overline{M}} \sin(\omega_k\tau)P_k + \cos(\omega_k\tau)P_{-k}. \tag{3.54}$$

In this continuum picture, it is straightforward to show that the Matsubara potential, kinetic energy, $A(\mathbf{Q})$, $B(\mathbf{Q})$ and the Matsubara phase are all integrals over imaginary time,

$$U_M(\mathbf{Q}) = \frac{1}{\beta\hbar}\int_0^{\beta\hbar} \mathrm{d}\tau\ V(q(\tau)) \tag{3.55}$$

$$\sum_{k=-\overline{M}}^{\overline{M}} \frac{P_k^2}{2m} = \frac{1}{\beta\hbar}\int_0^{\beta\hbar} \mathrm{d}\tau\ \frac{p(\tau)^2}{2m} \tag{3.56}$$

$$A(\mathbf{Q}) = \frac{1}{\beta\hbar}\int_0^{\beta\hbar} \mathrm{d}\tau\ A(q(\tau)) \tag{3.57}$$

$$B(\mathbf{Q}) = \frac{1}{\beta\hbar}\int_0^{\beta\hbar} \mathrm{d}\tau\ B(q(\tau)) \tag{3.58}$$

$$\theta(\mathbf{Q},\mathbf{P}) = \frac{1}{\beta\hbar}\int_0^{\beta\hbar} \mathrm{d}\tau\ p(\tau)q'(\tau). \tag{3.59}$$

Each of these is easily verified by inserting the Fourier decompositions of $q(\tau)$ (3.53) and $p(\tau)$ (3.54) into the relevant expressions in the previous section.

3.3 Symmetries

The quantum Kubo TCF for two operators $\hat{A} = A(\hat{q})$ and $\hat{B} = B(\hat{q})$ satisfies the following three symmetry relations,

1. Detailed balance: $C_{AB}(t) = C_{BA}(-t)$
2. Reality: $C_{AB}(t) = C^*_{AB}(t)$
3. Real-time reversal symmetry: $C_{AB}(-t) = C^*_{AB}(t)$.[c]

Detailed balance follows from the invariance of a trace under cyclic permutations. Reality follows from invariance of the TCF to a change in the direction of imaginary time (and is thus an example of imaginary-time reversal symmetry). The real-time reversal symmetry follows from the reality of $A(\hat{q})$ and $B(\hat{q})$ in the basis of eigenstates of a bound system. The last symmetry also holds for the standard quantum TCF but the first two do not;[55] rather than 1., the standard quantum TCF satisfies what is often called the spectroscopists' detailed balance relation instead,

$$I(-\omega) = e^{-\beta\hbar\omega}\, I(\omega), \tag{3.60}$$

where $I(\omega)$ is the Fourier transform of the standard quantum TCF. Matsubara dynamics shares all three of the listed symmetry properties with the quantum Kubo TCF, as we now demonstrate.

3.3.1 Time translation symmetries

Conservation of the Hamiltonian (real-time translation symmetry)

As for any classical dynamics, the Matsubara Hamiltonian is conserved because the Liouvillian is constructed from partial derivatives of the same Hamiltonian,

$$\mathcal{L}_M H(\mathbf{Q},\mathbf{P}) = \sum_{k=-\overline{M}}^{\overline{M}} \frac{\partial H(\mathbf{Q},\mathbf{P})}{\partial P_k}\frac{\partial H(\mathbf{Q},\mathbf{P})}{\partial Q_k} - \frac{\partial H(\mathbf{Q},\mathbf{P})}{\partial Q_k}\frac{\partial H(\mathbf{Q},\mathbf{P})}{\partial P_k} \tag{3.61}$$

$$= 0. \tag{3.62}$$

Conservation of the phase (imaginary-time translation symmetry)

Consider the effect that translation in imaginary time ($q(\tau) \to q(\tau+\tau')$) has on the Matsubara modes,

$$Q_k(\tau') = \begin{cases} \frac{\sqrt{2}}{\beta\hbar}\int_0^{\beta\hbar} \mathrm{d}\tau\ \cos(\omega_k\tau) q(\tau+\tau') & -\overline{M} \le k < 0 \\ \frac{\sqrt{2}}{\beta\hbar}\int_0^{\beta\hbar} \mathrm{d}\tau\ \sin(\omega_k\tau) q(\tau+\tau') & 0 < k \le \overline{M} \\ \frac{1}{\beta\hbar}\int_0^{\beta\hbar} \mathrm{d}\tau\ q(\tau+\tau') & k = 0. \end{cases} \tag{3.63}$$

[c] If the product $\hat{A}\hat{B}$ is odd with respect to $\hat{p} \to -\hat{p}$ then the following relation holds instead, $C_{AB}(-t) = -C^*_{AB}(t)$.

Bearing in mind that the imaginary-time path is periodic with period $\beta\hbar$, the centroid is unaffected by this translation. The fluctuation (non-centroid) modes are affected, however. The effect is a two-dimensional rotation of each pair of fluctuation modes Q_k and Q_{-k},

$$\begin{bmatrix} Q_k(\tau+\tau') \\ Q_{-k}(\tau+\tau') \end{bmatrix} = \begin{bmatrix} \cos(\omega_k\tau') & -\sin(\omega_k\tau') \\ \sin(\omega_k\tau') & \cos(\omega_k\tau') \end{bmatrix} \begin{bmatrix} Q_k(\tau) \\ Q_{-k}(\tau) \end{bmatrix}, \tag{3.64}$$

which is easily verified through integration by parts in (3.63). Given this equivalence between imaginary-time translation and two-dimensional rotation, it is natural for us to define for each pair of Matsubara modes, Q_k and Q_{-k}, a pair of polar coordinates ($k > 0$),

$$r_k = \sqrt{Q_k^2 + Q_{-k}^2} \tag{3.65}$$

$$\phi_k = \frac{1}{\omega_k} \tan^{-1}\left(\frac{Q_{-k}}{Q_k}\right), \tag{3.66}$$

where the angles ϕ_k have dimensions of time. Substitution of these variables into the Matsubara potential (3.55) gives

$$U_M(Q_0, \boldsymbol{r}, \boldsymbol{\phi}) = \frac{1}{\beta\hbar}\int_0^{\beta\hbar} \mathrm{d}\tau\ V\left[Q_0 + \sqrt{2}\sum_{k=1}^{\overline{M}} r_k \sin(\omega_k(\phi_k+\tau))\right]. \tag{3.67}$$

It is straightforward to show that the potential is invariant with respect to $\phi_k + \Delta\phi \to \phi_k$, $k = 1, 2, \ldots, \overline{M}$, due to the equivalence of this operation to translation of $q(\tau)$ in imaginary time,

$$\begin{aligned} U_M(Q_0, \boldsymbol{r}, \boldsymbol{\phi}) &= \frac{1}{\beta\hbar}\int_{-\Delta\phi}^{\beta\hbar-\Delta\phi} \mathrm{d}\tau\ V\left[Q_0 + \sqrt{2}\sum_{k=1}^{\overline{M}} r_k \sin(\omega_k(\phi_k+\Delta\phi+\tau))\right] \\ &= \frac{1}{\beta\hbar}\int_0^{\beta\hbar} \mathrm{d}\tau\ V\left[Q_0 + \sqrt{2}\sum_{k=1}^{\overline{M}} r_k \sin(\omega_k(\phi_k+\Delta\phi+\tau))\right] \\ &= U_M(Q_0, \boldsymbol{r}, \boldsymbol{\phi}+\Delta\phi). \end{aligned} \tag{3.68}$$

Defining $\boldsymbol{\Phi} = T\boldsymbol{\phi}$, where T is some orthogonal transformation matrix with $\Phi_0 = \sum_{k=1}^{\overline{M}} \phi_k$, we have

$$\frac{\partial U_M(Q_0, \boldsymbol{r}, \boldsymbol{\Phi})}{\partial \Phi_0} = 0. \tag{3.69}$$

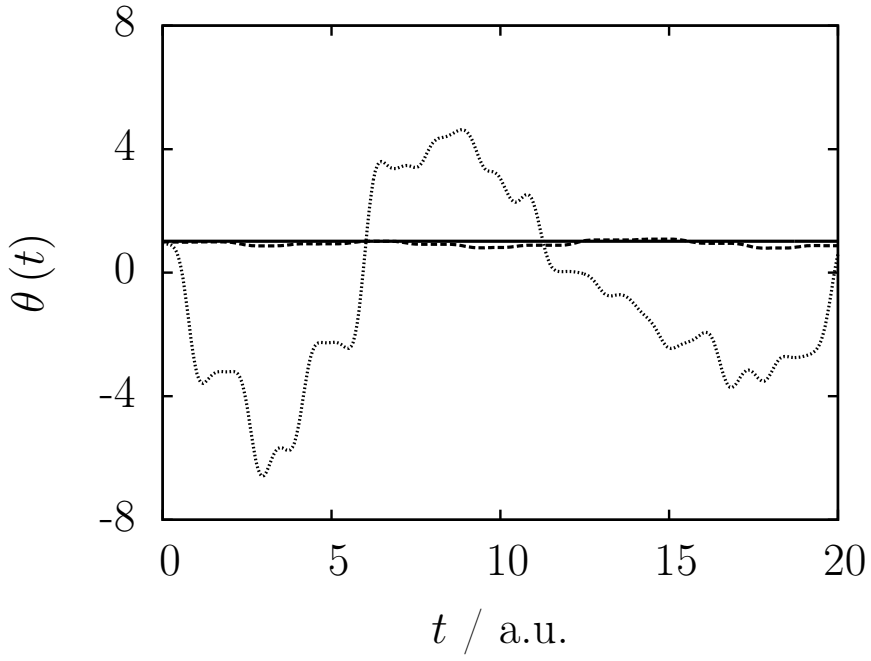

Figure 3.3: Conservation of the Matsubara phase in a quartic potential ($V(q) = q^4/4$ and $m = 1$ atomic unit) with $M = 5$, $N = 5$ (dots), 9 (dashes) and ∞ (solid line).

This means that Φ_0 is a cyclic (ignorable) coordinate so its conjugate momentum must be a constant of the motion. It turns out that the conjugate momentum is the Matsubara phase, as we now demonstrate.

The Matsubara Lagrangian in the polar coordinates is

$$L = \frac{1}{2}m\left[\dot{Q}_0^2 + \sum_{k=1}^{\overline{M}} \omega_k^2 \dot{\phi}_k^2 r_k^2 + \dot{r}_k^2\right] + U_M(Q_0, \boldsymbol{r}, \boldsymbol{\Phi}). \tag{3.70}$$

The conjugate momentum to Φ_0 is given by a derivative of this Lagrangian,

$$\frac{\partial L}{\partial \dot{\Phi}_0} = \sum_{k=1}^{\overline{M}} \frac{\partial L}{\partial \dot{\phi}_k} \frac{\partial \dot{\phi}_k}{\partial \dot{\Phi}_0} \tag{3.71}$$

$$= \sum_{k=1}^{\overline{M}} m\omega_k^2 \dot{\phi}_k r_k^2 \tag{3.72}$$

$$= \theta(\mathbf{Q}, \mathbf{P}), \tag{3.73}$$

thus proving that the Matsubara phase is conserved. In Ref. 43, we demonstrated the conservation of the Matsubara phase by appealing to Noether's theorem. A continuum-picture version of this demonstration is presented in Appendix B.5.

Figure 3.3 shows the numerical conservation of the phase. We propagated the normal modes ($\mathbf{Q}$, $\mathbf{P}$) according to the Matsubara Liouvillian (3.52) with the Matsubara potential replaced by

$$U_M(\mathbf{Q}) = \frac{1}{N}\sum_{l=1}^{N} V\left(\sum_{k=-\overline{M}}^{\overline{M}} T_{lk}\sqrt{N}Q_k\right), \tag{3.74}$$

for $M = 5$ and varied N. For $N = M$, the phase is time-dependent. For $N = 9$, the phase varies only very slightly and for $N \to \infty$ the phase is time-independent.

Detailed balance

Starting with the Matsubara dynamics TCF,

$$C_{AB}^{[M]}(t) = \frac{\alpha_M}{2\pi\hbar}\int \mathrm{d}\mathbf{Q}\int \mathrm{d}\mathbf{P}\; e^{-\beta H(\mathbf{Q},\mathbf{P})}e^{i\beta\theta(\mathbf{Q},\mathbf{P})}\, A(\mathbf{Q})\, e^{\mathcal{L}_M t}\, B(\mathbf{Q}), \tag{3.75}$$

if we expand the propagator $e^{\mathcal{L}_M t}$ in powers of t then repeatedly apply integration by parts in all Q_k and P_k we find

$$C_{AB}^{[M]}(t) = \frac{\alpha_M}{2\pi\hbar}\int \mathrm{d}\mathbf{Q}\int \mathrm{d}\mathbf{P}\; B(\mathbf{Q})e^{-\mathcal{L}_M t}e^{-\beta H(\mathbf{Q},\mathbf{P})}e^{i\beta\theta(\mathbf{Q},\mathbf{P})}\, A(\mathbf{Q}). \tag{3.76}$$

We have already shown that the propagator conserves the Matsubara Hamiltonian and Matsubara phase, thus the entire quantum Boltzmann distribution is conserved. The propagator therefore passes through the distribution to give,

$$C_{AB}^{[M]}(t) = \frac{\alpha_M}{2\pi\hbar}\int \mathrm{d}\mathbf{Q}\int \mathrm{d}\mathbf{P}\; e^{-\beta H(\mathbf{Q},\mathbf{P})}e^{i\beta\theta(\mathbf{Q},\mathbf{P})}\, B(\mathbf{Q})\, e^{-\mathcal{L}_M t}\, A(\mathbf{Q}) \tag{3.77}$$

$$= C_{BA}^{[M]}(-t), \tag{3.78}$$

thus proving detailed balance (2.10). As stated in Chapter 2, for the special case of $\hat{A} = \hat{I}$, this detailed balance relation implies that thermal expectation values are time-independent in Matsubara dynamics.

This time-independence of thermal expectation values is tested numerically in Figure 3.4. The graphs concern the quartic potential and the mildly anharmonic potential,[59]

$$V(q) = \frac{1}{4}q^4 \tag{3.79}$$

$$V(q) = \frac{1}{2}q^2 + \frac{1}{10}q^3 + \frac{1}{100}q^4, \tag{3.80}$$

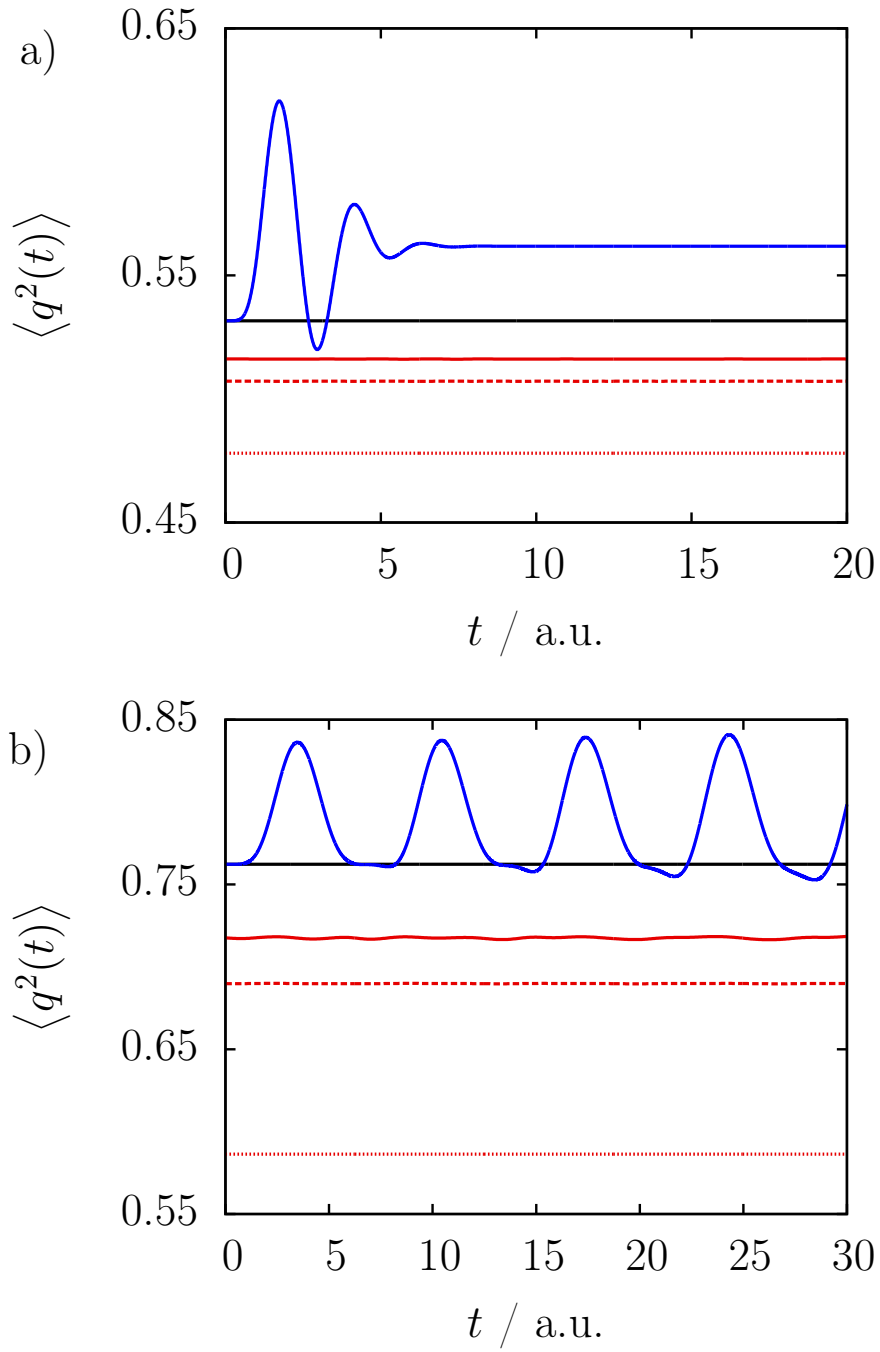

Figure 3.4: Conservation of the quantum Boltzmann distribution for the quartic potential (panel a) and the mildly anharmonic potential (panel b) at $\beta = 2$ atomic units. For each panel, the quantum result is shown in black, the LSC-IVR result in blue and the Matsubara dynamics results in red ($M = 1$ dots, $M = 3$ dashes and $M = 5$ solid).

with $m = 1$ atomic unit. The quantum results were calculated using the Colbert-Miller Discrete Variable Representation (DVR).[20] The LSC-IVR results were calculated using the Colbert-Miller DVR and evaluation of the Wigner transform by rectangular quadrature. The Matsubara dynamics results were calculated using Monte Carlo integration with importance sampling for the Hamiltonian part of the distribution. The exact Matsubara potential was used to avoid the fast Fourier transform (see Appendix B.4).

As shown in Figure 3.4, the LSC-IVR result starts at the correct initial value of $\langle q^2(t)\rangle$ for both potentials then oscillates. For the quartic potential (panel a), the LSC-IVR expectation value settles down to a value for $t > 10$ atomic units which is in error by some twenty percent. On the other hand, the Matsubara dynamics expectation values are time-independent, and gradually approach the correct value as the number of Matsubara modes increases.[d]

3.3.2 Time reversal symmetries

Real-time reversal symmetry

Suppose we change the direction of real time in the Matsubara dynamics TCF,

$$C_{AB}^{[M]}(-t) = \frac{\alpha_M}{2\pi\hbar}\int \mathrm{d}\mathbf{Q}\int \mathrm{d}\mathbf{P}\; e^{-\beta H(\mathbf{Q},\mathbf{P})}e^{i\beta\theta(\mathbf{Q},\mathbf{P})}\,A(\mathbf{Q})\,e^{-\mathcal{L}_M t}\,B(\mathbf{Q}). \tag{3.81}$$

The time reversal is equivalent to the transformation

$$\overline{P}_k = -P_k, \tag{3.82}$$

as is true for any classical dynamics, since the Liouvillian is only linearly dependent on each momentum,

$$-\mathcal{L}_M = \sum_k \frac{\overline{P}_k}{2m}\frac{\partial}{\partial Q_k} - \frac{\partial U_M(\mathbf{Q})}{\partial Q_k}\frac{\partial}{\partial \overline{P}_k}. \tag{3.83}$$

This variable transformation has no effect on the Matsubara Hamiltonian, nor on $A(\mathbf{Q})$ and $B(\mathbf{Q})$. The transformation does, however, have an effect on the Matsubara phase. The sign of the Matsubara phase is changed because of its linear dependence on the fluctuation momenta P_k ($k \neq 0$),

$$\theta(\mathbf{Q},\mathbf{P}) = -\theta(\mathbf{Q},\overline{\mathbf{P}}). \tag{3.84}$$

[d]The slight oscillation of the $M = 5$ Matsubara dynamics result in panel b of Figure 3.4 is within the error bars of the Monte Carlo integration.

Making the change of variables (3.82) in the TCF gives

$$C_{AB}^{[M]}(-t) = \frac{\alpha_M}{2\pi\hbar}\int \mathrm{d}\mathbf{Q}\int \mathrm{d}\mathbf{P}\; e^{-\beta H(\mathbf{Q},\mathbf{P})}e^{i\beta\theta(\mathbf{Q},\mathbf{P})}\,A(Q)\,e^{-\mathcal{L}_M t}\,B(\mathbf{Q}) \tag{3.85}$$

$$= \frac{\alpha_M}{2\pi\hbar}\int \mathrm{d}\mathbf{Q}\int \mathrm{d}\overline{\mathbf{P}}\; e^{-\beta H(\mathbf{Q},\overline{\mathbf{P}})}e^{-i\beta\theta(\mathbf{Q},\overline{\mathbf{P}})}\,A(\mathbf{Q})\,e^{\overline{\mathcal{L}}_M t}\,B(\mathbf{Q}) \tag{3.86}$$

$$= C_{AB}^{[M]*}(t), \tag{3.87}$$

where $\overline{\mathcal{L}}_M$ is the right-hand side of (3.83), and we have used

$$\int_{-\infty}^{\infty}\mathrm{d}P_k = \int_{-\infty}^{\infty}\mathrm{d}\overline{P}_k. \tag{3.88}$$

If we consider momentum-dependent observables $A(\mathbf{Q},\mathbf{P})$ and $B(\mathbf{Q},\mathbf{P})$ then (3.87) will only hold if the product $A(\mathbf{Q},\mathbf{P})B(\mathbf{Q},\mathbf{P})$ is even with respect to the transformation (3.82). If it is odd with respect to the transformation then instead we have

$$C_{AB}^{[M]}(-t) = -\,C_{AB}^{[M]*}(t). \tag{3.89}$$

These real-time reversal symmetries are the same as those satisfied by the quantum Kubo TCF.

Reality (imaginary-time reversal symmetry)

It is straightforward to show that the quantum Kubo TCF is necessarily real by reversing the direction of imaginary time. Consider what happens to the Matsubara position modes when we reverse the direction of imaginary time ($\tau \to \beta\hbar - \tau$),

$$\overline{Q}_k = \begin{cases} \frac{\sqrt{2}}{\beta\hbar}\int_0^{\beta\hbar}\mathrm{d}\tau\;\cos(\omega_k\tau)q(\beta\hbar-\tau) & -\overline{M}\le k<0 \\ \frac{\sqrt{2}}{\beta\hbar}\int_0^{\beta\hbar}\mathrm{d}\tau\;\sin(\omega_k\tau)q(\beta\hbar-\tau) & 0<k\le\overline{M} \\ \frac{1}{\beta\hbar}\int_0^{\beta\hbar}\mathrm{d}\tau\;q(\beta\hbar-\tau) & k=0. \end{cases} \tag{3.90}$$

The centroid is unaffected by this transformation as are all Matsubara modes $k<0$. However, the $k>0$ Matsubara modes change sign,

$$\overline{Q}_k = \begin{cases} Q_k & -\overline{M}\le k\le 0 \\ -Q_k & 0<k\le\overline{M}, \end{cases} \tag{3.91}$$

which is easily verified by integration by parts in (3.90). Of course, the same holds for the momentum modes as well. It is obvious that the Matsubara potential, kinetic

energy, $A(\mathbf{Q})$ and $B(\mathbf{Q})$ are insensitive to this transformation from their definitions in the continuum picture. The Matsubara phase, however, changes sign,

$$\begin{aligned}\theta(\mathbf{Q},\mathbf{P}) &= \frac{1}{\beta\hbar}\int_0^{\beta\hbar} \mathrm{d}\tau\ p(\tau)q'(\tau) && (3.92)\\ &= -\frac{1}{\beta\hbar}\int_0^{\beta\hbar} \mathrm{d}\tau\ p(\beta\hbar-\tau)\frac{\mathrm{d}}{\mathrm{d}\tau}q(\beta\hbar-\tau) && (3.93)\\ &= -\theta(\overline{\mathbf{Q}},\overline{\mathbf{P}}). && (3.94)\end{aligned}$$

Before we make this change of variables in the Matsubara dynamics TCF, note that the transformation is canonical since $\{\overline{Q}_k,\overline{Q}_j\} = \{\overline{P}_k,\overline{P}_j\} = 0$ and $\{\overline{Q}_k,\overline{P}_j\} = \delta_{jk}$, where the braces denote the Poisson bracket, so the Jacobian is unity. Given that the Hamiltonian in the $(\overline{Q}_k, \overline{P}_k)$ coordinates has exactly the same form as in the (Q_k, P_k) coordinates, the Liouvillian is unchanged (every (Q_k, P_k) is simply replaced with $(\overline{Q}_k, \overline{P}_k)$). Bringing everything together, we find the following for the Matsubara dynamics TCF,

$$\begin{aligned}C_{AB}^{[M]}(t) &= \frac{\alpha_M}{2\pi\hbar}\int \mathrm{d}\mathbf{Q}\int \mathrm{d}\mathbf{P}\ e^{-\beta H(\mathbf{Q},\mathbf{P})}e^{i\beta\theta(\mathbf{Q},\mathbf{P})}\,A(\mathbf{Q})\,e^{\mathcal{L}_M t}\,B(\mathbf{Q}) && (3.95)\\ &= \frac{\alpha_M}{2\pi\hbar}\int \mathrm{d}\overline{\mathbf{Q}}\int \mathrm{d}\overline{\mathbf{P}}\ e^{-\beta H(\overline{\mathbf{Q}},\overline{\mathbf{P}})}e^{-i\beta\theta(\overline{\mathbf{Q}},\overline{\mathbf{P}})}\,A(\overline{\mathbf{Q}})\,e^{\overline{\mathcal{L}}_M t}\,B(\overline{\mathbf{Q}}) && (3.96)\\ &= C_{AB}^{[M]*}(t). && (3.97)\end{aligned}$$

In other words, the Matsubara dynamics TCF is a real function of time.

The relation (3.97) in conjunction with the imaginary-time reversal symmetry (3.87) allows us to conclude that, for $A(\mathbf{Q})$ and $B(\mathbf{Q})$ dependent on the Matsubara position modes only, the Matsubara dynamics TCF is an even function of time, for

$$\begin{aligned}C_{AB}^{[M]}(-t) &= C_{AB}^{[M]*}(t) && (3.98)\\ &= C_{AB}^{[M]}(t). && (3.99)\end{aligned}$$

Again, this is true for the quantum Kubo TCF for operators $\hat{A} = A(\hat{q})$ and $\hat{B} = B(\hat{q})$ and also for the classical TCF. For more general observables $A(\mathbf{Q},\mathbf{P})$ and $B(\mathbf{Q},\mathbf{P})$ that depend on the Matsubara momentum modes, the TCF is an odd function of time if the product $A(\mathbf{Q},\mathbf{P})B(\mathbf{Q},\mathbf{P})$ is an odd function of the momenta, since in that case we have

$$\begin{aligned}C_{AB}^{[M]}(-t) &= -C_{AB}^{[M]*}(t) && (3.100)\\ &= -C_{AB}^{[M]}(t). && (3.101)\end{aligned}$$

For example, the linear position autocorrelation function $C_{qq}^{[M]}(t)$ is an even function of time, while the linear position-momentum TCF $C_{qp}^{[M]}(t)$ is an odd function of time. This final result holds for the quantum Kubo and classical TCFs as well.

3.4 Relation to CMD and RPMD

The Matsubara dynamics TCF for two observables $A(\mathbf{Q})$ and $B(\mathbf{Q})$ is

$$C_{AB}^{[M]}(t) = \frac{\alpha_M}{2\pi\hbar} \int \mathrm{d}\mathbf{Q} \int \mathrm{d}\mathbf{P}\; e^{-\beta H(\mathbf{Q},\mathbf{P})} e^{i\beta\theta(\mathbf{Q},\mathbf{P})}\, A(\mathbf{Q})\, e^{\mathcal{L}_M t}\, B(\mathbf{Q}). \tag{3.102}$$

Let us make the coordinate transformation

$$\overline{P}_k = P_k - im\omega_k Q_{-k}, \tag{3.103}$$

which we note has no effect on the centroid momentum, $\overline{P}_0 = P_0$, since the zeroth Matsubara frequency is zero. This transformation gives the following for the TCF,

$$C_{AB}^{[M]}(t) = \frac{\alpha_M}{2\pi\hbar} \int \mathrm{d}\mathbf{Q} \left[\prod_{k=-\overline{M}}^{\overline{M}} \int_{a_k}^{b_k} \mathrm{d}\overline{P}_k \right]\; e^{-\beta R(\mathbf{Q},\overline{\mathbf{P}})}\, A(\mathbf{Q}) e^{\mathcal{L}_M t}\, B(\mathbf{Q}), \tag{3.104}$$

where the integration limits are $a_k = -\infty - im\omega_k Q_{-k}$ and $b_k = \infty - im\omega_k Q_{-k}$. This is simply (3.102) in disguise, but at $t = 0$ we may use a standard contour integration trick to shift each $\overline{P}_k$ onto the real axis to give

$$C_{AB}^{[M]}(0) = \frac{\alpha_M}{2\pi\hbar} \int \mathrm{d}\mathbf{Q} \int \mathrm{d}\overline{\mathbf{P}}\; e^{-\beta R(\mathbf{Q},\overline{\mathbf{P}})}\, A(\mathbf{Q})\, B(\mathbf{Q}). \tag{3.105}$$

The standard contour integration trick is as follows. For the strip $0 \leq \mathrm{Im}\, p \leq \lambda$, if $f(p)$ is analytic everywhere and

$$\lim_{\mathrm{Re}\, p \to \pm\infty} \exp(-ap^2)\, f(p) = 0, \tag{3.106}$$

then

$$\int_{-\infty+i\lambda}^{\infty+i\lambda} \mathrm{d}p\;\, \exp(-ap^2)\, f(p) = \int_{-\infty}^{\infty} \mathrm{d}p\;\, \exp(-ap^2) f(p). \tag{3.107}$$

The proof involves writing the right and left-hand sides of (3.107) as two parts of a closed contour integral of width $2L$ in the $L \to \infty$ limit. Such a contour is shown for the $\overline{P}_k$ coordinate in Figure 3.5. Analyticity ensures that the contour integral

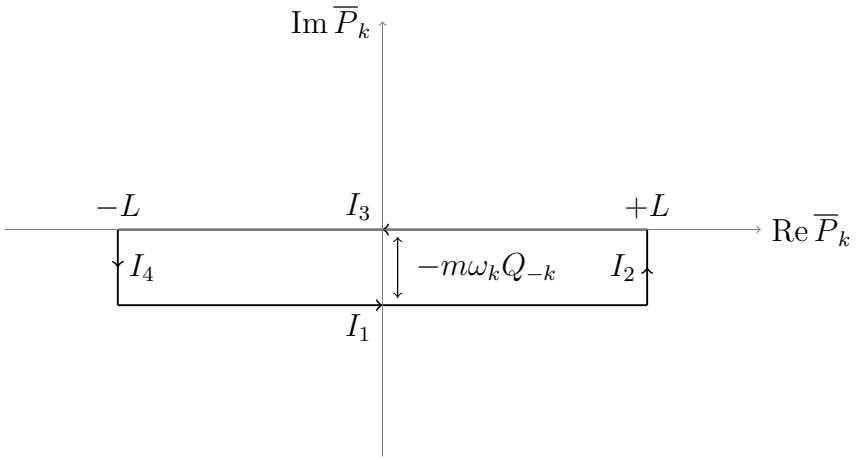

Figure 3.5: A closed contour for $\overline{P}_k$. We are interested in the $L \to \infty$ limit. We expect the integrals along I_2 and I_4 to be zero. Thus we expect the sum of the integrals along I_1 and I_3 to be zero, provided the integrand is analytic within the contour.

is zero and the limit (3.106) ensures that integration over the vertical sections of the contour gives zero in the $L \to \infty$ limit. The sum of the two horizontal contour integrals must therefore be zero in the $L \to \infty$ limit which gives the equality in (3.107).

Note that unlike (3.102), the integrand in the expression (3.105) is completely real, including the real ring-polymer distribution. This expression is the ring-polymer representation of the zero-time value of the quantum Kubo TCF in the space of M Matsubara modes. As stated before (see Section 3.2.4), in the $M \to \infty$ limit this expression will agree with the zero-time limit of the quantum Kubo TCF, which shows that Matsubara dynamics is exact in the $t \to 0$ limit.

3.4.1 CMD

A mean-field approximation over the fluctuation modes (Q_k, P_k, $k \neq 0$) can be made if $A(\mathbf{Q})$ is a function of just the centroid position Q_0, in which case we need only the Matsubara dynamics of the centroid reduced density,

$$b(Q_0, P_0, t) = \alpha_M \int \mathrm{d}\mathbf{Q}' \int \mathrm{d}\mathbf{P}' \; e^{-\beta H(\mathbf{Q},\mathbf{P})} e^{i\beta\theta(\mathbf{Q},\mathbf{P})} \, e^{\mathcal{L}_M t} B(\mathbf{Q}), \tag{3.108}$$

where the primes denote integration over all modes except Q_0 and P_0. Differentiation with respect to time and integration by parts gives

$$\frac{\partial b(Q_0, P_0, t)}{\partial t} = \alpha_M \int \mathrm{d}\mathbf{Q}' \int \mathrm{d}\mathbf{P}' \; e^{-\beta H(\mathbf{Q},\mathbf{P})} e^{i\beta\theta(\mathbf{Q},\mathbf{P})} \, \overline{\mathcal{L}} \, e^{\mathcal{L}_M t} B(\mathbf{Q}), \tag{3.109}$$

where

$$\overline{\mathcal{L}} = \frac{P_0}{m}\frac{\partial}{\partial Q_0} - \frac{\partial U_M(\mathbf{Q})}{\partial Q_0}\frac{\partial}{\partial P_0}. \tag{3.110}$$

We can split the force on the centroid into

$$-\frac{\partial U_M(\mathbf{Q})}{\partial Q_0} = -F'(Q_0) + F_{\text{fluct}}(\mathbf{Q}), \tag{3.111}$$

where $F'(Q_0)$ is the derivative of the centroid potential of mean force,

$$-F'(Q_0) = -\frac{\alpha_M}{Z(Q_0)}\int \mathrm{d}\mathbf{Q}' \int \mathrm{d}\mathbf{P}'\; e^{-\beta H(\mathbf{Q},\mathbf{P})} e^{i\beta\theta(\mathbf{Q},\mathbf{P})}\,\frac{\partial U_M(\mathbf{Q})}{\partial Q_0} \tag{3.112}$$

$$= -\frac{\alpha_M}{Z(Q_0)}\int \mathrm{d}\mathbf{Q}' \int \mathrm{d}\mathbf{P}'\; e^{-\beta R(\mathbf{Q},\mathbf{P})}\,\frac{\partial U_M(\mathbf{Q})}{\partial Q_0}, \tag{3.113}$$

with

$$Z(Q_0) = \alpha_M \int \mathrm{d}\mathbf{Q}' \int \mathrm{d}\mathbf{P}'\; e^{-\beta R(\mathbf{Q},\mathbf{P})}. \tag{3.114}$$

Note that we have used the contour integration trick to reach this expression and the final expression for the centroid potential of mean force (3.113). $F_{\text{fluct}}(\mathbf{Q})$ is the fluctuation force, as defined by (3.111) as the difference between the exact force and $-F'(Q_0)$. The time derivative of the centroid reduced density (3.109) separates into a sum,

$$\frac{\partial b(Q_0,P_0,t)}{\partial t} = \left[\frac{P_0}{m}\frac{\partial}{\partial Q_0} - F'(Q_0)\frac{\partial}{\partial P_0}\right] b(Q_0,P_0,t) \tag{3.115}$$

$$+ \alpha_M \int \mathrm{d}\mathbf{Q}' \int \mathrm{d}\mathbf{P}'\; e^{-\beta H(\mathbf{Q},\mathbf{P})} e^{i\beta\theta(\mathbf{Q},\mathbf{P})}\, F_{\text{fluct}}(\mathbf{Q})\frac{\partial}{\partial P_0} e^{\mathcal{L}_M t} B(\mathbf{Q}),$$

which is an exact rewriting of (3.109). Neglect of the integral term gives the following mean-field approximation for the first derivative,

$$\frac{\partial b(Q_0,P_0,t)}{\partial t} \approx \left[\frac{P_0}{m}\frac{\partial}{\partial Q_0} - F'(Q_0)\frac{\partial}{\partial P_0}\right] b(Q_0,P_0,t) \tag{3.116}$$

$$= \mathcal{L}_0\, b(Q_0,P_0,t). \tag{3.117}$$

By introducing time derivatives higher than first order, we may approximate as follows,

$$b(Q_0,P_0,t) \approx e^{\mathcal{L}_0 t} b(Q_0,P_0,0) \tag{3.118}$$

$$= e^{\mathcal{L}_0 t} e^{-\beta H(Q_0,P_0)}\, B(Q_0), \tag{3.119}$$

where $H(Q_0, P_0) = \frac{P_0^2}{2m} + F(Q_0)$ and we have used the 'classical operator' prescription to reach the last line. The TCF reduces to

$$C_{AB}^{[M]}(t) \approx \frac{1}{2\pi\hbar} \int \mathrm{d}Q_0 \int \mathrm{d}P_0 \; e^{-\beta H(Q_0,P_0)} \, A(Q_0) \, e^{\mathcal{L}_0 t} B(Q_0). \tag{3.120}$$

This TCF (3.120) is the CMD TCF in the space of M Matsubara modes. If we take the $M \to \infty$ limit, so that the centroid potential of mean force is fully converged, then (3.120) is identical to the standard CMD TCF presented earlier (2.44).

Therefore, CMD corresponds to an approximation to Matsubara dynamics where the fluctuation term has been left out of the Liouvillian. This result is not a surprise and is consistent with previous numerical findings that CMD causes errors through neglect of fluctuations.[64,65]

3.4.2 RPMD

Let us restate the Matsubara dynamics TCF in the aforementioned $\overline{\mathbf{P}}$ coordinates (3.103),

$$C_{AB}^{[M]}(t) = \frac{\alpha_M}{2\pi\hbar} \int \mathrm{d}\mathbf{Q} \left[\prod_{k=-\overline{M}}^{\overline{M}} \int_{a_k}^{b_k} \mathrm{d}\overline{P}_k \right] \; e^{-\beta R(\mathbf{Q},\overline{\mathbf{P}})} \, A(\mathbf{Q}) \, e^{\mathcal{L}_M t} \, B(\mathbf{Q}). \tag{3.121}$$

The Matsubara Liouvillian in terms of the new coordinates is

$$\mathcal{L}_M = \mathcal{L}^{[\mathrm{RP}]} + i\mathcal{L}^{[\mathrm{I}]}, \tag{3.122}$$

where

$$\mathcal{L}^{[\mathrm{RP}]} = \sum_{k=-\overline{M}}^{\overline{M}} \frac{\overline{P}_k}{2m} - \left[m\omega_k^2 Q_k + \frac{\partial U_M(\mathbf{Q})}{\partial Q_k} \right] \frac{\partial}{\partial \overline{P}_k} \tag{3.123}$$

is the RPMD Liouvillian in the space of M Matsubara modes and the imaginary part of the Liouvillian is

$$\mathcal{L}^{[\mathrm{I}]} = \sum_{k=-\overline{M}}^{\overline{M}} \omega_k \left(\overline{P}_k \frac{\partial}{\partial \overline{P}_{-k}} - Q_k \frac{\partial}{\partial Q_{-k}} \right). \tag{3.124}$$

Any resemblance to RPMD is at this stage illusory since the imaginary parts of $\overline{P}_k$ contribute terms that cancel the springs in $\mathcal{L}^{[\mathrm{RP}]}$ and the ring-polymer distribution

is complex. If we now try to shift $\overline{P}_k$ onto the real axis using the contour integration trick, we find that the dynamics generated by $\mathcal{L}_M$ propagates an initial distribution of real phase space points into the complex plane along numerically unstable trajectories. Such a trajectory in the complex plane is shown for example in Figure 3.6. This is a well-known problem.[107] While the total energy must be conserved by each trajectory, a complex kinetic energy can support a negative real part which allows the trajectory to explore large regions of the complex plane, even for bound potentials. Therefore, we do not know whether the contour integration trick remains valid for such trajectories. Even if it does, they appear to be at least as difficult to treat numerically as the sign problem in the original formulation of the Matsubara dynamics TCF (3.102).[44]

However, it is possible to follow a path along which each $\overline{P}_k$ is partially moved towards the real axis and $\mathcal{L}^{[\mathrm{I}]}$ is partially discarded so the contour integration trick remains valid. At the end of the path $\mathcal{L}^{[\mathrm{I}]}$ has been completely discarded and $\overline{P}_k$ has reached the real axis. This results in the approximation

$$C_{AB}^{[M]}(t) \approx \frac{\alpha_M}{2\pi\hbar} \int \mathrm{d}\mathbf{Q} \int \mathrm{d}\mathbf{P}\; e^{-\beta R(\mathbf{Q},\mathbf{P})}\, A(\mathbf{Q})\, e^{\mathcal{L}^{[\mathrm{RP}]}t}\, B(\mathbf{Q}), \tag{3.125}$$

which is the RPMD TCF in the space of M Matsubara modes.[e] The aforementioned path can be taken by letting λ change smoothly from one to zero in the Liouvillian

$$\mathcal{L}_\lambda = \mathcal{L}_M^{[\mathrm{RP}]} + i\lambda\mathcal{L}_M^{[\mathrm{I}]}, \tag{3.126}$$

whilst setting $\overline{P}_k = \Pi_k - i\lambda m\omega_k Q_{-k}$, where Π_k and Q_{-k} are real. If we write $\mathcal{L}_\lambda$ in terms of Π_k and Q_k we find

$$\mathcal{L}_\lambda = \sum_{k=-\overline{M}}^{\overline{M}} \frac{\Pi_k}{m}\frac{\partial}{\partial Q_k} - \left[\frac{\partial U_M(\mathbf{Q})}{\partial Q_k} + m(1-\lambda^2)\omega_k^2 Q_k\right]\frac{\partial}{\partial \Pi_k} \tag{3.127}$$

which shows that the dynamics of $\overline{\mathbf{P}}$ and $\mathbf{Q}$ maps onto a real dynamics in $\mathbf{\Pi}$ and $\mathbf{Q}$ at every value of λ between one and zero, and thus avoids the unstable trajectories in the complex plane. This procedure allows us to construct a TCF that is parametrically dependent on λ as follows,

$$C_{AB}^{[M]}(t;\lambda) = \frac{\alpha_M}{2\pi\hbar} \int \mathrm{d}\mathbf{Q} \int \mathrm{d}\mathbf{\Pi}\; e^{-\beta R_\lambda(\mathbf{Q},\mathbf{\Pi})}\, e^{i\lambda\beta\theta(\mathbf{Q},\mathbf{\Pi})}\, A(\mathbf{Q})\, e^{\mathcal{L}_\lambda t}\, B(\mathbf{Q}), \tag{3.128}$$

[e]Note that this also relates Matsubara dynamics to the standard formulation of RPMD in the space of N beads, since in the $N \to \infty$ limit the two formulations are identical.

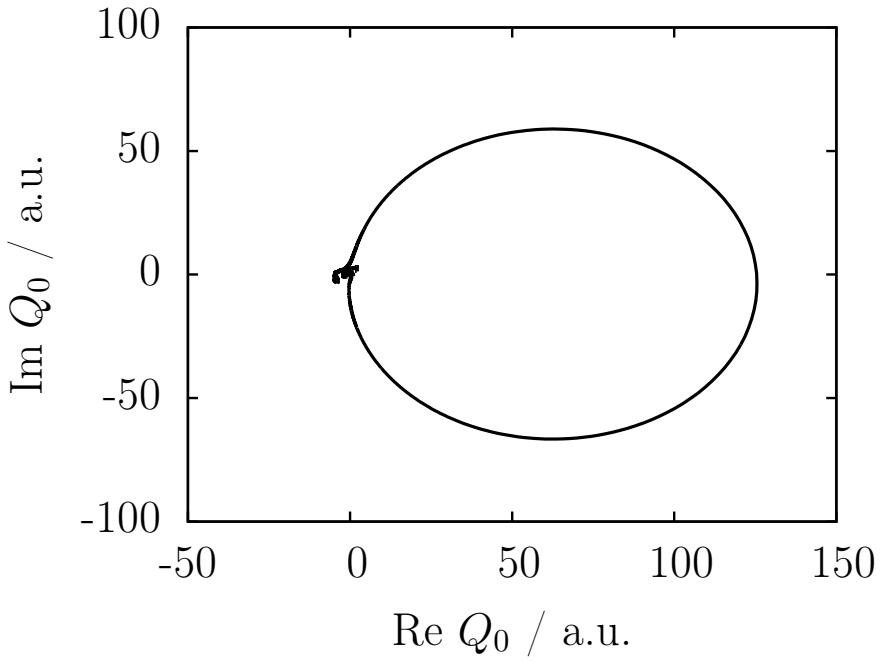

Figure 3.6: A centroid trajectory in the complex plane over 20 atomic time units for the quartic potential (3.79). The centroid position is initially real but becomes complex due to coupling to the fluctuation modes. The centroid traces a long excursion in the complex plane that is very difficult to converge numerically.

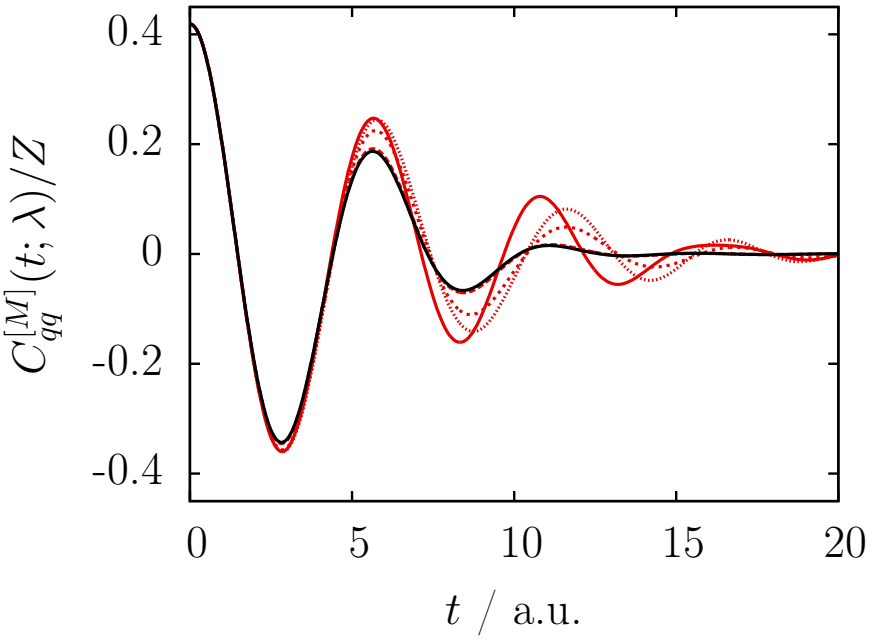

Figure 3.7: Interpolation between Matsubara dynamics and RPMD for $M = 3$ in the quartic potential (3.79) at $\beta = 2$ atomic units. The lines are $\lambda = 1.0$ (solid red), 0.5 (thin dotted red), 0.1 (thick dotted red), 0.05 (dashed red) and 0.0 (black).

where

$$R_\lambda(\mathbf{Q},\mathbf{\Pi}) = R(\mathbf{Q},\mathbf{\Pi}) - \frac{1}{2}m \sum_{k=-\overline{M}}^{\overline{M}} \lambda^2 \omega_k^2 Q_k^2. \tag{3.129}$$

For $\lambda = 1$, the TCF (3.128) is the Matsubara dynamics TCF. For $\lambda = 0$, it is the RPMD TCF in the space of M Matsubara modes. Note that the Liouvillian (3.127) conserves the Hamiltonian (3.129) and $e^{i\lambda\beta\theta(\mathbf{Q},\mathbf{\Pi})}$ so the distribution is conserved and detailed balance is satisfied for any $0 \leq \lambda \leq 1$. In other words, since both parts of the Matsubara Liouvillian $\mathcal{L}^{[\mathrm{RP}]}$ and $\mathcal{L}^{[\mathrm{I}]}$ independently conserve the ring-polymer Hamiltonian, the distribution is still conserved even when the imaginary part of the Liouvillian has been completely removed to give RPMD.

Figure 3.7 shows a graph of the linear position autocorrelation functions that resulted from various values of λ in the quartic potential at $\beta = 2$ atomic units. These results were calculated using Monte Carlo integration with importance sampling for the Hamiltonian part of the distribution. The exact Matsubara potential was used to avoid the fast Fourier transform as described in Appendix B.4.

Since the imaginary Liouvillian $\mathcal{L}^{[\mathrm{I}]}$ does not act directly on the centroid, it follows that an RPMD TCF involving linear operators will agree initially with the Matsubara dynamics TCF but will then lose accuracy as the errors in the fluctuation dynamics couple to the centroid through anharmonicity in the Matsubara potential. This is corroborated by the good agreement between the results for $t \to 0$ in Figure 3.7. In this context, it is the neglect of the imaginary Liouvillian in RPMD that leads to the spurious resonance problem due to the coupling of errors in the fluctuation dynamics to the centroid. Furthermore, even in the harmonic limit where there is no coupling between the centroid and the fluctuation modes, the neglect of the imaginary Liouvillian leads to a demonstrably incorrect fluctuation dynamics in non-linear TCFs. This last point is discussed in more detail in the following section.

3.5 Limits

3.5.1 The classical limit

The classical limit is recovered from the Matsubara dynamics TCF as a special case of one Matsubara mode (the centroid). For the centroid mode alone, the TCF is

$$C_{AB}(t) = \frac{1}{2\pi\hbar} \int \mathrm{d}Q_0 \int \mathrm{d}P_0 \; e^{-\beta H(Q_0,P_0)} \, A(Q_0) \, e^{\mathcal{L}_0 t} \, B(Q_0). \tag{3.130}$$

The Matsubara Hamiltonian reduces to the classical Hamiltonian,

$$H(Q_0, P_0) = \frac{P_0^2}{2m} + V(Q_0), \tag{3.131}$$

and the Matsubara Liouvillian reduces to the classical Liouvillian,

$$\mathcal{L}_0 = \frac{P_0}{2m}\frac{\partial}{\partial Q_0} - V'(Q_0)\frac{\partial}{\partial P_0}. \tag{3.132}$$

3.5.2 The harmonic limit

It is straightforward to show that, like LSC-IVR, Matsubara dynamics is exact for any observables $A(\mathbf{Q})$ and $B(\mathbf{Q})$ in the harmonic limit. The only approximation in the Matsubara dynamics derivation is the removal of the coupling between the Matsubara modes and non-Matsubara modes (see Section 3.2 and Appendix B.3), which allows us to integrate out the non-Matsubara modes in the $N \to \infty$ limit. However, since a harmonic potential does not couple any of the normal modes, the Matsubara dynamics approximation is not an approximation in this limit. In other words, the $M \to \infty$ limit of the Matsubara dynamics TCF (3.46) is just another way of writing the quantum Kubo TCF in the harmonic limit.

In particular, consider an external harmonic potential with natural frequency Ω, $V(q) = \frac{1}{2}m\Omega^2 q^2$. For M Matsubara modes the Matsubara potential is

$$U_M(\mathbf{Q}) = \frac{1}{2}m\Omega^2 \sum_{k=-\overline{M}}^{\overline{M}} Q_k^2. \tag{3.133}$$

Since the potential does not couple the Matsubara modes, the trajectories can be written down at once,

$$e^{\mathcal{L}_M t}Q_k = Q_k \cos(\Omega t) + \frac{P_k}{m\Omega}\sin(\Omega t) \tag{3.134}$$

$$e^{\mathcal{L}_M t}P_k = P_k \cos(\Omega t) - m\Omega Q_k \sin(\Omega t). \tag{3.135}$$

It is straightforward to show, by inserting these equations into (3.46), that the Matsubara dynamics linear position autocorrelation function is

$$\frac{C_{qq}^{[M]}(t)}{Z} = \frac{\cos(\Omega t)}{m\beta\Omega^2}, \tag{3.136}$$

which is independent of M since only the centroid contributes. This expression agrees with the quantum Kubo, classical, CMD and RPMD results. Using the

relations

$$\left\langle Q_j^2 Q_k^2 \right\rangle^{\mathrm{RP}} = (1+2\delta_{jk})\,\frac{1}{m\beta(\Omega^2+\omega_j^2)}\frac{1}{m\beta(\Omega^2+\omega_k^2)} \tag{3.137}$$

$$\left\langle Q_j^2 P_k^2 \right\rangle^{\mathrm{RP}} = \frac{1}{\beta^2(\Omega^2+\omega_j^2)}, \tag{3.138}$$

where $\langle\cdot\rangle^{\mathrm{RP}}$ denotes a ring-polymer average in the space of M Matsubara modes, along with (see Appendix C.1 for a proof)

$$\lim_{M\to\infty}\sum_{k=-\overline{M}}^{\overline{M}}\frac{1}{m\beta(\Omega^2+\omega_j^2)} = \frac{\hbar\,\coth(\beta\hbar\Omega/2)}{2m\Omega}, \tag{3.139}$$

it is straightforward to show that the Matsubara dynamics approximation to the non-linear position autocorrelation function is

$$\begin{aligned}&\lim_{M\to\infty}\frac{C^{[M]}_{q^2q^2}(t)}{Z}\\ &= \frac{\hbar^2}{4m^2\Omega^2}\left(\frac{2}{\beta\hbar\Omega}\coth(\beta\hbar\Omega/2)\cos(2\Omega t)+2\coth^2(\beta\hbar\Omega/2)-1\right),\end{aligned} \tag{3.140}$$

which agrees with the quantum Kubo result.[42] This is in contrast to CMD and RPMD which fail to reproduce the quantum result. The ring-polymer trajectories are

$$e^{\mathcal{L}^{[\mathrm{RP}]}t}Q_k = Q_k\cos(\overline{\omega}_k t)+\frac{P_k}{m\overline{\omega}_k}\sin(\overline{\omega}_k t) \tag{3.141}$$

$$e^{\mathcal{L}^{[\mathrm{RP}]}t}P_k = P_k\cos(\overline{\omega}_k t)-m\overline{\omega}_k Q_k\sin(\overline{\omega}_k t), \tag{3.142}$$

where $\overline{\omega}_k^2 = \omega_k^2+\Omega^2$ are the normal mode frequencies in the harmonic potential. For CMD, we need only consider the centroid ($k=0$). We find

$$\frac{C_{q^2q^2}(t)}{Z} = \frac{1}{(m\beta\Omega^2)^2}\left(1+2\cos^2(\Omega t)\right), \tag{3.143}$$

which is the classical result. On the other hand, the RPMD result is contaminated by the normal mode frequencies,[39]

$$\frac{C^{[N]}_{q^2q^2}(t)}{Z} = \frac{1}{m^2\beta^2}\sum_{k=-\overline{N}}^{\overline{N}}\left[\frac{1+\cos(2\overline{\omega}_k t)}{\overline{\omega}_k^4}+\sum_{j=-\overline{N}}^{\overline{N}}\frac{1}{\overline{\omega}_j^2\overline{\omega}_k^2}\right]. \tag{3.144}$$

A comparison of these results is given in Figure 3.8 for the choice $\beta=8$, $m=1$,

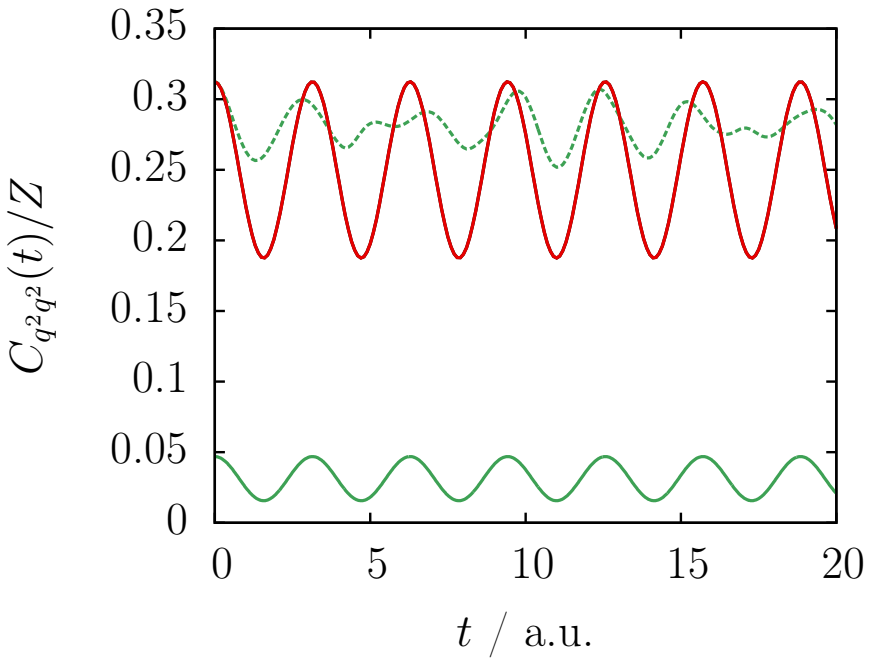

Figure 3.8: Comparison of Matsubara dynamics with quantum, CMD and RPMD results for a harmonic potential ($\Omega = 1$, $m = 1$ and $\beta = 8$ in atomic units). The lines correspond to quantum (black), Matsubara dynamics (red), CMD (solid green) and RPMD (dashed green).

and $\Omega = 1$ in atomic units. The RPMD result was calculated with $N = 128$, which we found to be sufficient for convergence. The CMD result (identical to the classical result) is out by nearly an order of magnitude at $t = 0$ which is a reflection of the inadequacy of CMD to reproduce a non-linear TCF such as this. While the RPMD result is in agreement with the exact result at $t = 0$, for $t > 0$ the oscillations are significantly damped and the TCF adopts a shape that clearly shows the superposition of harmonic oscillations at many spurious frequencies. This failure of RPMD is closely related to its incorrect description of the momentum distribution of the fluctuation modes (see Appendix B.6). The CMD and RPMD results are in stark contrast to the Matsubara dynamics result, which agrees with the quantum result at all time and oscillates only at the natural frequency of the harmonic oscillator Ω.

3.6 Numerical results for one-dimensional systems

The results in this section concern the Kubo quantum, LSC-IVR, CMD and RPMD linear and non-linear position autocorrelation functions. The Matsubara dynamics

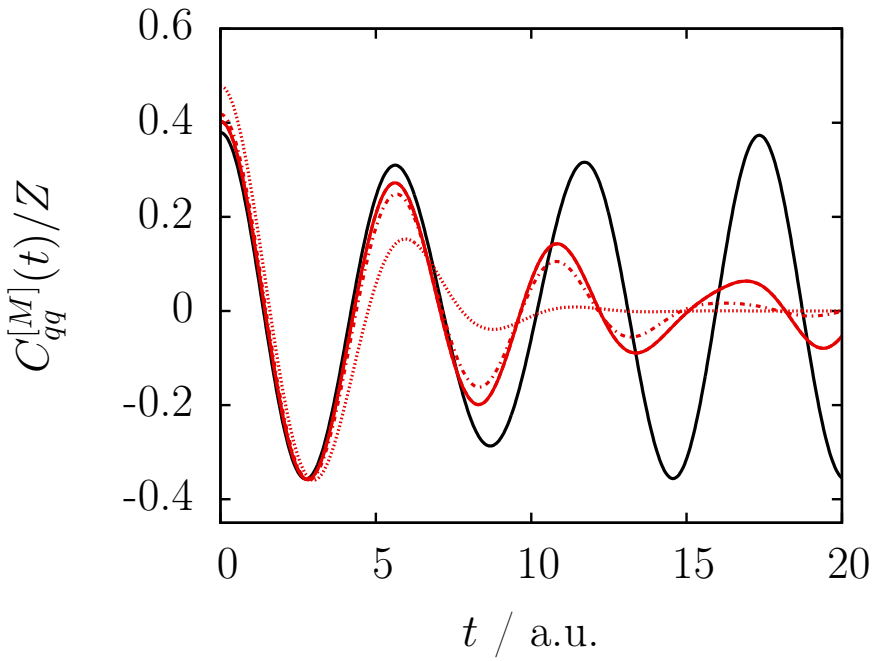

Figure 3.9: Convergence of the Matsubara dynamics linear position autocorrelation function. The results were generated with the quartic potential (3.79) at $\beta = 2$ atomic units. The red lines correspond to $M = 1$ (dots), 3 (chains), 5 (dashes) and 7 (solid). The solid black line is the quantum result.

results were calculated using Monte Carlo integration with importance sampling for the Hamiltonian part of the distribution. The exact Matsubara potential was used to avoid the fast Fourier transform as described in Appendix B.4. The quantum results were calculated using the Colbert-Miller DVR.[20] The LSC-IVR results were calculated using the Colbert-Miller DVR and rectangular quadrature for evaluation of the Wigner transforms. Standard techniques were used to calculate the CMD and RPMD results with $N = 8$, including the well-known symplectic propagator for ring-polymer evolution in normal mode coordinates.[55,14] The CMD centroid potential of mean force was calculated using centroid-constrained ring-polymer averages.

Figure 3.9 shows the convergence of the Matsubara dynamics linear position autocorrelation function as the number of Matsubara modes is increased. The simulation took place at an inverse temperature of $\beta = 2$ atomic units in the quartic potential (3.79). A total of 10^{11} Monte Carlo samples were required to converge the $M = 7$ result. Extending these calculations beyond $M = 7$ was prohibitively difficult. For $M = 7$, the Matsubara dynamics zero-time value is still slightly underconverged, showing a slight difference with the quantum result. We expect on the basis of RPMD simulations for this potential that $M = 9$ or $M = 11$ would

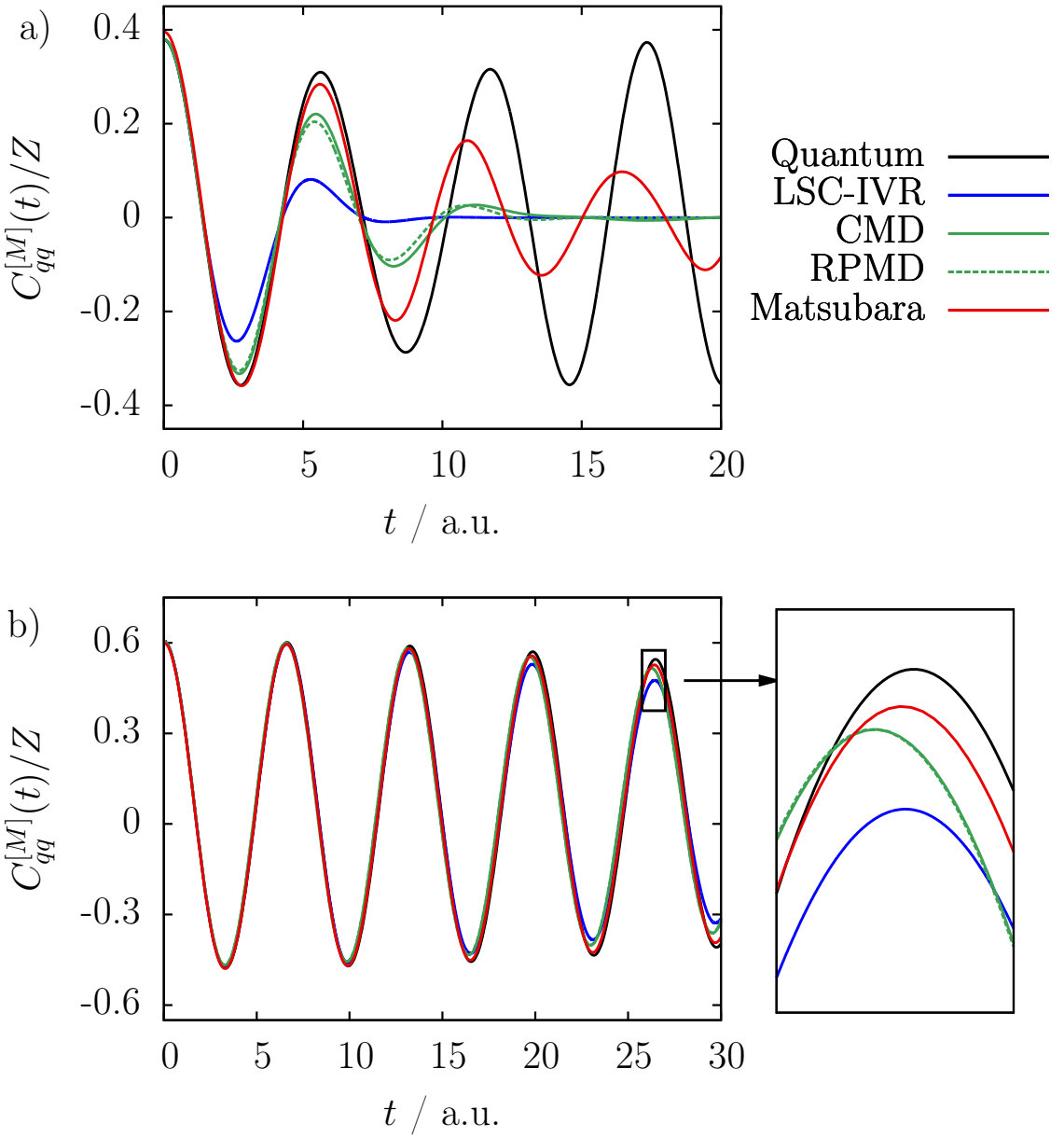

Figure 3.10: Comparison of Matsubara dynamics with practical methods for the linear position autocorrelation function. Panel a shows results for the quartic potential (3.79) and panel b shows results for the mildly anharmonic potential (3.80), both at $\beta = 2$ atomic units.

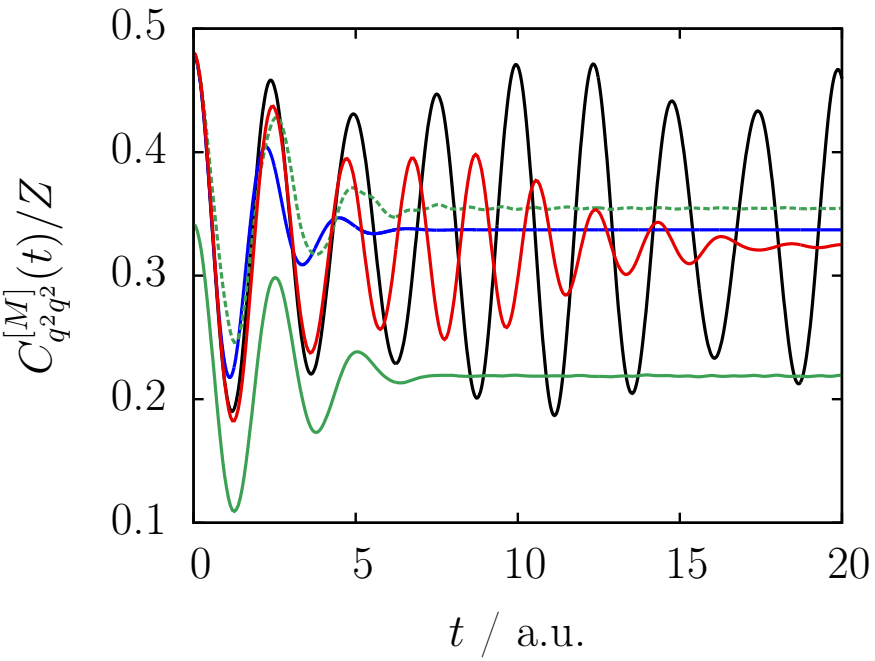

Figure 3.11: Comparison of Matsubara dynamics with practical methods for the non-linear position autocorrelation function in the quartic potential (3.79) at $\beta = 2$ atomic units. The same colour scheme is used as in Figure 3.10.

be sufficient for convergence at this temperature (the RPMD result is converged at $N = 8$). Nevertheless, the results in the figure are sufficient to show that the TCF converges with respect to M, although the convergence becomes slower at longer times. For the mildly anharmonic potential (3.80), we found convergence to within graphical accuracy with $M = 5$ at the same temperature.

Figure 3.10 compares linear position autocorrelation functions for the quartic and mildly anharmonic potentials at an inverse temperature of $\beta = 2$ atomic units. Panel a shows results for the quartic potential and panel b shows results for the mildly anharmonic potential. For Matsubara dynamics we used $M = 7$ and $M = 5$ Matsubara modes respectively. It is well known that the quartic potential is a severe test for which any method that neglects real-time coherence fails after a single recurrence. Nevertheless, we see that Matsubara dynamics gives a much better treatment than LSC-IVR, reproducing almost perfectly the first recurrence and decaying to zero more slowly. The Matsubara dynamics result is also better than both the CMD and RPMD results which have decayed to zero by $t = 15$ atomic units.

Figure 3.11 shows the non-linear position autocorrelation function for the quartic potential at the same temperature. The behaviours of CMD and RPMD are

qualitatively the same as for the harmonic potential at the higher inverse temperature of $\beta = 8$ atomic units (see Figure 3.8). The lower inverse temperature we used here leads to less pronounced spurious oscillation of the RPMD TCF and a smaller discrepancy at zero time for the CMD TCF. However, the situation has changed significantly for the LSC-IVR result which is no longer exact for this strongly anharmonic potential. The LSC-IVR TCF decays very quickly and has completely decorrelated by $t = 10$ atomic units, which we know to be roughly the time required for the LSC-IVR squared-position thermal expectation value to settle down to its incorrect final value (see Figure 3.4). On the other hand, while the Matsubara dynamics TCF is no longer in perfect agreement with the quantum result, it is promising to see that the agreement is good for $t \leq 5$ atomic units, by which time the other approximate results have almost completely decorrelated.

Chapter 4

The Planetary Model

4.1 Introduction

The planetary model of Poulsen *et al.* (described under the name FK-QCW(1) in Ref. 45) combines the Feynman-Kleinert approximation with a model dynamics involving a 'planet' that moves around the centroid. The model approximates the standard quantum TCF for two operators $\hat{A} = A(\hat{q})$ and $\hat{B} = B(\hat{q})$,

$$C_{AB}(t) = \mathrm{Tr}\left[e^{-\beta\hat{H}}\hat{A}\hat{B}(t)\right]. \tag{4.1}$$

The planetary model approximation to this TCF in one dimension is[45]

$$\begin{aligned} C_{AB}(t) = &\frac{1}{2\pi\hbar}\int \mathrm{d}Q_0 \int \mathrm{d}P_0 \; e^{-\beta\frac{P_0^2}{2m}-\beta W(Q_0)} \\ &\times \frac{1}{2\pi m\Omega a^2}\int \mathrm{d}\tilde{q}\int \mathrm{d}\tilde{p} \; e^{-\frac{\tilde{q}^2}{2a^2}-\frac{\tilde{p}^2}{2m^2\Omega^2a^2}} f_A(q,\tilde{p})\, e^{\mathcal{L}t}\, B(q). \end{aligned} \tag{4.2}$$

$W(Q_0)$ is the Feynman-Kleinert centroid potential of mean force and a and Ω are the (centroid-dependent) Feynman-Kleinert radius of gyration and frequency respectively (see Section 2.3). $q = Q_0 + \tilde{q}$ is the planet coordinate and $p = P_0 + \tilde{p}$ is its momentum. The Liouvillian that appears within the propagator is given by[a]

$$\begin{aligned} \mathcal{L} = &\frac{P_0}{m}\frac{\partial}{\partial Q_0} - W'(Q_0)\frac{\partial}{\partial P_0} \\ &+ \frac{\tilde{p}}{m}\frac{\partial}{\partial \tilde{q}} - m\Omega^2\tilde{q}\frac{\partial}{\partial \tilde{p}} \\ &+ \frac{P_0}{m}\frac{\partial \ln(m^2\Omega^2a^2)}{\partial Q_0}\frac{\tilde{p}}{2}\frac{\partial}{\partial \tilde{p}} + \frac{P_0}{m}\frac{\partial \ln(a^2)}{\partial Q_0}\frac{\tilde{q}}{2}\frac{\partial}{\partial \tilde{q}}. \end{aligned} \tag{4.3}$$

[a] Poulsen *et al.* do not use the Liouvillian formalism in Ref. 45. However, the Liouvillian formalism is more helpful for our purposes so we have recast their equations in this form.

This leads to the following equations of motion for the centroid,

$$\dot{Q}_0 = \frac{P_0}{m} \tag{4.4}$$

$$\dot{P}_0 = -\, W'(Q_0), \tag{4.5}$$

and for the planet,

$$\dot{\tilde{q}} = \frac{\tilde{p}}{m} + \frac{\tilde{q}}{2}\frac{\mathrm{d}}{\mathrm{d}t}\ln(a^2) \tag{4.6}$$

$$\dot{\tilde{p}} = -\, m\Omega^2\tilde{q} + \frac{\tilde{p}}{2}\frac{\mathrm{d}}{\mathrm{d}t}\ln(m^2\Omega^2a^2). \tag{4.7}$$

Notice that the planet is influenced by the centroid through the centroid-dependence of Ω^2 and a^2, but the centroid moves independently from the planet under the Feynman-Kleinert CMD equations of motion. In practice, integration of the equations of motion for the planet is simplified by transforming to the dimensionless coordinates $\overline{q} = \tilde{q}/a$ and $\overline{p} = \tilde{p}/m\Omega a$ which leads to the following simple equations of motion,[45]

$$\dot{\overline{q}} = \Omega\overline{p} \tag{4.8}$$

$$\dot{\overline{p}} = -\, \Omega\overline{q}. \tag{4.9}$$

This transformation arises naturally by introducing the integrating factor $1/a$ into (4.6) and $1/m\Omega a$ into (4.7). The function $f_A(q,\tilde{p})$ is defined according to the following Fourier transform,

$$f_A(q,\tilde{p}) = \frac{m\Omega a}{\sqrt{2\pi}\hbar}\, e^{+\frac{\tilde{p}^2}{2m^2\Omega^2a^2}} \int \mathrm{d}\Delta\; e^{i\Delta\tilde{p}/\hbar}\, e^{-\frac{m^2\Omega^2a^2}{2\hbar^2}\Delta^2} A(q+\Delta/2), \tag{4.10}$$

which arises from the Wigner transform $\left[e^{-\beta\hat{H}}A(\hat{q})\right](q,p)$ under the Feynman-Kleinert approximation for the centroid-constrained Boltzmann operator,

$$\begin{aligned}\langle q|\, e^{-\beta\hat{H}}\, |q'\rangle\,(Q_0) = \sqrt{\frac{m}{2\pi\beta\hbar^2}}e^{-\beta W(Q_0)}\frac{1}{\sqrt{2\pi}a}\,\exp\left\{-\frac{[(q+q')/2-Q_0]^2}{2a^2}\right\} \\ \times\,\exp\left\{-\frac{m\Omega\coth(\beta\hbar\Omega/2)}{4\hbar}(q-q')^2\right\}.\end{aligned} \tag{4.11}$$

This well-known expression is the contribution to the (Feynman-Kleinert) Boltzmann operator $\langle q|\, e^{-\beta\hat{H}}\, |q'\rangle$ from all imaginary-time paths whose centroids coincide with the given configuration space point Q_0.[108]

The Liouvillian formalism allows us to easily demonstrate that the distribution is conserved in the planetary model (which Poulsen *et al.* demonstrate equivalently using a time-dependent Jacobian). Expanding the propagator as a Taylor series in time and repeatedly applying integration by parts in each coordinate gives the following for the planetary model TCF,

$$C_{AB}(t) = \frac{1}{2\pi\hbar}\int \mathrm{d}Q_0 \int \mathrm{d}P_0 \int \mathrm{d}\tilde{q} \int \mathrm{d}\tilde{p}\; B(q) \sum_{k=0}^{\infty} \frac{1}{k!}\left[\frac{\mathcal{L}m\Omega a^2}{m\Omega a^2} - \mathcal{L}\right]^k \times \frac{1}{2\pi m\Omega a^2}\; e^{-\beta\frac{P_0^2}{2m} - \beta W(Q_0)}\, e^{-\frac{\tilde{q}^2}{2a^2} - \frac{\tilde{p}^2}{2m^2\Omega^2 a^2}}\, f_A(q,\tilde{p}). \tag{4.12}$$

Now, using the following result,

$$\frac{\mathcal{L}m\Omega a^2}{(m\Omega a^2)^2} = \mathcal{L}\frac{1}{m\Omega a^2}, \tag{4.13}$$

and conservation of energy,

$$\mathcal{L}\left[\frac{P_0^2}{2m} + W(Q_0) + \frac{\tilde{q}^2}{2\beta a^2} + \frac{\tilde{p}^2}{2\beta m^2\Omega^2 a^2}\right] = 0, \tag{4.14}$$

leads to

$$C_{AB}(t) = \frac{1}{2\pi\hbar}\int \mathrm{d}Q_0 \int \mathrm{d}P_0\; e^{-\beta\frac{P_0^2}{2m} - \beta W(Q_0)} \times \frac{1}{2\pi m\Omega a^2}\int \mathrm{d}\tilde{q} \int \mathrm{d}\tilde{p}\; e^{-\frac{\tilde{q}^2}{2a^2} - \frac{\tilde{p}^2}{2m^2\Omega^2 a^2}}\, B(q)\, e^{-\mathcal{L}t}\, f_A(q,\tilde{p}). \tag{4.15}$$

For the special case of $A(\hat{q}) = \hat{I}$, this implies

$$\frac{C_{IB}(t)}{Z} = \langle B \rangle\,, \tag{4.16}$$

which shows that thermal expectation values are time-independent.

In the following sections we demonstrate that the planetary model is related to Matsubara dynamics through several quantifiable approximations. First we outline how Matsubara dynamics approximates non-Kubo TCFs. Then we summarise the Feynman-Kleinert approximation in the context of the quantum canonical partition function and show that it is equivalent to making an approximation to the Matsubara potential. We then show that a model dynamics of the planet (a linear combination of Matsubara modes) that is based on this approximate potential allows us to integrate out the Matsubara phase which leads to (4.2) with a different Liouvillian. We find that this model dynamics gives a good approximation to the fluctuation part of

the exact Matsubara dynamics trajectory on the Feynman-Kleinert potential and is thus expected to be a good approximation for mildly anharmonic potentials. A slight modification to the dynamics of the planet recovers conservation of energy (and conservation of the quantum Boltzmann distribution), which leads to the equations of motion (4.6) and (4.7).

4.2 Matsubara dynamics for two-point correlation

The Matsubara dynamics TCF for two observables $A(\mathbf{Q})$ and $B(\mathbf{Q})$ is

$$C_{AB}^{[M]}(t) = \frac{\alpha_M}{2\pi\hbar} \int \mathrm{d}\mathbf{Q} \int \mathrm{d}\mathbf{P}\; e^{-\beta H(\mathbf{Q},\mathbf{P})} e^{i\beta\theta(\mathbf{Q},\mathbf{P})}\, A(\mathbf{Q})\, e^{\mathcal{L}_M t}\, B(\mathbf{Q}), \tag{4.17}$$

and approximates the quantum Kubo TCF. Remembering the definitions of $A(\mathbf{Q})$ and $B(\mathbf{Q})$ as imaginary-time integrals,

$$A(\mathbf{Q}) = \frac{1}{\beta\hbar} \int_0^{\beta\hbar} \mathrm{d}\tau A(q(\tau)), \tag{4.18}$$

(with $B(\mathbf{Q})$ defined equivalently) we may rewrite the TCF as follows,

$$C_{AB}^{[M]}(t) = \frac{1}{(\beta\hbar)^2} \int_0^{\beta\hbar} \mathrm{d}\tau \int_0^{\beta\hbar} \mathrm{d}\tau'\; C_{AB}^{[M]}(t;\tau;\tau'), \tag{4.19}$$

where

$$C_{AB}^{[M]}(t;\tau;\tau') = \frac{\alpha_M}{2\pi\hbar} \int \mathrm{d}\mathbf{Q} \int \mathrm{d}\mathbf{P}\; e^{-\beta H(\mathbf{Q},\mathbf{P})} e^{i\beta\theta(\mathbf{Q},\mathbf{P})}\, A(q(\tau))\, e^{\mathcal{L}_M t}\, B(q(\tau')). \tag{4.20}$$

This last quantity is the Matsubara dynamics TCF for two points on the imaginary time path $q(\tau)$ and $q(\tau')$. The imaginary-time path point $q(\tau)$ is, as defined in Chapter 3,

$$q(\tau) = Q_0 + \sqrt{2} \sum_{k=1}^{\overline{M}} \sin(\omega_k \tau) Q_k + \cos(\omega_k \tau) Q_{-k}. \tag{4.21}$$

Given the invariance of the Matsubara dynamics distribution under imaginary-time translation, $C_{AB}^{[M]}(t;\tau;\tau')$ is clearly only dependent on the imaginary-time difference $\Delta\tau = \tau - \tau'$. In other words, we may rewrite the Matsubara dynamics TCF as follows,

$$C_{AB}^{[M]}(t) = \frac{1}{\beta\hbar} \int_0^{\beta\hbar} \mathrm{d}\tau\; C_{AB}^{[M]}(t;\tau), \tag{4.22}$$

where $C_{AB}^{[M]}(t;\tau)$ is given by

$$C_{AB}^{[M]}(t;\tau) = \frac{\alpha_M}{2\pi\hbar}\int \mathrm{d}\mathbf{Q}\int \mathrm{d}\mathbf{P}\; e^{-\beta H(\mathbf{Q},\mathbf{P})}e^{i\beta\theta(\mathbf{Q},\mathbf{P})}\,A(q(\tau))\,e^{\mathcal{L}_M t}\,B(q(0)), \tag{4.23}$$

which we call the Matsubara dynamics two-point TCF. We may interpret this equation as the Matsubara dynamics approximation to the following quantum TCF,

$$C_{AB}(t;\tau) = \mathrm{Tr}\left[e^{-(\beta-\tau/\hbar)\hat{H}}\,\hat{A}\,e^{-\tau\hat{H}/\hbar}\hat{B}(t)\right], \tag{4.24}$$

where $0 \leq \tau \leq \beta\hbar$. In particular, the $\tau \to 0$ limit of (4.23) is the Matsubara dynamics approximation to the standard quantum TCF. Indeed, rather than unravelling the (Kubo) Matsubara dynamics TCF in this way, we may also repeat the derivation presented in Chapter 3 with the observables $A(\mathbf{q})$ and $B(\mathbf{z})$ replaced with $A(q_j)$ and $B(z_k)$ $(j \neq k)$ in the generalised quantum Kubo TCF (3.1). The result is (4.23).

4.3 The Feynman-Kleinert approximation

Suppose we make a locally harmonic approximation for the fluctuation modes Q_k $(k \neq 0)$ so that the Matsubara potential can be written as follows,

$$U_M(\mathbf{Q}) = L(Q_0) + \frac{1}{2}m\Omega^2\sum_{k\neq 0}Q_k^2, \tag{4.25}$$

where $\Omega^2 = \Omega^2(Q_0)$ is dependent on the centroid position (we omit this centroid dependence in the following to maintain a simple notation). With such a harmonic description of the fluctuation modes, the quantum canonical partition function in the space of M Matsubara modes is

$$Z = \frac{\alpha_M}{2\pi\hbar}\left(\frac{2\pi m}{\beta}\right)^{M/2}\int \mathrm{d}\mathbf{Q}\; e^{-\beta\left[L(Q_0)+\frac{1}{2}m\sum_{k\neq 0}(\Omega^2+\omega_k^2)Q_k^2\right]}. \tag{4.26}$$

By recognising that

$$\frac{1}{\alpha_M} = \int \mathrm{d}\mathbf{Q}'\int \mathrm{d}\mathbf{P}'\; e^{-\beta\sum_{k\neq 0}\frac{P_k^2}{2m}+\frac{1}{2}m\omega_k^2Q_k^2}, \tag{4.27}$$

where the primes denote integration over all the Matsubara fluctuation modes, and

$$\sum_{k=1}^{\infty}\int_0^{\Omega^2}\mathrm{d}\lambda\;\frac{1}{\lambda+\omega_k^2} = \ln\left[\frac{\sinh(\beta\hbar\Omega/2)}{\beta\hbar\Omega/2}\right], \tag{4.28}$$

it is straightforward to show by thermodynamic integration that the following result holds for the partition function in the $M \to \infty$ limit,

$$\lim_{M\to\infty} Z = \sqrt{\frac{m}{2\pi\beta\hbar^2}} \int \mathrm{d}Q_0 \; e^{-\beta L(Q_0)} \operatorname{csch}\left(\frac{\beta\hbar\Omega}{2}\right) \frac{\beta\hbar\Omega}{2}. \tag{4.29}$$

This integral can be rewritten as follows,

$$\lim_{M\to\infty} Z = \sqrt{\frac{m}{2\pi\beta\hbar^2}} \int \mathrm{d}Q_0 \; e^{-\beta W(Q_0)}, \tag{4.30}$$

where

$$W(Q_0) = L(Q_0) + \frac{1}{\beta} \ln\left[\frac{\sinh(\beta\hbar\Omega/2)}{\beta\hbar\Omega/2}\right], \tag{4.31}$$

and this last quantity is obviously to be interpreted as the centroid potential of mean force (see Section 2.3).

We would like to find the centroid potential of mean force $W(Q_0)$ that best approximates the true centroid potential of mean force $F(Q_0) = -\frac{1}{\beta}\ln[Z(Q_0)]$. From the Gibbs-Bogoliubov inequality we have the following upper bound for the true centroid potential of mean force,

$$F(Q_0) \leq -\left\langle \Delta H \right\rangle_0 + \frac{1}{\beta} \ln\left[\frac{\sinh(\beta\hbar\Omega/2)}{\beta\hbar\Omega/2}\right], \tag{4.32}$$

where $\left\langle \Delta H \right\rangle_0$ is the (centroid-dependent) expectation value of the energy difference within the harmonic approximation,

$$\left\langle \Delta H \right\rangle_0 = \lim_{M\to\infty} \int \mathrm{d}\mathbf{Q}' \; \rho(\mathbf{Q}) \left[U_M(\mathbf{Q}) - \frac{1}{2} m\Omega^2 \sum_{k\neq 0} Q_k^2\right], \tag{4.33}$$

and $\rho(\mathbf{Q})$ is the normalised harmonic distribution of the fluctuation modes,

$$\rho(\mathbf{Q}) = \frac{e^{-\beta\frac{1}{2}m\sum_{k\neq 0}(\Omega^2+\omega_k^2)Q_k^2}}{\int \mathrm{d}\mathbf{Q}' \; e^{-\beta\frac{1}{2}m\sum_{k\neq 0}(\Omega^2+\omega_k^2)Q_k^2}}. \tag{4.34}$$

It is straightforward to show (see Ref. 56), by introducing the Fourier representation of the Dirac delta function into the following rewriting of (4.33),

$$\begin{aligned}\left\langle \Delta H \right\rangle_0 = \lim_{M\to\infty} \int \mathrm{d}q \int \mathrm{d}\mathbf{Q}' \; \rho(\mathbf{Q}) \\ \times \left[U_M(\mathbf{Q}) - \frac{1}{2} m\Omega^2 \sum_{k\neq 0} Q_k^2\right] \delta(q - q(\tau)),\end{aligned} \tag{4.35}$$

that this expectation value reduces to the following simple form,

$$\langle \Delta H \rangle_0 = V_{a^2}(Q_0) - \frac{1}{2} m\Omega^2 a^2, \tag{4.36}$$

where $V_{a^2}(Q_0)$ is the convolution of the external potential with a Gaussian of width a,

$$V_{a^2}(Q_0) = \frac{1}{\sqrt{2\pi}a} \int_{-\infty}^{\infty} \mathrm{d}\tilde{q}\; e^{-\frac{\tilde{q}^2}{2a^2}}\, V(\tilde{q} + Q_0), \tag{4.37}$$

and a is the (expected) radius of gyration of the imaginary-time path within the harmonic approximation,

$$a^2 = \frac{2}{m\beta} \sum_{k=1}^{\infty} \frac{1}{\Omega^2 + \omega_k^2} \tag{4.38}$$

$$= \frac{\beta\hbar\Omega \coth\left(\frac{\beta\hbar\Omega}{2}\right) - 2}{2\beta m\Omega^2}. \tag{4.39}$$

Therefore, for $W(Q_0)$ to be variationally-optimal we equate it with the right-hand side of the inequality (4.32). This sets

$$L(Q_0) = V_{a^2}(Q_0) - \frac{1}{2} m\Omega^2 a^2, \tag{4.40}$$

and minimisation with respect to a^2 gives

$$m\Omega^2 = 2\frac{\partial V_{a^2}(Q_0)}{\partial a^2} \tag{4.41}$$

$$= \frac{1}{\sqrt{2\pi}a} \int_{-\infty}^{\infty} \mathrm{d}\tilde{q}\; e^{-\frac{\tilde{q}^2}{2a^2}}\, V''(\tilde{q} + Q_0). \tag{4.42}$$

These are the Feynman-Kleinert equations that define the variationally-optimal centroid potential of mean force in terms of the centroid position, the frequency Ω and radius of gyration a (see Section 2.3).

4.4 An approximate dynamics

According to the analysis in the previous section, making the Feynman-Kleinert approximation in Matsubara dynamics corresponds to approximation of the Matsubara potential (in the $M \to \infty$ limit) as follows,

$$U_M(\mathbf{Q}) \to L(Q_0) + \frac{1}{2} m\Omega^2 \sum_{k\neq 0} Q_k^2, \tag{4.43}$$

where $L(Q_0)$ and Ω^2 are defined according to (4.40) and (4.42) respectively. Modifying the potential in this way leads to the following expression for the Matsubara dynamics two-point TCF,

$$C_{AB}^{[M]}(t;\tau) = \frac{\alpha_M}{2\pi\hbar}\int \mathrm{d}\mathbf{Q}\int \mathrm{d}\mathbf{P}\; e^{-\beta\frac{P_0^2}{2m}-\beta L(Q_0)-\beta\sum_{k\neq 0}\frac{P_k^2}{2m}+\frac{1}{2}m\Omega^2 Q_k^2} \times\; e^{i\beta\theta(\mathbf{Q},\mathbf{P})}\, A(q(\tau))\, e^{\mathcal{L}_M t}\, B(q(0)). \tag{4.44}$$

For the Liouvillian this change leads to

$$\mathcal{L}_M = \frac{P_0}{m}\frac{\partial}{\partial Q_0} - \left[L'(Q_0) + \frac{1}{2}m\frac{\partial\Omega^2}{\partial Q_0}\sum_{k\neq 0}Q_k^2\right]\frac{\partial}{\partial P_0} + \sum_{k\neq 0}\frac{P_k}{m}\frac{\partial}{\partial Q_k} - m\Omega^2 Q_k\frac{\partial}{\partial P_k}. \tag{4.45}$$

The corresponding equations of motion for the centroid are

$$\dot{Q}_0 = \frac{P_0}{m} \tag{4.46}$$

$$\dot{P}_0 = -\frac{\partial L(Q_0)}{\partial Q_0} - \frac{1}{2}m\frac{\partial\Omega^2}{\partial Q_0}\sum_{k\neq 0}Q_k^2, \tag{4.47}$$

and for the fluctuation modes ($k \neq 0$),

$$\dot{Q}_k = \frac{P_k}{m} \tag{4.48}$$

$$\dot{P}_k = -m\Omega^2 Q_k. \tag{4.49}$$

Despite this harmonic approximation, the approximate Matsubara dynamics two-point TCF (4.44) is in general just as difficult to treat as Matsubara dynamics on the exact potential because each fluctuation mode Q_k ($k \neq 0$) rapidly acquires a non-linear dependence on the other fluctuation modes, making it impossible to integrate out the Matsubara phase. However, if the potential is not too strongly anharmonic, it seems reasonable to neglect these non-linear dependences by decoupling the centroid and the fluctuation modes to second order, i.e. to make the following approximation for the Matsubara Liouvillian,

$$\mathcal{L}_M = \mathcal{L}_0 + \sum_{k\neq 0}\frac{P_k}{m}\frac{\partial}{\partial Q_k} - m\Omega^2 Q_k\frac{\partial}{\partial P_k}, \tag{4.50}$$

where $\mathcal{L}_0$ concerns the centroid coordinates only. For example, we might propagate each centroid trajectory using a method such as CMD or RPMD, then insert the re-

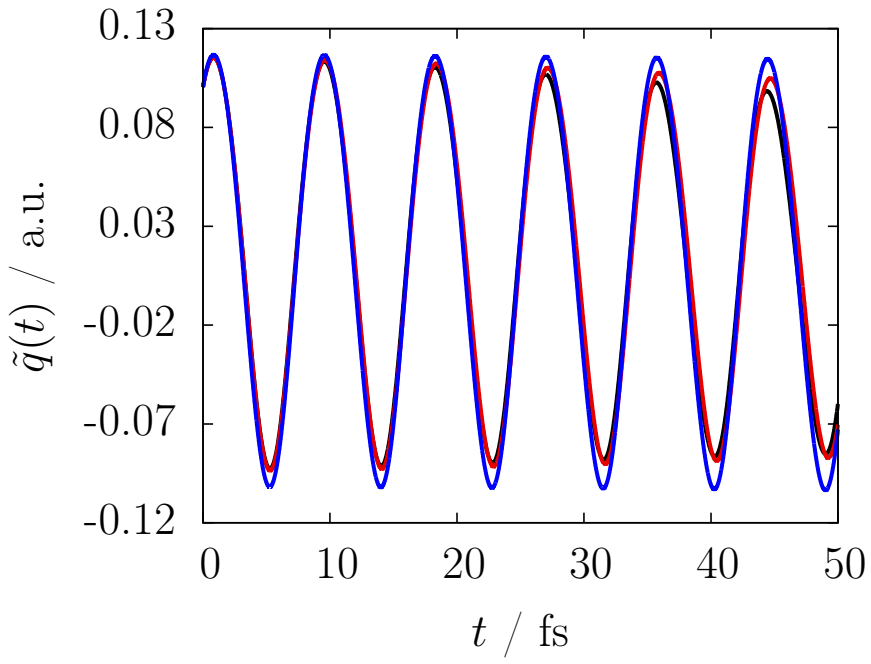

Figure 4.1: Comparison of trajectories for the q-TIP4P/F OH potential (4.51) at 300K. The plotted trajectories are from evolution under (4.45) (black line), (4.52) (red line) and the planetary model equations of motion (4.3) (blue line).

sulting time-dependent frequency into (4.49) to generate purely harmonic dynamics for each fluctuation mode.

We tested such an approximation on a one-dimensional model of the OH stretch in water based on the q-TIP4P/F potential,[109]

$$V_{OH}(q) = D_r \left[\alpha_r^2 (q - q_{eq})^2 - \alpha_r^3 (q - q_{eq})^3 + \frac{7}{12} \alpha_r^4 (q - q_{eq})^4 \right], \tag{4.51}$$

which is a fourth order expansion of a Morse potential. The parameters are $D_r = 116.09\,\text{kcal mol}^{-1}$, $\alpha_r = 2.287\,\text{Å}^{-1}$ and $q_{eq} = 0.942\,\text{Å}$. The mass is taken to be the reduced mass of the OH unit. We used the Feynman-Kleinert centroid potential of mean force to propagate the centroid trajectories. i.e. We evolved the system according to the following Liouvillian,

$$\begin{aligned} \mathcal{L}_M = & \frac{P_0}{m} \frac{\partial}{\partial Q_0} - W'(Q_0) \frac{\partial}{\partial P_0} \\ & + \sum_{k \neq 0} \frac{P_k}{m} \frac{\partial}{\partial Q_k} - m\Omega^2 Q_k \frac{\partial}{\partial P_k}, \end{aligned} \tag{4.52}$$

in which the dynamics of the centroid is unaffected by the fluctuation modes. In

Figure 4.1, this is compared with evolution under (4.45) and with evolution under the planetary model Liouvillian (4.3) from the same initial conditions. The plotted quantity is the fluctuation coordinate $\tilde{q}(0) = q(0) - Q_0$. To calculate the Feynman-Kleinert parameters we used Gauss-Hermite quadrature in the relevant integrals and found the fixed point iteration to converge after approximately five iterations. As is clear from the figure, this approximation has a small effect on the fluctuation trajectory. We found this behaviour to be typical at 150K, 300K and 600K with a range of initial conditions that were drawn in accordance with the quantum Boltzmann distribution.

4.5 Integrating out the Matsubara phase

The advantage of such a first-order approximation as presented in the previous section is that it allows us to integrate out the Matsubara phase in the approximate Matsubara dynamics two-point TCF (4.44). The dynamics of any linear combination of fluctuation modes, e.g. $\tilde{q}(\tau) = q(\tau) - Q_0$, obey the following first-order linear differential equations (as is easily verified by inspecting $\mathcal{L}_M \tilde{q}(\tau)$ and $\mathcal{L}_M \tilde{p}(\tau)$) with $\mathcal{L}_M$ defined by (4.52)),

$$\dot{\tilde{q}}(\tau) = \frac{\tilde{p}(\tau)}{m} \tag{4.53}$$

$$\dot{\tilde{p}}(\tau) = -m\Omega^2 \tilde{q}(\tau). \tag{4.54}$$

The fluctuation coordinate $\tilde{q}(\tau)$ at time t is therefore only dependent on the initial conditions $(\tilde{q}(\tau), \tilde{p}(\tau), Q_0, P_0)$ and the dependence on the initial $\tilde{q}(\tau)$ and $\tilde{p}(\tau)$ is linear. The upshot of this is that, taking the approximate Matsubara dynamics two-point TCF,

$$\begin{aligned} C_{AB}^{[M]}(t;\tau) = \frac{\alpha_M}{2\pi\hbar} \int \mathrm{d}\mathbf{Q} \int \mathrm{d}\mathbf{P}\ & e^{-\beta \frac{P_0^2}{2m} - \beta L(Q_0) - \beta \sum_{k\neq 0} \frac{P_k^2}{2m} + \frac{1}{2} m\Omega^2 Q_k^2} \\ & \times\ e^{i\beta\theta(\mathbf{Q},\mathbf{P})}\, A(q(\tau))\, e^{\mathcal{L}_M t}\, B(q(0)), \end{aligned} \tag{4.55}$$

the Liouvillian may be replaced as follows,

$$\begin{aligned} \mathcal{L}_M \to\ & \frac{P_0}{m}\frac{\partial}{\partial Q_0} - W'(Q_0)\frac{\partial}{\partial P_0} \\ & + \frac{\tilde{p}(0)}{m}\frac{\partial}{\partial \tilde{q}(0)} - m\Omega^2 \tilde{q}(0)\frac{\partial}{\partial \tilde{p}(0)}. \end{aligned} \tag{4.56}$$

This enables us to integrate out the Matsubara phase in the $M \to \infty$ limit. The approach is to insert Dirac delta functions to rewrite as follows,

$$\begin{aligned} C_{AB}^{[M]}(t;\tau) = & \frac{\alpha_M}{2\pi\hbar} \int \mathrm{d}\mathbf{x} \int \mathrm{d}\mathbf{Q} \int \mathrm{d}\mathbf{P}\ e^{-\beta\frac{P_0^2}{2m} - \beta L(Q_0) - \beta\sum_{k\neq 0}\frac{P_k^2}{2m} + \frac{1}{2}m\Omega^2 Q_k^2} \\ & \times \delta\left(\tilde{q}_2 - \tilde{q}(\tau)\right)\, \delta\left(\tilde{p}_2 - \tilde{p}(\tau)\right)\, \delta\left(\tilde{q}_1 - \tilde{q}(0)\right)\, \delta\left(\tilde{p}_1 - \tilde{p}(0)\right) \\ & \times\ e^{i\beta\theta(\mathbf{Q},\mathbf{P})}\, A(q(\tau))\, e^{\mathcal{L}_M t}\, B(q(0)), \end{aligned} \tag{4.57}$$

where $\mathbf{x}^T = (\tilde{q}_1, \tilde{p}_1, \tilde{q}_2, \tilde{p}_2)$. By exploiting the Fourier transform identity for the Dirac delta function it is straightforward to show that, in the $M \to \infty$ limit, this expression reduces to (see Appendix C.2)

$$\begin{aligned} C_{AB}(t;\tau) = & \frac{1}{2\pi\hbar} \int \mathrm{d}Q_0 \int \mathrm{d}P_0\ e^{-\beta\frac{P_0^2}{2m} - \beta W(Q_0)} \\ & \times \frac{1}{(2\pi)^2\sqrt{\det(G)}} \int \mathrm{d}\mathbf{x}\ e^{-\frac{1}{2}\mathbf{x}^T G^{-1}\mathbf{x}} A(q_2)\, e^{\mathcal{L}t}\, B(q_1), \end{aligned} \tag{4.58}$$

where the 4×4 symmetric matrix G is given by

$$G = \begin{bmatrix} a^2 & 0 & b^2(\tau) & ic^2(\tau) \\ 0 & m^2\Omega^2 a^2 & -ic^2(\tau) & m^2\Omega^2 b^2(\tau) \\ b^2(\tau) & -ic^2(\tau) & a^2 & 0 \\ ic^2(\tau) & m^2\Omega^2 b^2(\tau) & 0 & m^2\Omega^2 a^2. \end{bmatrix}. \tag{4.59}$$

The a^2 that appears in this matrix is the Feynman-Kleinert radius of gyration (4.39), $b^2(\tau)$ is the following hyperbolic function,

$$b^2(\tau) = \frac{2}{m\beta}\left(\frac{\beta\hbar}{4\Omega}\frac{\cosh\left(\beta\hbar\Omega/2 - \Omega\tau\right)}{\sinh\left(\beta\hbar\Omega/2\right)} - \frac{1}{2\Omega^2}\right) \tag{4.60}$$

and $c^2(\tau)$ is

$$c^2(\tau) = \frac{\hbar}{2}\,\mathrm{csch}\left(\frac{\beta\hbar\Omega}{2}\right)\sinh\left(\frac{\beta\hbar\Omega}{2} - \Omega\tau\right), \tag{4.61}$$

which is related to the first derivative of $b^2(\tau)$ with respect to τ. The Liouvillian is, of course, the same as in (4.56) but with the following replacements $\tilde{q}(0) \to \tilde{q}_1$ and $\tilde{p}(0) \to \tilde{p}_1$ (in accordance with the Dirac delta functions in (4.57)). Note that $\det(G)$ is positive provided $\Omega^2 > 0$ since $c^2(\tau) \geq 0$, $a^2 \geq b^2(\tau)$ and

$$\det(G) = \left[c^4(\tau) + m^2\Omega^2(a^4 - b^4(\tau))\right]^2 \tag{4.62}$$

$$> 0. \tag{4.63}$$

Note also that the imaginary entries in G are the residual phase, representing the correlation between $\tilde{q}_1$ and $\tilde{p}_2$,

$$\langle \tilde{q}_1 \tilde{p_2} \rangle = ic^2(\tau). \tag{4.64}$$

To remove this residual phase, we recognise that since the Liouvillian does not involve $\tilde{q}_2$ and $\tilde{p}_2$, we may formally integrate over these coordinates to give

$$\begin{aligned} C_{AB}(t;\tau) =& \frac{1}{2\pi\hbar} \int \mathrm{d}Q_0 \int \mathrm{d}P_0 \; e^{-\beta\frac{P_0^2}{2m} - \beta W(Q_0)} \\ & \times \frac{1}{2\pi m\Omega a^2} \int \mathrm{d}\tilde{q} \int \mathrm{d}\tilde{p} \; e^{-\frac{\tilde{q}^2}{2a^2} - \frac{\tilde{p}^2}{2m^2\Omega^2 a^2}} f_A(q,\tilde{p})\, e^{\mathcal{L}t}\, B(q), \end{aligned} \tag{4.65}$$

where the subscripts have been dropped from q_1 and p_1 to simplify the notation because only one planet remains. Of course, the form of $f_A(q,\tilde{p})$ depends on the observable $A(q_2)$. By the usual route for writing a multivariate normal distribution as a product of a conditional and marginal distribution, it is straightforward to show that the function $f_A(q,\tilde{p})$ has the following general form,

$$f_A(q,\tilde{p}) = \frac{1}{2\pi\sqrt{\det(\Sigma)}} \int \mathrm{d}\mathbf{x} \; e^{-\frac{1}{2}(\mathbf{x}-\boldsymbol{\mu})^T \Sigma^{-1} (\mathbf{x}-\boldsymbol{\mu})}\, A(q_2), \tag{4.66}$$

where Σ is the Schur complement of G_{22} in G,[b]

$$\Sigma = G_{11} - G_{12}G_{22}^{-1}G_{21}, \tag{4.67}$$

G_{ab} being a 2×2 submatrix of G (G_{11} the upper left submatrix etc.), $\mathbf{x}$ is

$$\mathbf{x} = \begin{bmatrix} \tilde{q}_2 \\ \tilde{p}_2 \end{bmatrix}, \tag{4.68}$$

and $\boldsymbol{\mu}$ is

$$\boldsymbol{\mu} = G_{12}G_{22}^{-1} \begin{bmatrix} \tilde{q} \\ \tilde{p} \end{bmatrix}. \tag{4.69}$$

By taking the Taylor series of $A(q_2)$ and using the following relation for the k^{th}

[b] Notice that $\det(\Sigma) = \det(G)/m^2\Omega^2a^4$ which is positive provided $\Omega^2 > 0$.

probabilists' Hermite polynomial,

$$H_k(x) = \left(\frac{1}{i\sigma}\right)^k \frac{1}{\sqrt{2\pi}\sigma} \int_{-\infty}^{\infty} \mathrm{d}y \; e^{-\frac{y^2}{2\sigma^2}} \; (y + i\sigma x)^k \,, \tag{4.70}$$

the general form of $f_A(q, \tilde{p})$ (4.66) reduces to

$$f_A(q, \tilde{p}) = \sum_{k=0}^{\infty} \frac{A^k \, (Q_0 + \tilde{q} \, b^2(\tau)/a^2)}{k!} \, (i\sigma)^k \, H_k(\xi \tilde{p}). \tag{4.71}$$

The constants ξ and σ are given by the following pair of equations,

$$\sigma\xi = \frac{c^2(\tau)}{m^2\Omega^2 a^2} \tag{4.72}$$

$$\sigma^2 = a^2 - \frac{b^4(\tau)}{a^2} + \frac{c^4(\tau)}{m^2\Omega^2 a^2}. \tag{4.73}$$

This expression can be made more compact as follows,

$$f_A(q, \tilde{p}) = e^{+\frac{\xi^2\tilde{p}^2}{2}} A \left[Q_0 + \frac{b^2(\tau)}{a^2}\tilde{q} + \frac{\sigma}{i\xi}\frac{\partial}{\partial \tilde{p}} \right] e^{-\frac{\xi^2\tilde{p}^2}{2}}, \tag{4.74}$$

where this equation is to be understood as a formal rewriting of (4.71), having equated terms in the infinite series and made use of Rodrigues' formula for the probabilists' Hermite polynomials,

$$H_k(x) = (-1)^k e^{+\frac{x^2}{2}} \frac{\mathrm{d}^k}{\mathrm{d}x^k} e^{-\frac{x^2}{2}}. \tag{4.75}$$

Of course, we have ignored the radius of convergence of the Taylor series of $A(q_2)$ in this analysis. However, polynomials in q_2 (as we might encounter with a non-linear dipole moment) and e^{ikq_2} (as we might encounter for the intermediate scattering function) are entire functions. This justifies taking the Taylor expansion in (4.66) in those cases.

As it stands, (4.65) is completely general in the sense that it encompasses all approximate Matsubara dynamics two-point TCFs for $0 \leq \tau \leq \beta\hbar$ within the Feynman-Kleinert approximation. However, to compare with the planetary model we take the $\tau \to 0$ limit, since $C_{AB}(t;\tau)$ in the $\tau \to 0$ limit is the Matsubara dynamics approximation to the standard quantum TCF. In this limit we have

$$\lim_{\tau\to 0} b^2(\tau) = a^2 \tag{4.76}$$

$$\lim_{\tau\to 0} c^2(\tau) = \frac{\hbar}{2}, \tag{4.77}$$

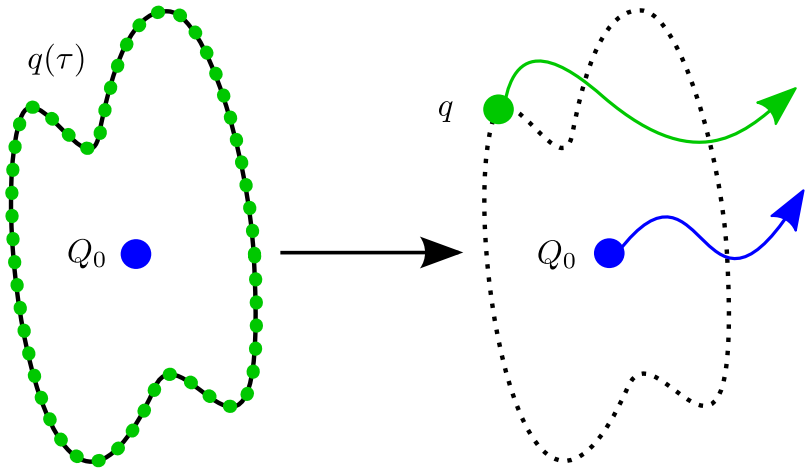

Figure 4.2: Schematic diagram comparing the entire imaginary-time path that is evolved in (Kubo) Matsubara dynamics (left) with a single point on the imaginary-time path (the 'planet') which evolves about the centroid in the approximate Matsubara dynamics two-point TCF (right).

and the function $f_A(q,\tilde{p})$ becomes

$$f_A(q,\tilde{p}) = \sum_{k=0}^{\infty} \frac{A^k(q)}{k!} \left(\frac{i\hbar}{2m\Omega a}\right)^k H_k\left(\frac{\tilde{p}}{m\Omega a}\right) \tag{4.78}$$

$$= e^{+\frac{\tilde{p}^2}{2m^2\Omega^2a^2}} A\left[q + \frac{\hbar}{2i}\frac{\partial}{\partial\tilde{p}}\right] e^{-\frac{\tilde{p}^2}{2m^2\Omega^2a^2}}. \tag{4.79}$$

The Matsubara dynamics approximation to the standard quantum TCF within the Feynman-Kleinert approximation is therefore

$$\begin{aligned} C_{AB}(t) =& \frac{1}{2\pi\hbar}\int \mathrm{d}Q_0 \int \mathrm{d}P_0\; e^{-\beta\frac{P_0^2}{2m}-\beta W(Q_0)} \\ &\times \frac{1}{2\pi m\Omega a^2}\int \mathrm{d}\tilde{q}\int \mathrm{d}\tilde{p}\; e^{-\frac{\tilde{q}^2}{2a^2}-\frac{\tilde{p}^2}{2m^2\Omega^2a^2}} f_A(q,\tilde{p})\, e^{\mathcal{L}t}\, B(q), \end{aligned} \tag{4.80}$$

which correlates one point on the imaginary-time path $q = q(0)$ (the 'planet') with itself at a later time t. A schematic diagram of this transformation from the full imaginary-time path to the planet coordinate is shown in Figure 4.2.

We now demonstrate that the function $f_A(q,\tilde{p})$ presented here is identical to that in the planetary model (4.10). Using the well-known formula for the Fourier transform of a Gaussian, we may write

$$\int_{-\infty}^{\infty} \mathrm{d}\Delta\; e^{i\Delta\tilde{p}/\hbar}\, e^{-\frac{m^2\Omega^2a^2\Delta^2}{2\hbar^2}} = \frac{\sqrt{2\pi}\hbar}{m\Omega a} e^{-\frac{\tilde{p}^2}{2m^2\Omega^2a^2}}. \tag{4.81}$$

Inserting this identity into (4.79) leads to

$$f_A(q,\tilde{p}) = \frac{m\Omega a}{\sqrt{2\pi}\hbar}\, e^{+\frac{\tilde{p}^2}{2m^2\Omega^2a^2}} \int_{-\infty}^{\infty} \mathrm{d}\Delta\; e^{-\frac{m^2\Omega^2a^2\Delta^2}{2\hbar^2}}\, A\left[q + \frac{\hbar}{2i}\frac{\partial}{\partial\tilde{p}}\right] e^{i\Delta\tilde{p}/\hbar} \tag{4.82}$$

$$= \frac{m\Omega a}{\sqrt{2\pi}\hbar}\, e^{+\frac{\tilde{p}^2}{2m^2\Omega^2a^2}} \int_{-\infty}^{\infty} \mathrm{d}\Delta\; e^{i\Delta\tilde{p}/\hbar}\, e^{-\frac{m^2\Omega^2a^2\Delta^2}{2\hbar^2}}\, A\left(q + \Delta/2\right), \tag{4.83}$$

which is the same as in the planetary model (4.10).

4.6 Recovering conservation of energy

The only remaining difference between the approximate Matsubara dynamics two-point TCF presented in the previous section (4.80) and the planetary model TCF (4.2) is the Liouvillian. We restate the approximate Matsubara Liouvillian for the centroid and the planet,

$$\mathcal{L} = \frac{P_0}{m}\frac{\partial}{\partial Q_0} - W'(Q_0)\frac{\partial}{\partial P_0} + \frac{\tilde{p}}{m}\frac{\partial}{\partial\tilde{q}} - m\Omega^2\tilde{q}\frac{\partial}{\partial\tilde{p}}. \tag{4.84}$$

If we interpret the exponentiated part of the integrand in (4.80) as the total energy of the centroid and the planet we find

$$H(Q_0,P_0,\tilde{q},\tilde{p}) = \frac{P_0^2}{2m} + W(Q_0) + \frac{\tilde{q}^2}{2\beta a^2} + \frac{\tilde{p}^2}{2\beta m^2\Omega^2a^2}. \tag{4.85}$$

Now, the energy is not conserved since

$$\mathcal{L}H(Q_0,P_0,\tilde{q},\tilde{p}) = \frac{\tilde{q}^2}{2\beta}\frac{P_0}{2m}\frac{\partial a^{-2}}{\partial Q_0} + \frac{\tilde{p}^2}{2\beta}\frac{P_0}{2m}\frac{\partial(m\Omega a)^{-2}}{\partial Q_0} \tag{4.86}$$

$$= -\left[\frac{P_0}{m}\frac{\partial\ln(m^2\Omega^2a^2)}{\partial Q_0}\frac{\tilde{p}}{2}\frac{\partial}{\partial\tilde{p}} + \frac{P_0}{m}\frac{\partial\ln(a^2)}{\partial Q_0}\frac{\tilde{q}}{2}\frac{\partial}{\partial\tilde{q}}\right] \times\; H(Q_0,P_0,\tilde{q},\tilde{p}), \tag{4.87}$$

which is generally non-zero outside the harmonic limit because the Feynman-Kleinert radius of gyration and frequency are dependent on the centroid position. However, the form of (4.87) shows that if we modify the Liouvillian according to

$$\mathcal{L} \to \frac{P_0}{m}\frac{\partial}{\partial Q_0} - W'(Q_0)\frac{\partial}{\partial P_0} + \frac{\tilde{p}}{m}\frac{\partial}{\partial\tilde{q}} - m\Omega^2\tilde{q}\frac{\partial}{\partial\tilde{p}} + \frac{P_0}{m}\frac{\partial\ln(m^2\Omega^2a^2)}{\partial Q_0}\frac{\tilde{p}}{2}\frac{\partial}{\partial\tilde{p}} + \frac{P_0}{m}\frac{\partial\ln(a^2)}{\partial Q_0}\frac{\tilde{q}}{2}\frac{\partial}{\partial\tilde{q}}, \tag{4.88}$$

then this remedies the non-conservation of energy and leads to the same Liouvillian as in the planetary model (4.3). This completes our demonstration of the relationship between Matsubara dynamics and the planetary model of Poulsen *et al.* in one dimension.

4.7 Limits and momentum-dependent observables

4.7.1 The zero-time limit

Notice that while $f_A(q,\tilde{p})$ is in general a complicated function of q and $\tilde{p}$, it may be replaced with $A(q)$ in the $t \to 0$ limit provided the observable $B(q)$ is only dependent on position. Using the Hermite polynomial representation of $f_A(q,\tilde{p})$ (4.78), we have

$$\begin{aligned} C_{AB}(0) = &\frac{1}{2\pi\hbar}\int \mathrm{d}Q_0 \int \mathrm{d}P_0 \; e^{-\beta\frac{P_0^2}{2m}-\beta W(Q_0)} \\ &\times \frac{1}{2\pi m\Omega a^2}\int \mathrm{d}\tilde{q}\int \mathrm{d}\tilde{p}\; e^{-\frac{\tilde{q}^2}{2a^2}-\frac{\tilde{p}^2}{2m^2\Omega^2a^2}}\, B(q) \\ &\times \sum_{k=0}^{\infty}\frac{A^k(q)}{k!}\left(\frac{i\hbar}{2m\Omega a}\right)^k H_k\left(\frac{\tilde{p}}{m\Omega a}\right). \end{aligned} \tag{4.89}$$

Now, since the zeroth Hermite polynomial is $H_0\left(\frac{\tilde{p}}{m\Omega a}\right) = 1$ and all the Hermite polynomials are orthogonal with respect to the weight $w(\tilde{p}) = e^{-\frac{\tilde{p}^2}{2m^2\Omega^2a^2}}$, it is clear that

$$\frac{1}{\sqrt{2\pi}m\Omega a}\int \mathrm{d}\tilde{p}\; e^{-\frac{\tilde{p}^2}{2m^2\Omega^2a^2}} H_k\left(\frac{\tilde{p}}{m\Omega a}\right) = \begin{cases} 1 & k = 0 \\ 0 & k > 0. \end{cases} \tag{4.90}$$

Therefore, only the zeroth term in the series survives and we are left with

$$\begin{aligned} C_{AB}(0) = &\frac{1}{2\pi\hbar}\int \mathrm{d}Q_0 \int \mathrm{d}P_0 \; e^{-\beta\frac{P_0^2}{2m}-\beta W(Q_0)} \\ &\times \frac{1}{2\pi m\Omega a^2}\int \mathrm{d}\tilde{q}\int \mathrm{d}\tilde{p}\; e^{-\frac{\tilde{q}^2}{2a^2}-\frac{\tilde{p}^2}{2m^2\Omega^2a^2}}\, A(q)\, B(q), \end{aligned} \tag{4.91}$$

which is the same as (4.89) but for $f_A(q,\tilde{p})$ replaced with $A(q)$. For example, for $A(q) = q$ and $B(q) = q$, this leads to

$$\frac{C_{qq}(0)}{Z} = \left\langle Q_0^2 + a^2 \right\rangle, \tag{4.92}$$

where the thermal average is taken over the Feynman-Kleinert distribution for the centroid.

4.7.2 The harmonic limit

The various approximations made to the Matsubara dynamics two-point TCF do not need to be made in the harmonic limit. As stated earlier, the Feynman-Kleinert approximation is equivalent to approximation of the Matsubara potential as follows,

$$U_M(\mathbf{Q}) = L(Q_0) + \frac{1}{2}m\Omega^2 \sum_{k\neq 0} Q_k^2. \tag{4.93}$$

However, in the harmonic limit the Matsubara potential already has this form with $L(Q_0) = \frac{1}{2}m\omega^2 Q_0^2$ and $\Omega = \omega$ (the constant natural frequency of the harmonic potential). The approximate Matsubara dynamics two-point TCF (4.65) is therefore exact for a harmonic potential with any imaginary-time separation τ. Of course, for $\tau \to 0$ this implies that the planetary model TCF is exact as well.

4.7.3 Momentum-dependent observables

The analysis in this chapter may be repeated with the observable $A(q_2)$ dependent only on momentum as opposed to position. The form of the approximate Matsubara dynamics two-point TCF (4.65) is identical but $f_A(q, \tilde{p})$ must be replaced with

$$f_A(\tilde{q}, p) = \sum_{k=0}^{\infty} \frac{A^k \left(P_0 + \tilde{p}\, b^2(\tau)/a^2\right)}{k!} (i\sigma)^k H_k(\xi\tilde{q}) \tag{4.94}$$

$$= e^{+\frac{\xi^2\tilde{q}^2}{2}} A \left[P_0 + \frac{b^2(\tau)}{a^2}\tilde{p} + \frac{\sigma}{i\xi}\frac{\partial}{\partial\tilde{q}}\right] e^{-\frac{\xi^2\tilde{q}^2}{2}}, \tag{4.95}$$

where

$$\sigma\xi = -\frac{c^2(\tau)}{a^2} \tag{4.96}$$

$$\sigma^2 = \frac{c^4(\tau)}{a^2} + m^2\Omega^2 a^2 - \frac{b^4(\tau)m^2\Omega^2}{a^2}. \tag{4.97}$$

For $\tau \to 0$, the function $f_A(\tilde{q}, p)$ becomes

$$f_A(\tilde{q}, p) = \sum_{k=0}^{\infty} \frac{A^k \left(P_0 + \tilde{p}\right)}{k!} \left(\frac{\hbar}{2ia}\right)^k H_k\left(\frac{\tilde{q}}{a}\right) \tag{4.98}$$

$$= e^{+\frac{\tilde{q}^2}{2a^2}} A \left[P_0 + \tilde{p} + \frac{i\hbar}{2}\frac{\partial}{\partial\tilde{q}}\right] e^{-\frac{\tilde{q}^2}{2a^2}}, \tag{4.99}$$

which would be used to approximate the standard quantum TCF for $\hat{A} = A(\hat{p})$.

4.8 Multidimensional generalisation

The multidimensional generalisation of the foregoing analysis is straightforward, with every quantity having a simple vector or matrix analogue. The centroid potential of mean force for a system with F degrees of freedom within the Feynman-Kleinert approximation is

$$W(\mathbf{Q}_0) = L(\mathbf{Q}_0) + \frac{1}{\beta}\mathrm{Tr}\left[\ln\left(\frac{\Omega^{-1}\sinh(\beta\hbar\Omega/2)}{\beta\hbar/2}\right)\right], \tag{4.100}$$

where

$$L(\mathbf{Q}_0) = \frac{1}{(2\pi)^{F/2}\det(A)}\int_{-\infty}^{\infty}\mathrm{d}\tilde{\mathbf{q}}_M\; e^{-\frac{1}{2}\tilde{\mathbf{q}}_M^T A^{-2}\tilde{\mathbf{q}}_M}\; V(\tilde{\mathbf{q}}+\mathbf{Q}_0) - \frac{1}{2}\mathrm{Tr}\left[\Omega^2 A^2\right]. \tag{4.101}$$

The vector $\tilde{\mathbf{q}}_M = M^{1/2}\tilde{\mathbf{q}}$ is the mass-weighted coordinate corresponding to $\tilde{\mathbf{q}}$ and M is the $F \times F$ mass matrix for the system. The Feynman-Kleinert frequency matrix that optimises the centroid potential of mean force is defined through

$$\Omega^2 = \frac{1}{(2\pi)^{F/2}\det(A)}\int_{-\infty}^{\infty}\mathrm{d}\tilde{\mathbf{q}}\; e^{-\frac{1}{2}\tilde{\mathbf{q}}_M^T A^{-2}\tilde{\mathbf{q}}_M}\; \overline{H}(\tilde{\mathbf{q}}+\mathbf{Q}_0), \tag{4.102}$$

where $\overline{H}(\tilde{\mathbf{q}}+\mathbf{Q}_0)$ is the mass-weighted Hessian and the Feynman-Kleinert radius of gyration matrix A is related to the frequency via

$$A^2 = \frac{1}{\beta}\Omega^{-2}\left[\frac{\beta\hbar\Omega}{2}\coth(\beta\hbar\Omega/2) - 1\right]. \tag{4.103}$$

Note that the Feynman-Kleinert radius of gyration matrix is simply a function of the frequency, thus they are simultaneously diagonalisable. The multidimensional planetary model TCF is

$$\begin{aligned} C_{AB}(t) = &\frac{1}{(2\pi\hbar)^F}\int\mathrm{d}\mathbf{Q}_0\int\mathrm{d}\mathbf{P}_0\; e^{-\beta\frac{1}{2}\mathbf{P}_0^T M^{-1}\mathbf{P}_0 - \beta W(\mathbf{Q}_0)}\,\frac{1}{(2\pi)^F\det\left(\Omega A^2\right)} \\ &\times\int\mathrm{d}\tilde{\mathbf{q}}_M\int\mathrm{d}\tilde{\mathbf{p}}_M\; e^{-\frac{1}{2}\tilde{\mathbf{q}}_M^T A^{-2}\tilde{\mathbf{q}}_M - \frac{1}{2}\tilde{\mathbf{p}}_M^T(\Omega A)^{-2}\tilde{\mathbf{p}}_M} f_A(\mathbf{q},\tilde{\mathbf{p}})\, e^{\mathcal{L}t}\, B(\mathbf{q}), \end{aligned} \tag{4.104}$$

where $\tilde{\mathbf{p}}_M = M^{-1/2}\tilde{\mathbf{p}}$ is the mass-weighted coordinate corresponding to $\tilde{\mathbf{p}}$. The function $f_A(\mathbf{q},\tilde{\mathbf{p}})$ is

$$f_A(\mathbf{q},\tilde{\mathbf{p}}) = e^{+\frac{1}{2}\tilde{\mathbf{p}}_M^T(\Omega A)^{-2}\tilde{\mathbf{p}}_M} A\left[\mathbf{Q}_0 + \tilde{\mathbf{q}} + \frac{\hbar}{2i}\nabla_{\tilde{\mathbf{p}}}\right] e^{-\frac{1}{2}\tilde{\mathbf{p}}_M^T(\Omega A)^{-2}\tilde{\mathbf{p}}_M}, \tag{4.105}$$

where $\nabla_x^T = \left(\frac{\partial}{\partial x_1}, \frac{\partial}{\partial x_2}, \cdots, \frac{\partial}{\partial x_F}\right)$. Notice that for $A(\mathbf{q}) = \mathbf{q}$, the function $f_A(\mathbf{q},\tilde{\mathbf{p}})$

is simply

$$f_A(\mathbf{q},\tilde{\mathbf{p}}) = \mathbf{q} + i\hbar M^{-1/2}(\Omega A)^{-2}\tilde{\mathbf{p}}_M, \tag{4.106}$$

which we will use later in the thesis. By projecting $\tilde{\mathbf{q}}_M$ and $\tilde{\mathbf{p}}_M$ onto the eigenvectors of the Feynman-Kleinert frequency matrix, $f_A(\mathbf{q},\tilde{\mathbf{p}})$ can be written in terms of the probabilists' Hermite polynomials as in the one-dimensional case. This provides the relation between the function $f_A(\mathbf{q},\tilde{\mathbf{p}})$ presented here and in Ref. 46. The multidimensional planetary model Liouvillian is

$$\begin{aligned}\mathcal{L} =& \mathbf{P}_0^T M^{-1}\nabla_{\mathbf{Q}_0} - \nabla_{\mathbf{Q}_0}^T W(\mathbf{Q}_0)\nabla_{\mathbf{P}_0} \\ &+ \tilde{\mathbf{p}}_M^T\nabla_{\tilde{\mathbf{q}}_M} - \tilde{\mathbf{q}}_M^T\Omega^2\nabla_{\tilde{\mathbf{p}}_M} \\ &- \tilde{\mathbf{q}}_M^T\sum_{j=1}^{F}\frac{P_0^j}{m_j}\frac{\partial A^{-1}}{\partial Q_0^j}A\nabla_{\tilde{\mathbf{q}}_M} \\ &- \tilde{\mathbf{p}}_M^T\sum_{j=1}^{F}\frac{P_0^j}{m_j}\frac{\partial\,(A\Omega)^{-1}}{\partial Q_0^j}A\Omega\nabla_{\tilde{\mathbf{p}}_M}.\end{aligned} \tag{4.107}$$

This leads to the Feynman-Kleinert CMD equations of motion for the centroids,

$$\dot{\mathbf{Q}}_0 = M^{-1}\mathbf{P}_0 \tag{4.108}$$

$$\dot{\mathbf{P}}_0 = -\nabla_{\mathbf{Q}_0}W(\mathbf{Q}_0), \tag{4.109}$$

and the following equations of motion for the planets,

$$\dot{\tilde{\mathbf{q}}}_M = \tilde{\mathbf{p}}_M - A\dot{A}^{-1}\tilde{\mathbf{q}}_M \tag{4.110}$$

$$\dot{\tilde{\mathbf{p}}}_M = -\Omega^2\tilde{\mathbf{q}}_M - A\Omega(\dot{A\Omega})^{-1}\tilde{\mathbf{p}}_M. \tag{4.111}$$

As in one dimension, to facilitate integration of these equations we insert the integrating factor A^{-1} into the first equation and $(A\Omega)^{-1}$ into the second to give

$$\frac{\mathrm{d}}{\mathrm{d}t}A^{-1}\tilde{\mathbf{q}}_M = A^{-1}\tilde{\mathbf{p}}_M \tag{4.112}$$

$$\frac{\mathrm{d}}{\mathrm{d}t}(A\Omega)^{-1}\tilde{\mathbf{p}}_M = -\Omega A^{-1}\tilde{\mathbf{q}}_M. \tag{4.113}$$

Defining the dimensionless coordinates $\overline{\mathbf{q}} = A^{-1}\tilde{\mathbf{q}}_M$ and $\overline{\mathbf{p}} = (A\Omega)^{-1}\tilde{\mathbf{p}}_M$ we get

$$\dot{\overline{\mathbf{q}}} = \Omega\overline{\mathbf{p}} \tag{4.114}$$

$$\dot{\overline{\mathbf{p}}} = -\Omega\overline{\mathbf{q}}, \tag{4.115}$$

which have exactly the same form as they do in one dimension (see (4.8) and (4.9)). Note that if we choose to project the dimensionless coordinates onto the eigenvectors of the Feynman-Kleinert frequency matrix by taking $D^T\overline{\mathbf{q}} \to \overline{\mathbf{q}}$ and $D^T\overline{\mathbf{p}} \to \overline{\mathbf{p}}$, where D is the (centroid-dependent) matrix of eigenvectors, then the equations of motion become

$$\dot{\overline{q}}_j = \Omega_j \overline{p}_j - \left(D^T \dot{D}\, \overline{\mathbf{q}}\right)_j \tag{4.116}$$

$$\dot{\overline{p}}_j = -\,\Omega_j \overline{q}_j - \left(D^T \dot{D}\, \overline{\mathbf{p}}\right)_j , \tag{4.117}$$

where Ω_j is the square root of the j^{th} eigenvalue of Ω^2. Poulsen *et al.* integrate these equations with an algorithm that is accurate to first order in the size of the time step (see Appendix in Ref. 46). We instead integrate the equations (4.114) and (4.115) directly. By using Jacobi's formula for the derivative of a determinant and conservation of energy, it is straightforward to use the same approach as in the one-dimensional case to demonstrate the conservation of the multidimensional distribution.

4.9 Practicalities

4.9.1 Imaginary frequencies

For a general potential, the square of the Feynman-Kleinert frequency matrix is not guaranteed to remain positive definite. In this case the distribution for the planet momentum in the planetary model TCF becomes ill-defined. To remedy this problem we set any negative eigenvalues of the square of the effective frequency matrix to zero, in accordance with the procedure described in the original formulation of the planetary model in Ref. 45 under the name FK-QCW(1), which is consistent with the limiting distribution of the planet momentum as a Dirac delta function. This modification does not affect the conservation of the quantum Boltzmann distribution and maintains the exactness of the TCF in the harmonic limit which is otherwise lost if the planet momentum distribution is heuristically modified (as in FK-QCW(2) in Ref. 45) to extend the method to incorporate imaginary frequencies.

4.9.2 Two practical modifications

To apply the planetary model to large systems we need a practical means of evaluating the Feynman-Kleinert centroid potential of mean force and frequency that

bypasses the non-linear simultaneous equations in (4.102) and (4.103). In previous simulations of large systems using the Feynman-Kleinert approximation, this problem has been greatly simplified by approximating the potential as a linear combination of Gaussian functions.[46,91,94] This allows for exact evaluation of the Gaussian integrals in the definition of the Feynman-Kleinert centroid potential of mean force and frequency. However, we would rather not make this approximation since it limits the method to potentials that can be expanded in this way, which is of course impossible for any sophisticated *ab initio* treatment. Rather, we suggest the use of an alternative to the Feynman-Kleinert frequency.

Since the square of the Feynman-Kleinert frequency is an integral of harmonic fluctuations over the mass-weighted Hessian, it seems likely that a satisfactory frequency would be obtained by integrating the mass-weighted Hessian over the exact fluctuations instead, i.e. by defining the following 'path integral frequency',

$$m\Omega^2 = \frac{1}{N}\sum_{l=1}^{N}\left\langle V''(q_l)\,\delta\left(x - \frac{1}{N}\sum_{j=1}^{N} q_j\right)\right\rangle, \tag{4.118}$$

where $\Omega^2 = \Omega^2(x)$, and the thermal expectation value is taken in the space of N ring-polymer beads,

$$\langle A\rangle = \lim_{N\to\infty}\frac{1}{Z}\frac{1}{(2\pi\hbar)^N}\int \mathrm{d}\mathbf{q}\int \mathrm{d}\mathbf{p}\; e^{-\beta_N R(\mathbf{q},\mathbf{p})}A(\mathbf{q}). \tag{4.119}$$

In the normal mode coordinates (as defined previously in (2.62)) we have

$$\sum_{l=1}^{N}\frac{\partial^2 U(\mathbf{q})}{\partial q_l^2} = \sum_{k=-\overline{N}}^{\overline{N}}\frac{\partial^2 U(\mathbf{Q})}{\partial Q_k^2}, \tag{4.120}$$

where $U(\mathbf{q}) = \sum_{l=1}^{N} V(q_l)$ and $\overline{N} = (N-1)/2$. Note that since the potential does not couple the ring-polymer bead coordinates, we also have

$$\frac{1}{N}\sum_{l=1}^{N}\frac{\partial^2 U(\mathbf{q})}{\partial q_l^2} = \frac{\partial^2 U(\mathbf{Q})}{\partial Q_0^2}. \tag{4.121}$$

This allows us to rewrite (4.118) as follows,

$$m\Omega^2 = \frac{1}{N-1}\sum_{k\neq 0}\left\langle \frac{\partial^2 U(\mathbf{Q})}{\partial Q_k^2}\,\delta\left(x - \frac{Q_0}{\sqrt{N}}\right)\right\rangle. \tag{4.122}$$

To avoid evaluation of the Hessian, we use integration by parts to give the following

equivalent estimator,

$$m\Omega^2 = \frac{\beta_N}{N-1}\sum_{k\neq 0}\left\langle \left[F_k^2 - m\omega_k^2 Q_k F_k\right]\, \delta\left(x - \frac{Q_0}{\sqrt{N}}\right)\right\rangle, \tag{4.123}$$

where F_k is the force on the k^{th} normal mode coordinate,

$$F_k = -\frac{\partial U(\mathbf{Q})}{\partial Q_k}. \tag{4.124}$$

This is the first practical modification we propose for the planetary model.

The second practical modification concerns the centroid dynamics and centroid distribution. In the original formulation of the planetary model, Poulsen *et al.* perform the centroid dynamics using Feynman-Kleinert CMD in accordance with the Feynman-Kleinert centroid potential of mean force that appears in the centroid part of the distribution. An approximation to the Feynman-Kleinert centroid potential of mean force could be calculated with the path integral frequency outlined above. However, since the path integral frequency is determined stochastically using (4.123), the method is more computationally stable if we do away with the Feynman-Kleinert approximation for the centroid distribution and rewrite the planetary model TCF as follows,

$$\begin{aligned} C_{AB}(t) = &\int \mathrm{d}Q_0 \int \mathrm{d}P_0\ \rho(Q_0, P_0) \\ &\times \frac{1}{2\pi m\Omega a^2}\int \mathrm{d}\tilde{q}\int \mathrm{d}\tilde{p}\ e^{-\frac{\tilde{q}^2}{2a^2} - \frac{\tilde{p}^2}{2m^2\Omega^2 a^2}} f_A(q,\tilde{p})\, e^{\mathcal{L}t}\, B(q), \end{aligned} \tag{4.125}$$

where $\rho(Q_0, P_0)$ is the exact centroid distribution,[c] and the Liouvillian is modified to

$$\begin{aligned} \mathcal{L} = &\mathcal{L}_0 + \frac{\tilde{p}}{m}\frac{\partial}{\partial\tilde{q}} - m\Omega^2\tilde{q}\frac{\partial}{\partial\tilde{p}} \\ &+ \frac{P_0}{m}\frac{\partial \ln(m^2\Omega^2a^2)}{\partial Q_0}\frac{\tilde{p}}{2}\frac{\partial}{\partial\tilde{p}} + \frac{P_0}{m}\frac{\partial\ln(a^2)}{\partial Q_0}\frac{\tilde{q}}{2}\frac{\partial}{\partial\tilde{q}}, \end{aligned} \tag{4.126}$$

where $\mathcal{L}_0$ is some (to be determined) Liouvillian for the centroid that conserves the distribution $\rho(Q_0, P_0)$. Of course, CMD, RPMD and TRPMD all conserve this distribution. Since our aim is to use the planetary model in the simulation of infrared absorption spectra, we advise against the use of CMD for this purpose because of the curvature problem. We also advise against the use of RPMD because of the

[c] Note that use of the exact centroid distribution with the Feynman-Kleinert description of the fluctuation was proposed in a different context by Liu and Miller in Appendix A of Ref. 89.

spurious resonance problem. Instead, we propose the use of TRPMD which has the advantage of being cheap and efficient and, of course, also allows us to easily evaluate the path integral frequency (4.123) on the fly.

These considerations translate immediately into the multidimensional case. The matrix elements of the multidimensional analogue of the path integral frequency (4.123) are

$$\Omega^2_{ab} = \frac{\beta_N}{N-1} \sum_{k\neq 0} \left\langle \left[\frac{F^a_k F^b_k}{\sqrt{m_a m_b}} - \omega_k^2 \sqrt{\frac{m_a}{m_b}} Q^a_k F^b_k \right] \delta\left(\mathbf{x} - \frac{\mathbf{Q}_0}{\sqrt{N}} \right) \right\rangle , \tag{4.127}$$

where F^a_k is the force on the k^{th} normal mode coordinates of the a^{th} degree of freedom and m_a is the mass associated with that degree of freedom. We direct the reader to Appendix C.3 for a discussion about the computational efficiency of the path integral frequency estimator.

A partial rationalisation of why the path integral frequency might be a good approximation to the Feynman-Kleinert frequency can be made by considering the low and high temperature limits. Using Ramirez and López-Ciudad's minimum energy wavepacket analysis of the centroid-constrained Boltzmann operator,[66] described in more detail in Appendix C.4, it is straightforward to show that, in the $T \to 0$ limit, $m\Omega^2$ is the (pure state) expectation value of $V''(\hat{x})$ taken over the minimum energy wavepacket whose average position is Q_0. In other words,

$$\lim_{T\to 0} m\Omega^2 = \left\langle \Psi(Q_0) \right| V''(\hat{x}) \left| \Psi(Q_0) \right\rangle , \tag{4.128}$$

where $|\Psi(Q_0)\rangle$ is normalised and minimises the energy, $\langle \Psi(Q_0)| \hat{H} |\Psi(Q_0)\rangle$, subject to $\langle \Psi(Q_0)| \hat{x} |\Psi(Q_0)\rangle = Q_0$. Within the Feynman-Kleinert approximation, the same limiting behaviour holds but $\langle x|\Psi(Q_0\rangle$ is further constrained to be a Gaussian. In the $T \to \infty$ limit, both the path integral frequency and the Feynman-Kleinert frequency tend to the same value,

$$\lim_{T\to\infty} m\Omega^2 = V''(Q_0), \tag{4.129}$$

since the ring polymer radius of gyration and the Feynman-Kleinert radius of gyration tend to zero in this limit. These ideas are easily extended to the multidimensional case.

To further explore the effect of our proposed modifications, we compared trajectories for the one-dimensional q-TIP4P/F model of the OH stretch (4.51). This comparison is shown in Figure 4.3. Panel a shows a comparison of the centroid

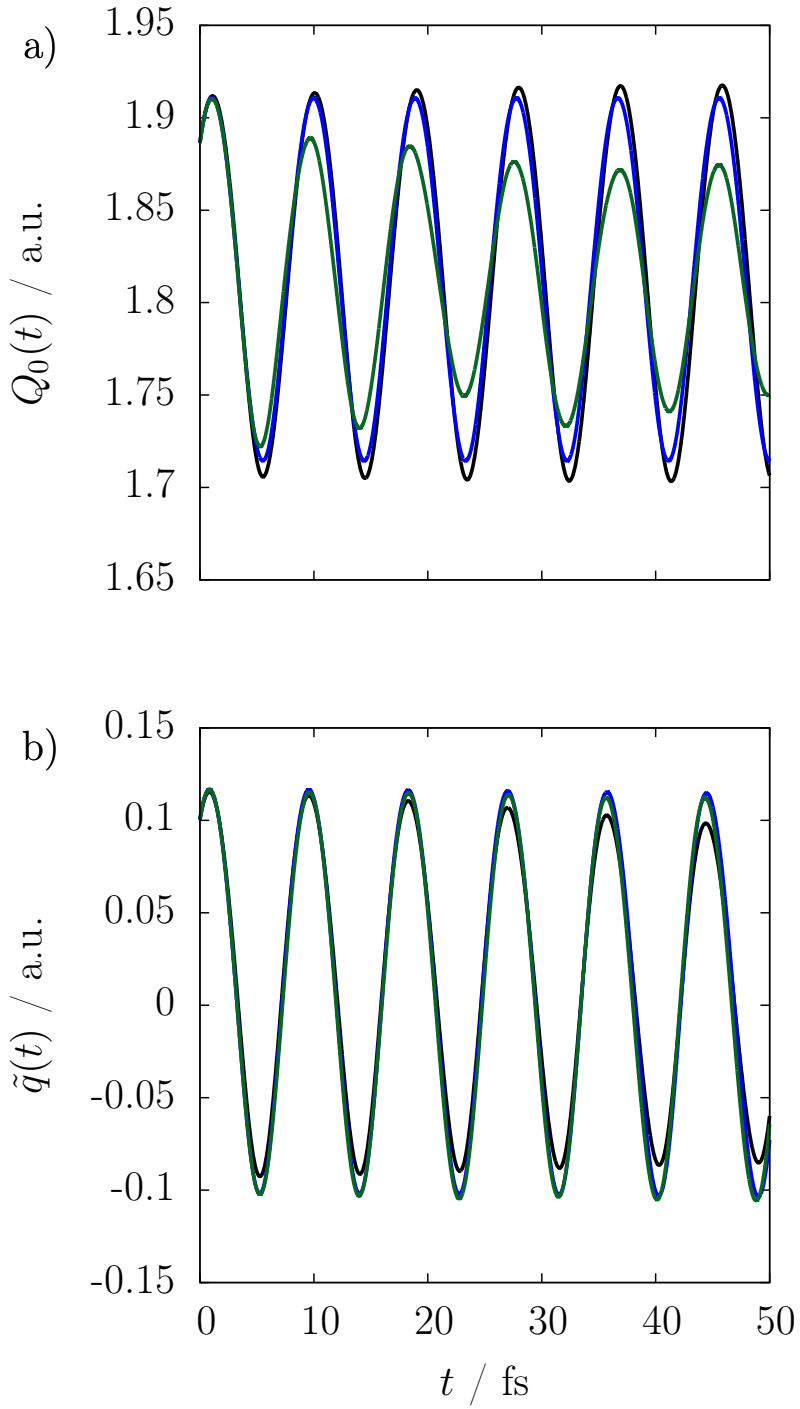

Figure 4.3: Comparison of trajectories for the one-dimensional q-TIP4P/F model (4.51) of the OH stretch at 300K. Panel a shows centroid trajectories while panel b shows trajectories in the fluctuation coordinate $\tilde{q} = q - Q_0$. The black line corresponds to Matsubara dynamics within the Feynman-Kleinert approximation, the blue line corresponds to the original formulation of the planetary model and the green line corresponds to the planetary model with our proposed modifications.

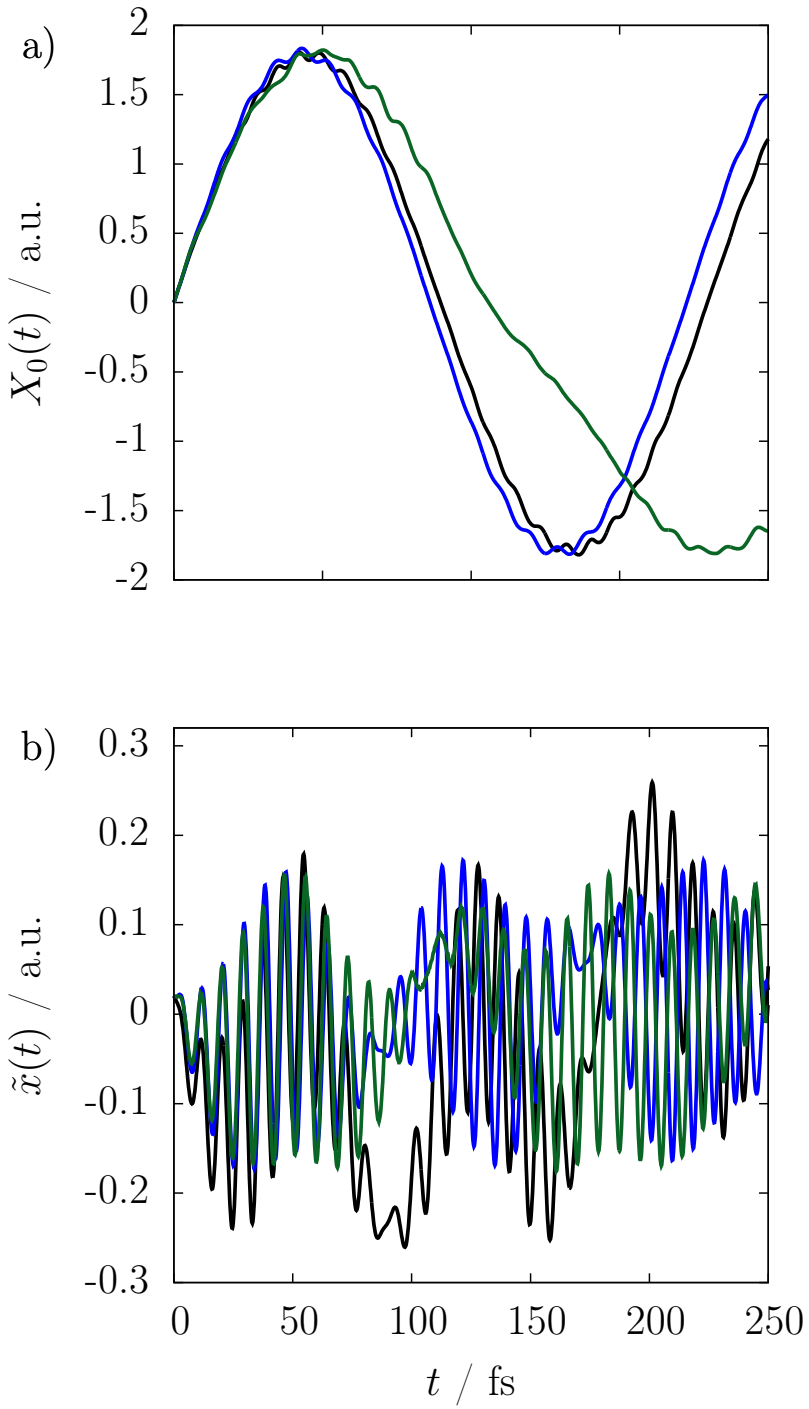

Figure 4.4: Comparison of trajectories for the q-TIP4P/F champagne bottle model of the OH stretch at 300K. Panel a shows centroid trajectories while panel b shows trajectories in the fluctuation coordinate $\tilde{x} = x - X_0$. The black line corresponds to Matsubara dynamics within the Feynman-Kleinert approximation, the blue line corresponds to the original formulation of the planetary model and the green line corresponds to the planetary model with our proposed modifications.

trajectories and panel b shows a comparison of trajectories for the relative planet coordinate $\tilde{q} = q - Q_0$. While the centroid trajectories are significantly different (owing to the coupling of the centroid to the thermostatted fluctuation modes in TRPMD), the planet trajectories with and without the modifications presented in this section are reassuringly similar.

We also compared trajectories for the two-dimensional 'champagne bottle' analogue of the q-TIP4P/F model (a simple extension of (4.51) in polar coordinates where the potential is evaluated in the distance coordinate and the angular coordinate is cyclic). These results are shown in Figure 4.4. Due to the circular symmetry of the potential, the Feynman-Kleinert frequency matrix (and the path integral frequency matrix) can be diagonalised as follows,

$$\Omega^2(\mathbf{Q}_0) = R^T(\theta)\Omega^2(r)R(\theta), \tag{4.130}$$

where $r = \sqrt{X_0^2 + Y_0^2}$, $\theta = \tan^{-1}(Y_0/X_0)$, $\Omega^2(r)$ is a diagonal matrix and $R(\theta)$ is a two-dimensional rotation matrix. One of the diagonal elements of $\Omega^2(r)$ accounts for vibration in the direction of $\mathbf{Q}_0$ (i.e. radially). This manifests itself in the fast oscillations in panel b of Figure 4.4. The other accounts for vibration in the orthogonal direction (i.e. transversally). The latter frequency becomes imaginary for small values of the radial coordinate due to the curvature of the potential. Clearly a harmonic approximation for the dynamics in the orthogonal direction is inadequate since motion in this direction corresponds to rotation, which can only be described harmonically for infinitesimal displacements. This problem is inextricably linked to the harmonic approximation and suggests that the planetary model will be unable to describe rotational dynamics.

Chapter 5

Infrared Absorption Spectroscopy of Water

5.1 Simulation of infrared absorption spectra

According to the golden rule of time-dependent perturbation theory, the product of the Beer-Lambert absorption coefficient $\alpha(\omega)$ and the frequency-dependent refractive index $n(\omega)$ of a liquid with dipole moment operator $\hat{\mu}$ is[69]

$$n(\omega)\alpha(\omega) = \frac{\pi\omega}{2\hbar cV\epsilon_0}\left[1 - e^{-\beta\hbar\omega}\right] I(\omega), \tag{5.1}$$

where $I(\omega)$ is the Fourier transform of the standard quantum dipole moment autocorrelation function,

$$I(\omega) = \frac{1}{2\pi}\int_{-\infty}^{\infty} \mathrm{d}t\; e^{-i\omega t}\,\frac{C_{\mu\mu}(t)}{Z}. \tag{5.2}$$

It is straightforward to show that we may also write

$$n(\omega)\alpha(\omega) = \frac{\pi\omega}{\hbar cV\epsilon_0}\tanh\left(\beta\hbar\omega/2\right) I(\omega), \tag{5.3}$$

where $I(\omega)$ is now the Fourier transform of the real part of the standard quantum dipole moment autocorrelation function. By making use of the harmonic correction factor (2.28) that relates the Fourier transforms of the standard and Kubo quantum TCFs, we may rewrite as follows,

$$n(\omega)\alpha(\omega) = \frac{\pi\beta\omega^2}{3cV\epsilon_0} I(\omega), \tag{5.4}$$

where $I(\omega)$ is the Fourier transform of the quantum Kubo dipole moment autocorrelation function instead.

Of course, the three equations (5.1), (5.3) and (5.4) are equivalent provided $I(\omega)$ is the Fourier transform of an exact quantum dipole moment autocorrelation function. For approximate methods, different infrared absorption spectra $n(\omega)\alpha(\omega)$ will result in general depending on which type of quantum dipole moment autocorrelation function is approximated. Since CMD, RPMD and TRPMD approximate the quantum Kubo TCF, the third form (5.4) is used with those methods. Since the planetary model approximates the standard quantum TCF, we have used the second form (5.3) for the planetary model in this study. Note that it is common when comparing with classical simulations to use the Fourier transform of the classical dipole moment autocorrelation function with the Kubo form (5.4), since this gives the exact result in the harmonic limit if the dipole moment is a linear operator.[69] We followed this convention in this study.

5.2 The q-TIP4P/F model of water

We performed our water simulations with the q-TIP4P/F potential of Habershon *et al.*[109] which has the advantage of being cheap in comparison to other more sophisticated water potentials (e.g. TTM3-F,[110] PS,[111] MB-pol[112,113,114]), while still capturing the important quantum properties of water in the condensed phase. The other commonly used simple point charge water model for approximate quantum simulations is q-SPC/FW of Paesani *et al.*[115] However, owing to its harmonic description of the OH covalent bond stretch, q-SPC/FW is known to incorrectly predict distinct symmetric and antisymmetric stretch peaks in the infrared absorption spectrum of the room temperature liquid which is at odds with experiment.[109] Since the infrared absorption spectrum of liquid water is precisely what we would like to describe, we opted for q-TIP4P/F over q-SPC/FW in this study.

The q-TIP4P/F potential is an empirical water potential based on TIP4P/2005.[116] The intermolecular potential is pairwise additive and identical to that in TIP4P/2005,

$$V_{\text{inter}}(\boldsymbol{r}) = \sum_i \sum_{j>i} \left\{ 4\epsilon \left[\left(\frac{\sigma}{r_{ij}} \right)^{12} - \left(\frac{\sigma}{r_{ij}} \right)^{6} \right] + \sum_{m \in i} \sum_{n \in j} \frac{q_m q_n}{r_{mn}} \right\}, \tag{5.5}$$

where r_{ij} is the distance between the oxygen atoms and r_{mn} is the distance between the partial charge sites in molecules i and j. Two positive charges of magnitude $q_M/2$ are placed on the hydrogen atoms of each molecule and a negative charge of

$-q_M$ is placed at a point $\boldsymbol{r}_M$ a fraction γ along the vector connecting the oxygen atom to the centre of mass of the two hydrogen atoms,

$$\boldsymbol{r}_M = \gamma \boldsymbol{r}_0 + \frac{(1-\gamma)}{2}(\boldsymbol{r}_{H_1} + \boldsymbol{r}_{H_2}). \tag{5.6}$$

The intramolecular part of the potential comprises a harmonic potential for the HOH bend angle and a fourth-order expansion of a Morse potential for each OH covalent bond distance,[109]

$$V_{\text{intra}}(\boldsymbol{r}) = \sum_i \left[V_{OH}(r_{i1}) + V_{OH}(r_{i2}) + \frac{1}{2} k_\theta (\theta_i - \theta_{eq})^2 \right], \tag{5.7}$$

where

$$V_{OH}(r) = D_r \left[\alpha_r^2 (r - r_{eq})^2 - \alpha_r^3 (r - r_{eq})^3 + \frac{7}{12} \alpha_r^4 (r - r_{eq})^4 \right], \tag{5.8}$$

as was described earlier in the thesis (4.51). The variables r_{i1} and r_{i2} are the two OH bond distances and θ_i is the HOH bond angle in the i^{th} water molecule. The four parameters for the intermolecular part of the potential are the same as in TIP4P/2005, while the intramolecular parameters were optimised by Habershon *et al.* in a set of path integral calculations to give good agreement with experimental data for liquid structure, self-diffusion constant and infrared absorption frequencies. All nine of the parameters are to be found in Ref. 109. In practice, evaluation of the intermolecular part of the potential is much more computationally demanding than the intramolecular part. However, the short-range Lennard-Jones interactions can be treated using a sensible cut-off distance, and the long range Coulombic interactions can be accounted for with the Ewald summation technique.[117,118] We employed both of these computational tools in this study.

Since q-TIP4P/F is a point charge model of water, the total dipole moment of a collection of water molecules is simply a linear combination of the atomic displacements,

$$\boldsymbol{\mu}(\boldsymbol{r}) = q_M \gamma \sum_i \left(\boldsymbol{r}^i_{H_1} + \boldsymbol{r}^i_{H_2} \right)/2 - \boldsymbol{r}^i_O, \tag{5.9}$$

where $r^i_{H_1}$ is the position of the first hydrogen atom in molecule i etc.

The linearity of the dipole moment means that the function $f_A(\mathbf{q}, \tilde{\mathbf{p}})$ that appears in the planetary model has the following simple form for the dipole moment in (5.9),

$$f_\mu(\mathbf{q}, \tilde{\mathbf{p}}) = \boldsymbol{\mu}(\mathbf{q}) + i\hbar M^{-1/2} \boldsymbol{\mu} \left[(\Omega A)^{-2} \tilde{\mathbf{p}}_M \right], \tag{5.10}$$

where M is the $F \times F$ mass matrix for the F-dimensional system and $\tilde{\mathbf{p}}_M = M^{-1/2}\tilde{\mathbf{p}}$. Therefore, $f_\mu(\mathbf{q}, \tilde{\mathbf{p}})$ may be replaced with $\boldsymbol{\mu}(\mathbf{q})$ in the real part of the autocorrelation function, i.e.

$$\begin{aligned}\mathrm{Re}\, C_{\mu\mu}(t) =& \frac{1}{(2\pi\hbar)^F} \int \mathrm{d}\mathbf{Q}_0 \int \mathrm{d}\mathbf{P}_0 \; \rho(\mathbf{Q}_0, \mathbf{P}_0) \, \frac{1}{(2\pi)^F \det(\Omega A^2)} \\ & \times \int \mathrm{d}\tilde{\mathbf{q}}_M \int \mathrm{d}\tilde{\mathbf{p}}_M \; e^{-\frac{1}{2}\tilde{\mathbf{q}}_M^T A^{-2} \tilde{\mathbf{q}}_M - \frac{1}{2}\tilde{\mathbf{p}}_M^T (\Omega A)^{-2} \tilde{\mathbf{p}}_M} \, \boldsymbol{\mu}(\mathbf{q}) \cdot e^{\mathcal{L}t} \boldsymbol{\mu}(\mathbf{q}). \end{aligned} \tag{5.11}$$

By again exploiting the linearity of the dipole moment ($\boldsymbol{\mu}(\mathbf{q}) = \boldsymbol{\mu}(\mathbf{Q}_0) + \boldsymbol{\mu}(\tilde{\mathbf{q}})$) we find,

$$\begin{aligned}\mathrm{Re}\, C_{\mu\mu}(t) =& \, \overline{C}_{\mu\mu}(t) + \frac{1}{(2\pi\hbar)^F} \int \mathrm{d}\mathbf{Q}_0 \int \mathrm{d}\mathbf{P}_0 \; \rho(\mathbf{Q}_0, \mathbf{P}_0) \, \frac{1}{(2\pi)^F \det(\Omega A^2)} \\ & \times \int \mathrm{d}\tilde{\mathbf{q}}_M \int \mathrm{d}\tilde{\mathbf{p}}_M \; e^{-\frac{1}{2}\tilde{\mathbf{q}}_M^T A^{-2} \tilde{\mathbf{q}}_M - \frac{1}{2}\tilde{\mathbf{p}}_M^T (\Omega A)^{-2} \tilde{\mathbf{p}}_M} \, \boldsymbol{\mu}(\tilde{\mathbf{q}}) \cdot e^{\mathcal{L}t} \boldsymbol{\mu}(\tilde{\mathbf{q}}), \end{aligned} \tag{5.12}$$

where $\overline{C}_{\mu\mu}(t)$ is the TRPMD dipole moment autocorrelation function. This conveniently splits the planetary model autocorrelation function into two parts which need not be evaluated simultaneously. In practice, we have found that many more initial centroid phase space points must be sampled to converge the TRPMD part of (5.12) than the planetary part. This separation is therefore extremely helpful, since calculation of the planetary part for a given initial centroid phase space point is inherently more time-consuming because it requires calculation of the path integral frequency matrix (4.127). Of course, the same separation applies with the original formulation of the planetary model as well. In that case $\overline{C}_{\mu\mu}(t)$ is the Feynman-Kleinert CMD dipole moment autocorrelation function.

5.3 The single molecule

The infrared absorption spectrum of water in the gas phase is extremely complex. The vibrations of the water molecule involve combinations of symmetric stretching, asymmetric stretching and bending of the covalent bonds. These vibrations are coupled to the rotational motion of the molecule which leads to a complicated rotational fine structure. To accurately reproduce the infrared absorption spectrum requires the use of a sophisticated potential and dipole moment surface in combination with a quantum treatment of the nuclear dynamics in order to account for quantum coherence. Of course, such a treatment is beyond the intended scope of the methods described in this thesis.

However, by calculating an exact quantum autocorrelation function for the q-

TIP4P/F potential, and by heuristically damping its oscillations to simulate quantum decoherence, we may generate an approximation to the quantum infrared absorption spectrum of condensed-phase q-TIP4P/F water. By then comparing the result with single-molecule infrared absorption spectra from approximate methods, this approach enables us to better assess the accuracy of those methods in a genuine condensed phase simulation where a quantum calculation is too computationally expensive. Of course, we may also compare with experiment in the condensed phase. However, the approximate nature of the q-TIP4P/F potential will inevitably contribute to observed differences that may then be incorrectly attributed to deficiencies in the approximate method rather than the potential.

5.3.1 Computational details

To calculate the quantum results in this study, we implemented the q-TIP4P/F potential and dipole moment surface into the DVR3D package of Tennyson *et al.*[6] This package gives the energy levels of the system and the matrix elements of the dipole moment operator in the basis of eigenstates. We combined these to compute the real part of the standard quantum dipole moment autocorrelation function. To simulate the effect of rapid quantum decoherence in the condensed phase, we applied a Hann window (raised cosine) to the quantum autocorrelation function before taking its Fourier transform. The Hann window is given by[119]

$$w(t,\Delta t) = \begin{cases} \frac{1}{2}\left(\cos\left(\pi t/\Delta t\right)+1\right) & |t| \leq \Delta t \\ 0 & \text{elsewhere} \end{cases}. \tag{5.13}$$

At each temperature, we chose the parameter Δt to be commensurate with the correlation time of the classical dipole moment autocorrelation function ($\Delta t = 500\,\text{fs}$ (150K), 400 fs (300K) and 300 fs (600K)). We extended the autocorrelation function to $t < 0$ through reflection about $t = 0$ (the real part of the autocorrelation function is an even function of time) before applying the Hann window. We then calculated its Fourier transform using an algorithm that is based on the fast Fourier transform.[84] The result was then inserted into (5.3) with an arbitrary volume to produce the infrared absorption spectrum.

To calculate the classical and TRPMD results, we calculated each dipole moment autocorrelation over a total of 10^6 independent trajectories of length 2 ps. These were then treated using the same Hann window as for the quantum results before taking their Fourier transforms (to mitigate ringing in the spectra). To ensure independence of trajectories for the classical simulations we employed an Andersen

thermostat to resample momenta.[120] We used a time step of $\Delta t = 0.25\,\text{fs}$ for both methods with a symmetric velocity Verlet algorithm (classical) and the algorithm described in Ref. 47 to integrate the TRPMD equations of motion. To converge the TRPMD results with respect to the number of ring-polymer beads we used $N = 64$ (150K), 32 (300K) and 16 (600K).

To calculate the planetary model results, we used the same TRPMD code with a symmetric algorithm for alternating propagation of the centroids (TRPMD) and planets (see equations (4.114) and (4.115)) with a time step of $\Delta t = 0.25\,\text{fs}$. At each temperature we used the same number of ring polymer beads as mentioned previously for the TRPMD simulations. To calculate the path integral frequency matrix, we spawned an independent TRPMD centroid-constrained trajectory of length 64 fs at each time step and calculated the thermal average (4.127) as a time average along the trajectory. We used a total of 64 independent initial planet phase space points (drawn from the relevant normal distribution: $\overline{q}_j, \overline{p}_j \sim \mathcal{N}(0,1)$ for $j = 1, 2, \ldots F$) to converge the integrals over the distribution of the planets. We calculated the dipole moment autocorrelation over a total of 10^4 independent centroid trajectories of length 2 ps (one for each of the 64 initial positions and momenta of the planets). The aforementioned Hann window and Fourier transform procedure was then used for each autocorrelation function to generate the infrared absorption spectra.

5.3.2 Infrared absorption spectra

The effect of the Hann window on the quantum infrared absorption spectrum at 300K is shown in Figure 5.1. Without application of the Hann window, the infrared absorption spectrum shows the presence of hundreds of lines representing the many rovibrational transitions that are thermally accessible to the molecule. After application of the Hann window, the rotation band adopts a broad lineshape, the bend band shows two distinct peaks and the stretch band shows a broad lineshape with the remnants of a little rotational structure. The bend band comprises the P, Q and R branches of the bend vibration with an unpronounced Q branch (the bend vibration changes the dipole moment along the molecular symmetry axis). The stretch band comprises the P, Q and R branches of the symmetric and asymmetric stretch vibrations. The Q branch of the asymmetric stretch is pronounced since it changes the dipole moment along an axis that is perpendicular to the molecular symmetry axis. The symmetric stretch contributes much less to the stretch band since it is associated with a smaller change in dipole moment. Application of the Hann window also washes out the first overtone of the bend vibration at approximately $3200\,\text{cm}^{-1}$.[121,122]

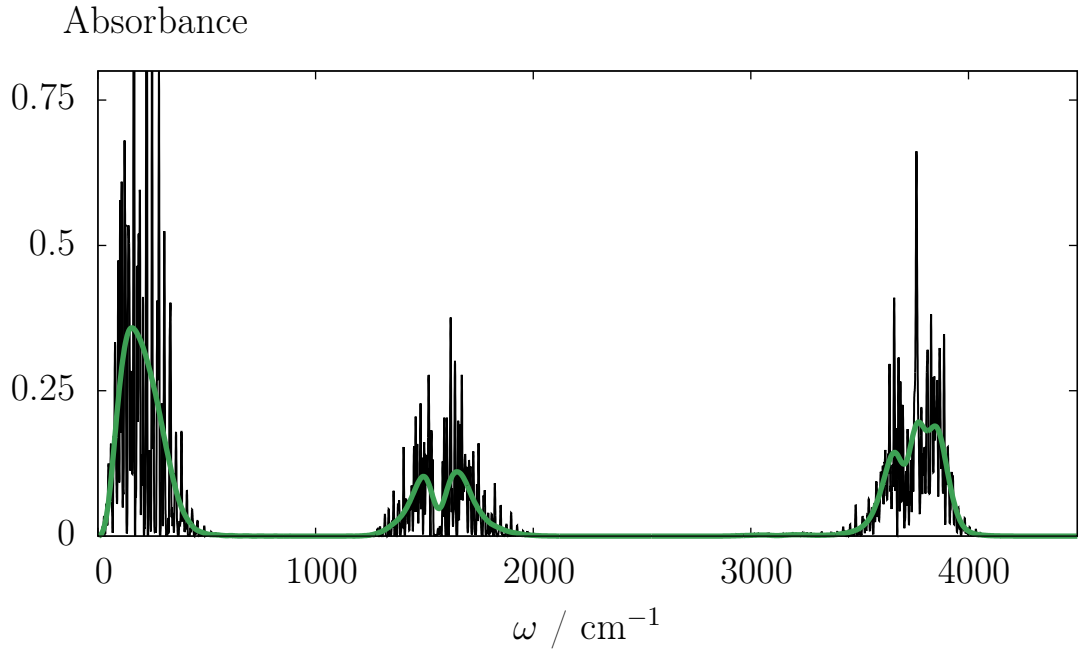

Figure 5.1: Infrared absorption spectrum for the q-TIP4P/F water molecule at 300K. The absorbance is given in arbitrary units. The black and green lines show the infrared absorption spectra with the use of the Hann window (green) and without (black).

The infrared absorption spectra for all of the methods at 150K, 300K and 600K are shown in Figure 5.2. The insets show the stretch band over 3300 cm^{-1} to 4250 cm^{-1}. The first point to note is that the classical stretch band is shifted to the blue at all temperatures (and by some 100 cm^{-1} relative to the quantum stretch band at 150K). This relative shift is accounted for by the significant zero-point energy of the anharmonic OH covalent bond and highlights the importance of a correct description of the quantum Boltzmann statistics in water. The planetary model and TRPMD stretch bands are much closer to the quantum result at the three plotted temperatures because they correctly account for the quantum Boltzmann statistics.

The second point to note is the emergence of a shoulder in the rotation band for the planetary model at 300K, and the emergence of a spurious peak between the rotation and bend band at 150K. We found that setting the lowest six eigenvalues of the path integral frequency matrix to zero removed the shoulder and spurious peak. These are therefore caused by the harmonic description of the free rotation of the water molecule as described previously (see Chapter 4). This effect becomes more pronounced as the temperature decreases for two reasons. Firstly, the spurious frequencies associated with rotation increase because the ring polymer in the path integral frequency estimator becomes more delocalised along the rotation co-

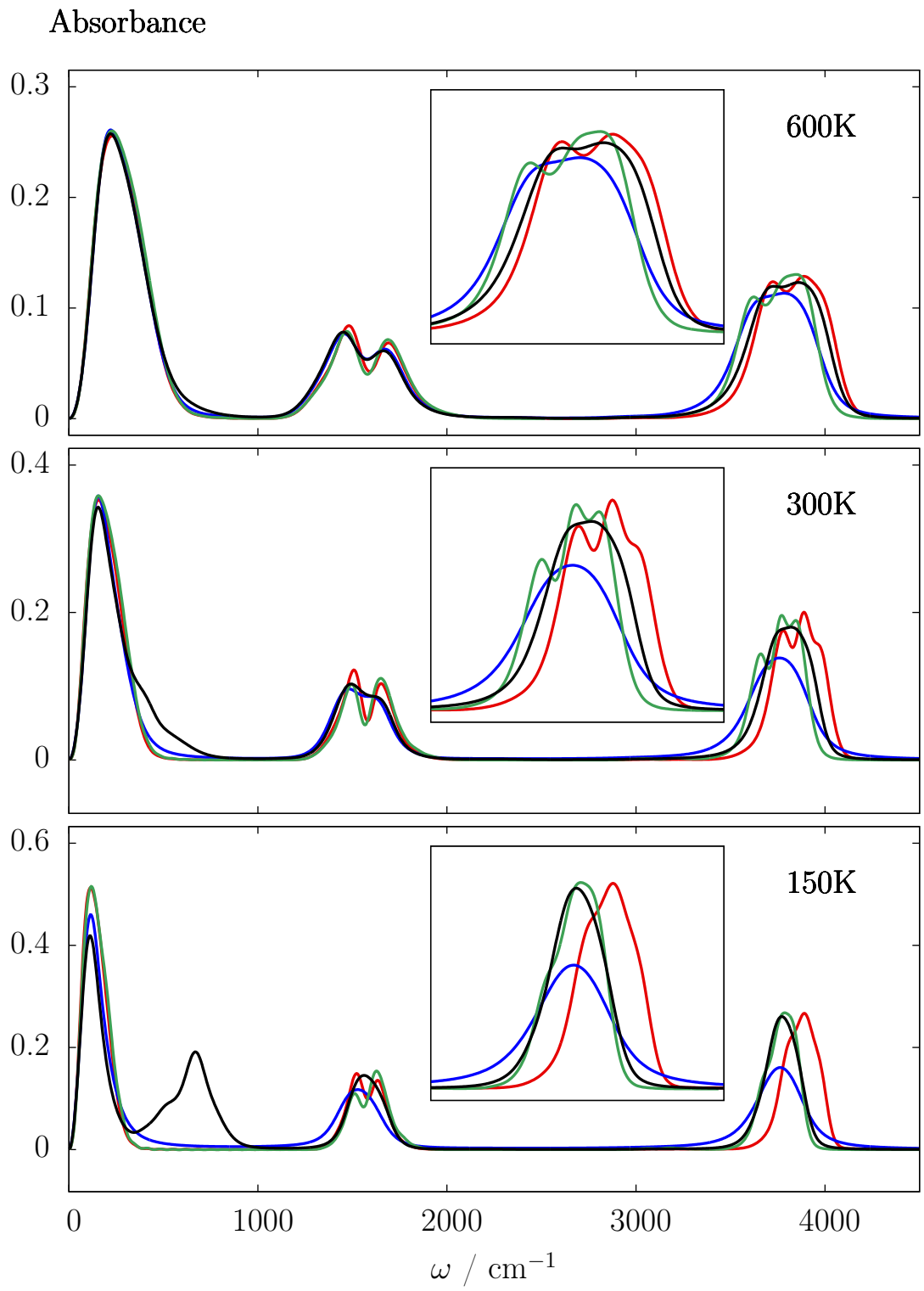

Figure 5.2: Infrared absorption spectra for the q-TIP4P/F water molecule at 150K, 300K and 600K. The absorbance is given in arbitrary units. The lines correspond to the planetary model (black), classical (red), TRPMD (blue) and quantum (green). The insets show the stretch band over 3300 cm^{-1} to 4250 cm^{-1}.

ordinates. Secondly, the weight of the planetary contribution to the dipole moment autocorrelation function increases relative to the centroid contribution (see (5.12)). This is seen as a loss of absorbance of the rotational band in the correct region, which results from the adequate TRPMD description of rotation, and an increase in absorbance of the spurious peak. As alluded to previously, these results suggest that the planetary model spectra should not be trusted for low frequencies.

However, at 150K where the rotation band is most poorly described, the stretch band of the planetary model result is in remarkably good agreement with the quantum result in position, absorbance and lineshape. This is in contrast to the TRPMD result which shows a broadened lineshape and an absorbance that is nearly a factor of two too small. This promising observation suggests that the incorrect planetary model description of the rotational dynamics of the molecule does not contaminate the vibrational dynamics. This is a useful property since the stretch band is the portion of the spectrum that is most poorly described by CMD, RPMD and TRPMD at low temperatures.

Notice further that the planetary model and TRPMD results do not show rotational structure to the same extent that the classical and quantum results do. For instance, the bend band of the spectrum is not split at all for either method at 150K. This is caused by the thermostatting of the fluctuation modes in TRPMD which suppresses dynamical coupling of the vibrational and rotational motion. The absence of this structure is not so concerning since our intention is to adequately describe the infrared absorption spectroscopy of water in the condensed phase and condensed-phase infrared absorption spectra of water are almost devoid of rotational structure. While the original formulation of the planetary model by Poulsen *et al.* does lead to the presence of rotational structure in the stretch and bend bands for the single q-TIP4P/F molecule, the infrared absorption spectrum at 150K exhibits a spurious combination band that results from the modulation of the planetary model rotation frequencies at a rate governed by the centroid stretching motion. This point is developed further in Appendix D.1.

5.4 The condensed phase

5.4.1 Computational details

We used the i-PI package of Ceriotti *et al.*[123] (including the packaged q-TIP4P/F driver) to calculate the classical, TRPMD and planetary model infrared absorption spectra of q-TIP4P/F water in the condensed phase. We simulated hexagonal ice

at 150K, liquid at 300K and (compressed) liquid at 600K under periodic boundary conditions. Our simulation box consisted of 96 water molecules for hexagonal ice and 128 water molecules for the liquid at 300K and 600K.[a] These are the same thermodynamic conditions as were used by Rossi *et al.* in Ref. 124. To determine the size of the simulation box we used the experimental density of hexagonal ice and the liquids at the relevant temperatures, which at 600K was the density of the liquid at the liquid-vapour coexistence point. To generate initial hexagonal ice geometries at 150K we used a Monte Carlo procedure[125] to ensure consistency with the Bernal-Fowler rules[126] which were then evolved under thermostatted ring-polymer or classical (Andersen thermostatted) dynamics. The initial liquid configurations were generated straightforwardly using only the thermostatted ring-polymer or classical dynamics.

We used a time step of $\Delta t = 0.25\,\text{fs}$ for all the simulations and $N = 64$ (150K), 32 (300K) and 16 (600K) ring-polymer beads for the TRPMD and planetary model simulations in accordance with the previous study by Rossi *et al.*[124] For the classical and TRPMD simulations we calculated the autocorrelation of the total dipole moment derivative of the simulation box over 256 independent trajectories of length 10 ps. We then applied the aforementioned Hann window and Fourier transform procedure ($\Delta t = 500\,\text{fs}$) to the autocorrelation functions to generate the infrared absorption spectra, making use of the following relation,

$$\frac{1}{2\pi}\int_{-\infty}^{\infty} \mathrm{d}t\; e^{-i\omega t}\,\langle \dot{\boldsymbol{\mu}}\cdot\dot{\boldsymbol{\mu}}(t)\rangle = \frac{\omega^2}{2\pi}\int_{-\infty}^{\infty} \mathrm{d}t\; e^{-i\omega t}\,\langle \boldsymbol{\mu}\cdot\boldsymbol{\mu}(t)\rangle\,. \tag{5.14}$$

There are three important computational differences between how we calculated the planetary model infrared absorption spectra for the single molecule and the condensed phase. Firstly, we found that we need not calculate the path integral frequency matrix every 0.25 fs, but could rather calculate it every 1 fs and use linear interpolation to approximate the intervening matrices without any loss in quality of the resulting infrared absorption spectra. Secondly, we found the eigenvalues of the path integral frequency matrix to converge more slowly in the condensed phase than for the single molecule for the following reason. The converged path integral frequency matrix is sparse and nearly block diagonal when fully converged, but noise in the underconverged matrix elements associated with pairs of atoms that are well-separated in space leads to a slow convergence of the eigenvalues. To remedy this problem we took the Hadamard product of the following screening matrix with the

[a] We also simulated the 300K and 600K liquids with a simulation box of 64 water molecules and found the resulting infrared absorption spectra to be almost indistinguishable to graphical accuracy.

path integral frequency matrix,

$$S_{ab} = \exp\left(-\gamma^2 r_{ab}^2\right), \tag{5.15}$$

where γ is an adjustable parameter and r_{ab} is the distance between the centroids that pertain to the a^{th} and b^{th} degrees of freedom. We found that a value of $\gamma = 0.10\,\text{a.u.}^{-1}$ was sufficient to give the same result as with a smaller value (we also simulated with $\gamma = 0.25, 0.13, 0.11, 0.09, 0.08\,\text{a.u.}^{-1}$) but without the expense of significantly longer centroid-constrained TRPMD trajectories. With this modification we were able to use centroid-constrained TRPMD trajectories of length 128 fs. Thirdly, we exploited the different convergence properties of the TRPMD and planetary parts of the autocorrelation function in (5.12) by calculating each part in a separate simulation. We have already described the calculation of the TRPMD part, while for the planetary part we found we obtained a converged infrared absorption spectrum by correlating the total dipole moment of the simulation box over only 8 trajectories of length 2 ps at each temperature. As for the simulations of the single q-TIP4P/F water molecule, we used a total of 64 independent initial planet phase space points to converge the integrals over the phase space distribution of the planets. The aforementioned Hann window and Fourier transform procedure ($\Delta t = 500\,\text{fs}$) was then applied to these autocorrelation functions to generate the planetary contributions to the infrared absorption spectra.

For comparison, we extracted CMD infrared absorption spectra data for the same thermodynamic conditions from Ref. 124. The authors present their infrared absorption spectra in arbitrary units so we scaled the extracted CMD data by the same ratio as that required to match the absorbances of our TRPMD results with the TRPMD results in the same paper.[124]

5.4.2 Infrared absorption spectra

The results of our simulations of condensed-phase q-TIP4P/F water are shown in Figure 5.3. Hydrogen bonding in the condensed phase has a pronounced effect on the infrared absorption spectrum of water as is clear from a comparison of Figure 5.2 and Figure 5.3. For example, hindered rotation of hydrogen-bonded molecules leads to a blueshift of the libration (rotation) band in comparison to that for the single molecule. Hydrogen bonding also leads to a redshift of the stretch band since it weakens the OH covalent bond stiffness. This is the opposite effect to what is found for the bend band, which is blueshifted relative to that for the single molecule. All three of these effects become more pronounced with a decrease in temperature

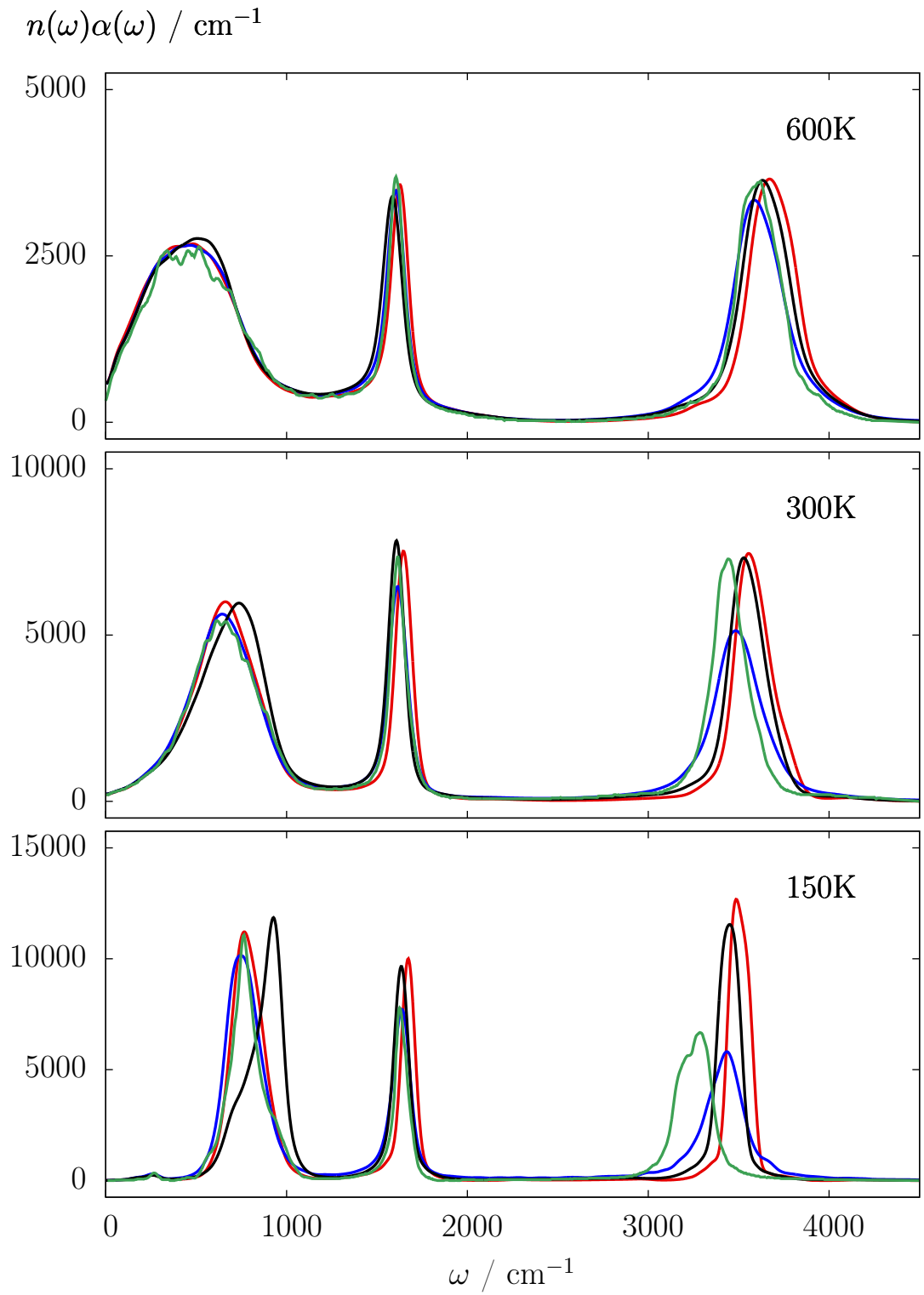

Figure 5.3: Infrared absorption spectra for q-TIP4P/F hexagonal ice (150K), liquid (300K) and compressed liquid (600K). The lines correspond to the planetary model (black), classical (red), TRPMD (blue) and CMD (green).

because the hydrogen bond network is longer-lived at lower temperatures.

The most noticeable difference between the planetary model results in the single-molecule and condensed-phase figures is the improvement in the appearance of the libration (rotation) band. At 150K the planetary model libration band is shifted to the blue and shows a shoulder (the underlying TRPMD peak) but has not bifurcated like it has in the single molecule case. Clearly, the harmonic approximation is less crude for hindered rotation in the condensed phase than for free rotation in the single molecule.

Besides the libration band, the relative positions and absorbances of the planetary model and TRPMD bands are very similar between the single-molecule and condensed-phase figures. For example, at 150K the absorbance of the planetary model stretch band is approximately twice that of TRPMD for both the single-molecule and condensed-phase infrared absorption spectra. Likewise, the positions of the planetary model and TRPMD stretch bands are in very good agreement at 150K in both figures; the maximum of the planetary model stretch band lies approximately $10\,\mathrm{cm}^{-1}$ to the blue of the TRPMD maximum (see Appendix D.2 for tabulated spectroscopic data). By comparing with the exact quantum result for the single water molecule, we were able to determine that the planetary model provides a good representation of the stretch band for that system at 150K. We are unable to make such a comparison with an exact quantum q-TIP4P/F condensed-phase infrared absorption spectrum because the calculation of such a result is infeasible. However, it is reassuring to see that the planetary model and TRPMD stretch bands respond consistently to changes in the composition of the system. This observation leads us to speculate that the planetary model provides a good representation of the stretch band in both the condensed-phase and single-molecule systems, especially at 150K.

As for the single-molecule results, the agreement between the absolute positions of the maxima of the planetary model and TRPMD stretch bands is excellent at 150K but slightly worse at 300K and 600K, where the maximum of the planetary model stretch band lies approximately $50\,\mathrm{cm}^{-1}$ to the blue of the TRPMD maximum at both temperatures. However, the agreement with the positions of the CMD stretch band is significantly worse at 150K and 300K. At 150K, the CMD stretch band is shifted to the red from the TRPMD and planetary model results by some $150\,\mathrm{cm}^{-1}$. This discrepancy is almost certainly the result of the curvature problem in CMD at this low temperature, but at 300K the importance of the curvature problem for condensed-phase water simulations with CMD is not fully resolved.

This is partly because the position of the stretch band in a PA-CMD infrared

absorption spectrum is strongly affected by the details of the thermostatting of the fluctuation modes.[95,124] The absolute position of the stretch band is also strongly dependent on the water potential and dipole moment surface. For the condensed-phase q-TIP4P/F and q-SPC/FW models, the CMD stretch band is consistently redshifted relative to TRPMD/RPMD at 300K.[69,47] A comparison of Figure 5.2 and Figure 5.3 suggests that the curvature problem is responsible for this difference in the q-TIP4P/F water model since the TRPMD stretch band position is in good agreement with the quantum result in Figure 5.2. However, Medders *et al.* have shown that the position of the CMD stretch band at 300K is in good agreement with experiment for the MB-pol potential and dipole moment surface (MB-μ).[61]

Comparisons between CMD and LSC-IVR have also been made in the literature which have led to different conclusions about the importance of the curvature problem at room temperature. For example, with the TTM3-F potential and dipole moment surface, the CMD stretch band at 300K was found by Liu to be redshifted relative to the experimental result but blueshifted relative to the LSC-IVR result.[35] On the other hand, with the q-SPC/FW potential and dipole moment surface, Liu *et al.* found the CMD stretch band at 298K to be significantly redshifted relative to the LSC-IVR result, with both blueshifted relative to the experiment.[93] However, LSC-IVR infrared absorption spectra must be interpreted with caution since the stretch band position is known to be susceptible to a redshift that is dependent on how strongly the TCF is damped before its Fourier transform is taken.[95] Of course, strong damping minimises the long-time contribution of the TCF to its Fourier transform. Since the non-conservation of the quantum Boltzmann distribution becomes increasingly important at long times, the redshift in LSC-IVR is likely to be closely related to this well-known shortcoming.

5.5 Motional narrowing and lineshapes

The results in this chapter lead us to speculate on the importance of explicit time-dependence in the path integral frequency matrix. Are the planetary model spectra in Figure 5.3 simply a reflection of the static distribution of the path integral frequencies (the square roots of the eigenvalues of (4.127))?

To answer this question we repeated the planetary model simulations with the path integral frequency matrix held constant for the dynamics of the planets. This, of course, keeps the radius of gyration matrix constant as well. The infrared absorption spectrum that resulted from the planetary part of (5.12) at 300K is shown in Figure 5.4. As is clear from the figure, this modification has a drastic effect

which suggests that the planetary model spectra are not simply a reflection of the static distribution of frequencies. In particular, the bend and stretch bands are distorted through broadening and appear to no longer hold a Lorentzian lineshape. The stretch band is of a broad Gaussian shape that is some three to four times wider than the full width at half maximum of the previously-presented planetary model stretch band. We found this modification to have the same effect at 150K and 600K as well (results omitted).

The relevant theory to describe this phenomenon is that of motional narrowing. In the absence of a time-dependent path integral frequency matrix, the dynamics of the planets can be mapped onto an exact harmonic dynamics with each eigenfrequency constant in time. This leads to the broad bands in Figure 5.4 that directly reflect the static distribution of eigenfrequencies. However, with a time-dependent path integral frequency matrix, the modulation of each eigenfrequency can sharpen these peaks.

The physics of motional narrowing in this context is described concretely by Kubo's stochastic theory of lineshape.[48] Kubo identifies two important quantities for the effect of frequency modulation on lineshapes by a stationary process. These are the time-independent standard deviation of the frequency,

$$\Delta = \left\langle \Omega^2 \right\rangle^{1/2}, \tag{5.16}$$

and its correlation time,

$$\tau_c = \frac{1}{\Delta^2} \int_0^\infty \mathrm{d}t \, \langle \Omega\Omega(t) \rangle \, . \tag{5.17}$$

These equations are for a one-dimensional system but, of course, for a multidimensional system the frequency $\Omega(t)$ represents one of many eigenfrequencies. If the condition $\Delta\tau_c \gg 1$ is satisfied then the modulation of the frequency is slow, while if $\Delta\tau_c \ll 1$ is satisfied then the modulation is fast. For fast modulation the spectrum of an oscillator that moves under the stochastic frequency $\Omega(t)$ shows motional narrowing: the lineshape becomes sharp with Lorentzian form. In the opposite limit, the lineshape is a direct reflection of the random distribution of the frequency.[48]

To reach this conclusion, Kubo assumes that the environment, as experienced by the system through the stochastic frequency $\Omega(t)$, is insensitive to the motion of the system. This is precisely the situation in the planetary model where the centroid is to be identified with the environment and the planet with the system. We therefore conclude that the planetary model infrared absorption spectra show the phenomenon of motional narrowing due to the unidirectional interaction of the

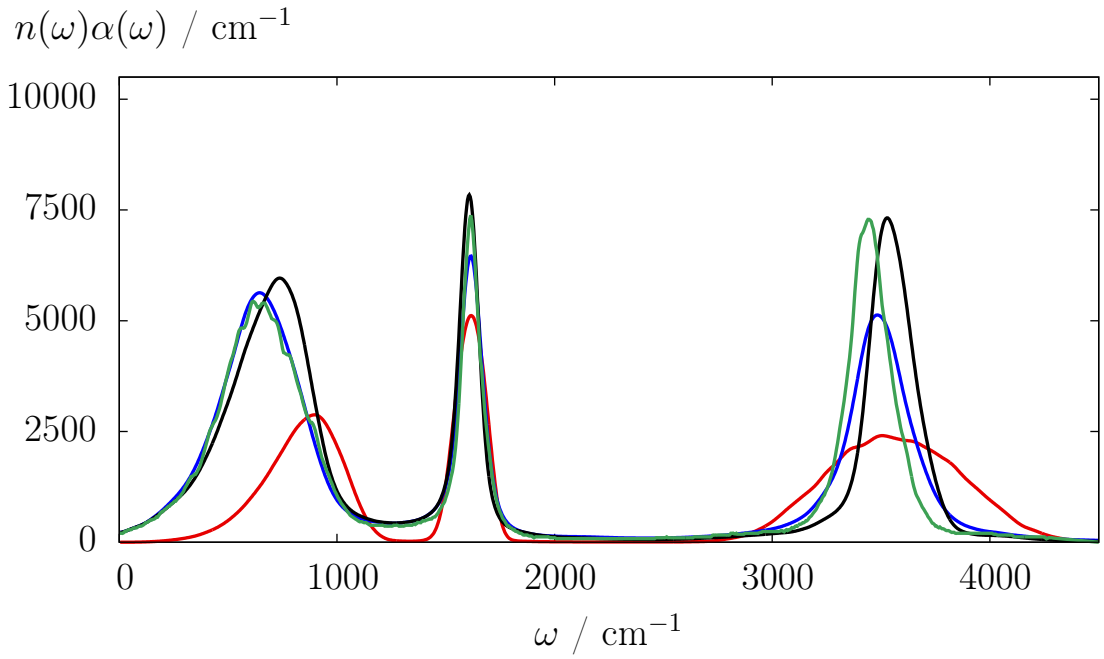

Figure 5.4: Infrared absorption spectra for q-TIP4P/F liquid water at 300K. The lines correspond to the planetary model (black), TRPMD (blue), CMD (green) and the planetary model with a time-independent path integral frequency matrix (red).

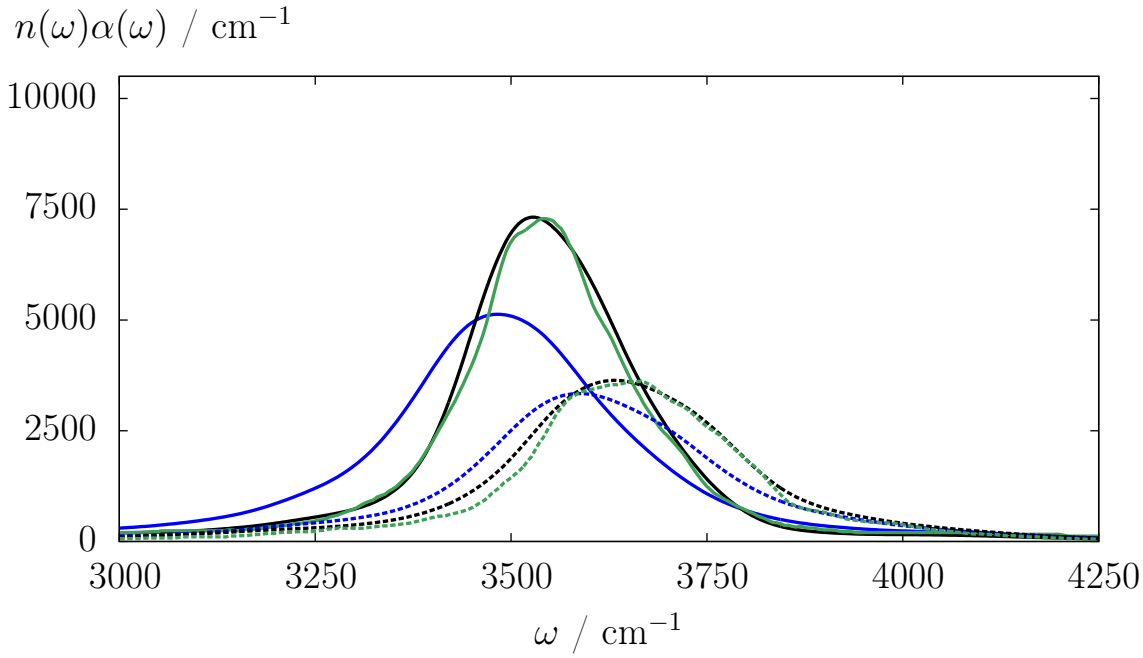

Figure 5.5: Comparison of stretch band lineshapes for the q-TIP4P/F liquid (300K) and compressed liquid (600K). The lines correspond to the planetary model (black), TRPMD (blue) and CMD (green). The 300K results are plotted with solid lines while the 600K results are plotted with dotted lines. At each temperature, the CMD band has been shifted to overlap with the planetary model band.

planet with the centroid through the time-dependent path integral frequency matrix.

Notice that the standard deviation of the frequency (5.16) is a static property and the correlation time (5.17) is a zero-frequency property of the system. It is well known that CMD, RPMD and TRPMD provide a consistent description of zero-frequency properties like the self-diffusion constant.[68] This suggests that for calculation of infrared absorption spectra, all of these methods would reproduce the effect of motional narrowing, and to the same extent, and the question of which in particular to use for the planetary model boils down to one of convenience.[b] In other words, all three of the methods when used with the planetary model would lead to the same, consistent description of the fluctuation dynamics.

To further investigate the accuracy of the narrowed stretch band in the planetary model infrared absorption spectra, we compare the stretch bands of the CMD, TRPMD and planetary model condensed-phase results at 300K and 600K in Figure 5.5. To aid the comparison of lineshapes and absorbances, we shifted the CMD stretch bands to match their median values with the planetary model results. As is clear from the figure, at both temperatures the CMD and planetary model lineshapes and absorbances are in remarkably good agreement. On the other hand, the TRPMD lineshape is noticeably distorted at 300K because of the thermostatting of the fluctuation modes. While the absolute positions of the planetary model and CMD stretch bands differ, these results suggest that CMD and the planetary model provide an equivalent description of the non-trivial structure of the stretch band for q-TIP4P/F at temperatures exceeding 300K through fundamentally different approaches. This is a promising result for motional narrowing in the planetary model since CMD in conjunction with the TTM3-F water model has been shown to give a good description of experimental lineshapes for condensed-phase infrared absorption spectra.[127] These considerations strengthen our earlier speculation that the planetary model provides a good representation of the stretch band of the condensed-phase infrared absorption spectrum of q-TIP4P/F at 150K, where the CMD stretch band is unambiguously distorted and redshifted by the curvature problem.

[b] Of course, LSC-IVR does not provide a consistent description of zero-frequency properties since the quantum Boltzmann distribution is not conserved.[37]

Chapter 6

Conclusions

In this thesis we have derived Matsubara dynamics, a theory for rigorously combining quantum statistics and classical dynamics in approximate quantum time-correlation functions (TCFs).[43] Matsubara dynamics is based on the classical dynamics of the Fourier coefficients (Matsubara modes) of an imaginary-time path in the quantum Kubo TCF. We have shown that, remarkably, if this imaginary-time path is constrained to remain a smooth function of imaginary time (a linear combination of Matsubara modes), then the quantum dynamics reduces to the classical dynamics of the Matsubara modes. Owing to its invariance with respect to imaginary-time translation, Matsubara dynamics conserves a complex phase factor that appears in the quantum Boltzmann distribution. Since the Matsubara phase and Hamiltonian are constants of the motion, the quantum Boltzmann distribution is conserved.

Before our development of Matsubara dynamics, the pre-eminent theory for combining quantum statistics and classical dynamics in approximate quantum TCFs that exclude quantum coherence was the Linearised Semiclassical Initial Value Representation (LSC-IVR).[35] In principle, the LSC-IVR description of water could predict the spontaneous boiling of the liquid at room temperature.[2] Of course, the neglect of quantum coherence is not to blame for this shortcoming. The source of this and other spurious predictions is, as is well known, the erroneous redistribution of energy over time which results from the non-conservation of the quantum Boltzmann distribution.[37]

The fact that LSC-IVR fails to conserve the quantum Boltzmann distribution renders it inadequate as a theory from which to derive any approximate method that does, such as the popular Centroid Molecular Dynamics (CMD) and Ring Polymer Molecular Dynamics (RPMD) methods.[38,55] CMD and RPMD were generally considered to be *ad hoc*, but we have shown that both result from quantifiable approximations to the Matsubara dynamics TCF. In the case of CMD, the approxi-

mation is that of a mean field taken over the fluctuation (non-centroid) modes, while for RPMD it is the neglect of an imaginary part of the Matsubara Liouvillian that governs the dynamics of a set of analytically-continued Matsubara modes.[44] Since the RPMD approximation only affects the dynamics of the fluctuation modes, this analysis shows that RPMD is ultimately a short-time approximation to Matsubara dynamics for TCFs involving observables that are linearly-dependent on position. This analysis also explains the origin of the shortcomings of CMD and RPMD, which are most apparent in non-linear TCFs, and ultimately result from their incorrect description of the (Matsubara) fluctuation dynamics.

Like CMD and RPMD, the recently-developed approximate method of Poulsen *et al.*, the planetary model,[45] also conserves the quantum Boltzmann distribution, suggesting that it is related to Matsubara dynamics. We have shown that the planetary model is indeed equivalent to an approximation to the Matsubara dynamics two-point TCF for a particular imaginary-time separation $\tau = 0$ of two points on the imaginary-time path. This approximation arises naturally from Matsubara dynamics by invoking the Feynman-Kleinert approximation,[56] a variationally-optimal locally-harmonic approximation for the fluctuation modes, then uncoupling the dynamics of these modes from the centroid. By comparing trajectories, we found that this approximation is a faithful approximation to Matsubara dynamics for weakly anharmonic systems but does not work well for low-frequency anharmonic motions such as rotations and librations.

To make the planetary model more practical for the simulation of large systems, we have proposed two practical modifications. The first is the use of thermostatted RPMD (TRPMD)[47] instead of Feynman-Kleinert CMD for the evolution of the centroid coordinate. The second is the use of an alternative to the Feynman-Kleinert frequency that is consistent with the ring-polymer distribution in TRPMD. Using these practical modifications, we applied the planetary model to a study of the infrared absorption spectroscopy of the q-TIP4P/F water model[109] in the gas phase and condensed phase.

We found, by comparison with exact quantum calculations, that the planetary model gives a good representation of the high frequency portion of infrared absorption spectra for the single molecule but a poor representation of the low-frequency (rotation) band. For the condensed phase, we showed that the libration band is better reproduced by the planetary model than the rotation band for the single molecule. We also demonstrated that the planetary model provides a good representation (in position, lineshape and absorbance) of the stretch band in the condensed-phase infrared absorption spectra with a Lorentzian lineshape that is significantly

different from the static distribution of stretch frequencies. We have rationalised this difference on the basis of Kubo's stochastic theory of lineshape[48] which suggests that CMD, RPMD and TRPMD would all give the same, consistent description of fluctuation dynamics when used with the planetary model.

Given that Matsubara dynamics underlies CMD, RPMD and the planetary model, it would be interesting to search for other approximate methods based on the Matsubara dynamics theory in the future. For example, it might be possible to maintain at least part of the imaginary part of the Matsubara Liouvillian that is discarded in RPMD, e.g. by using constraints on the fluctuation modes to stabilise the complex dynamics. It might also be possible to apply a less-severe alternative to the CMD mean-field approximation that does not lead to the curvature problem.

It would certainly be interesting to apply the planetary model to more sophisticated water potentials and dipole moment surfaces (e.g. MB-pol and MB-μ) for infrared absorption spectroscopy or polarisability tensors (e.g. MB-α) for Raman spectroscopy.[112,113,114] To the extent that the planetary model provides a faithful approximation to Matsubara dynamics, it might also be possible to use the planetary model as a tool for determining the importance of an explicit description of fluctuation dynamics for non-linear TCFs. From a practical point of view, this would help to determine the range of validity of centroid-based methods like CMD and RPMD for non-linear dynamical properties. In other words, it would help to clarify the importance of the non-linear operator problem for these methods.[42] More fundamentally, such an analysis would help us to understand how explicit non-linear terms in the Matsubara dynamics TCF affect observable properties like the dynamic structure factor, for example, which is probed in neutron scattering experiments.[128]

Appendix A

Background Theory Appendix

A.1 The classical propagator

We would like to prove the following result for a classical propagator $e^{\mathcal{L}t}$,

$$e^{\mathcal{L}t}\left[ab\right] = \left[e^{\mathcal{L}t}a\right]\left[e^{\mathcal{L}t}b\right]. \tag{A.1}$$

We start by taking the Taylor expansion of $e^{\mathcal{L}t}$,

$$e^{\mathcal{L}t}\left[ab\right] = \sum_{k=0}^{\infty}\frac{1}{k!}\mathcal{L}^k t^k\left[ab\right]. \tag{A.2}$$

Using the Leibniz product rule (which is valid for any linear operator involving only first derivatives like $\mathcal{L}$) we get

$$\begin{aligned} e^{\mathcal{L}t}\left[ab\right] =& \sum_{k=0}^{\infty}\sum_{l=0}^{k}\frac{1}{k!}\binom{k}{l}t^k\left[\mathcal{L}^{k-l}a\right]\left[\mathcal{L}^l b\right] && \text{(A.3)}\\ =& \sum_{k=0}^{\infty}\sum_{l=0}^{\infty}\frac{1}{k!}\frac{1}{l!}t^k t^l\left[\mathcal{L}^k a\right]\left[\mathcal{L}^l b\right] && \text{(A.4)}\\ =& \left[e^{\mathcal{L}t}a\right]\left[e^{\mathcal{L}t}b\right]. && \text{(A.5)} \end{aligned}$$

The key step is recognising (A.3) as a Cauchy product. This result means that for any function $f(q,p)$ and any Liouvillian $\mathcal{L}$ that involves only first derivatives we may write

$$\begin{aligned} e^{\mathcal{L}t}f(q,p) =& f(e^{\mathcal{L}t}q, e^{\mathcal{L}t}p) && \text{(A.6)}\\ =& f(q_t, p_t), && \text{(A.7)} \end{aligned}$$

since the Taylor series of $f(q,p)$ will involve products in q and p, and we know from (A.1) that the propagator $e^{\mathcal{L}t}$ is distributive over any product. This argument breaks down if the Liouvillian contains derivatives of higher order than first, e.g. the quantum Liouvillian outside the harmonic limit, since then the Leibniz product rule does not hold.

A.2 Trajectories in LSC-IVR

Another way to understand the LSC-IVR approximation is to consider the Wigner-transformed operator $\left[\hat{B}(t)\right](q,p)$ as a function of three variables $b(q,p,t)$. The relationship between $b(q_0,p_0,t)$ and $b(q_t,p_t,0)$ is given without approximation by

$$b(q_0,p_0,t) - b(q_t,p_t,0) = \int_L \nabla b(q,p,t') \cdot \mathrm{d}\boldsymbol{v}, \tag{A.8}$$

where $\boldsymbol{v} = (q,p,t')$ and L is any directed line connecting the points $\boldsymbol{v} = (q_t,p_t,0)$ to $\boldsymbol{v} = (q_0,p_0,t)$. Now,

$$\frac{\partial b(q,p,t')}{\partial t'} = \frac{p}{m}\frac{\partial b(q,p,t')}{\partial q} - V'(q)\frac{\partial b(q,p,t')}{\partial p} + \mathcal{O}\left(\hbar^2\right) \tag{A.9}$$

so

$$\begin{aligned}
&b(q_0,p_0,t) - b(q_t,p_t,0) \\
&= \int_0^t dt' \left[\frac{\partial b(q,p,t')}{\partial q}\dot{q} + \frac{\partial b(q,p,t')}{\partial p}\dot{p} + \frac{\partial b(q,p,t')}{\partial t'}\right] &\text{(A.10)}\\
&= \int_0^t dt' \left[\frac{\partial b(q,p,t')}{\partial q}\left(\dot{q} + \frac{p}{m}\right) + \frac{\partial b(q,p,t')}{\partial p}\left(\dot{p} - V'(q)\right)\right] + \mathcal{O}\left(\hbar^2\right). &\text{(A.11)}
\end{aligned}$$

Therefore, if q and p satisfy the following first-order ordinary differential equations,

$$\dot{q} = -\frac{p}{m} \tag{A.12}$$

$$\dot{p} = V'(q), \tag{A.13}$$

then the integrand in (A.11) is zero at every point on the line L and we have

$$\begin{aligned}
b(q_t,p_t,0) &= b(q_0,p_0,t) + \mathcal{O}\left(\hbar^2\right) &\text{(A.14)}\\
&\approx b(q_0,p_0,t). &\text{(A.15)}
\end{aligned}$$

Note that $t \to -t$ transforms (A.12) and (A.13) into Hamilton's equations.

Appendix B

Matsubara Dynamics Appendix

B.1 Exactness of the generalised quantum Kubo time-correlation function

The first step in the proof of

$$C_{AB}(t) = \lim_{N\to\infty} C_{AB}^{[N]}(t), \tag{B.1}$$

is to recognise that, since the weight $1/N$ of any $A(q_l + \Delta_l/2)$ becomes vanishingly small in the $N \to \infty$ limit, we may anticipate this limit and rewrite (3.1) as

$$\begin{aligned} C_{AB}^{[N]}(t) = &\int \mathrm{d}\mathbf{q} \int \mathrm{d}\mathbf{\Delta} \int \mathrm{d}\mathbf{z}\; A(\mathbf{q}+\mathbf{\Delta}/2)B(\mathbf{z}) \\ &\times \prod_{l=1}^{N} \langle q_{l-1} - \Delta_{l-1}/2|\, e^{-\beta_N \hat{H}}\, |q_l + \Delta_l/2\rangle \\ &\times \langle q_l + \Delta_l/2|\, e^{i\hat{H}t/\hbar}\, |z_l\rangle \, \langle z_l|\, e^{-i\hat{H}t/\hbar}\, |q_l - \Delta_l/2\rangle\,. \end{aligned} \tag{B.2}$$

Now we make the following change of variables,

$$x_l = q_l + \Delta_l/2 \tag{B.3}$$

$$y_l = q_l - \Delta_l/2, \tag{B.4}$$

which has unit Jacobian. This gives the following for the generalised quantum Kubo TCF,

$$C_{AB}^{[N]}(t) = \lim_{N\to\infty} \frac{1}{N^2} \sum_{j=1}^{N}\sum_{k=1}^{N} \mathrm{Tr}\left[\prod_{l=1}^{N} f_{jl}(e^{i\hat{H}t/\hbar}, \hat{B}) e^{-i\hat{H}t/\hbar} f_{kl}(e^{-\beta_N \hat{H}}, \hat{A})\right], \tag{B.5}$$

where for convenience we have defined

$$f_{jk}(\mathcal{A},\mathcal{B}) = (1-\delta_{jk})\mathcal{A} + \delta_{jk}\mathcal{A}\mathcal{B}. \tag{B.6}$$

Notice that for $l \neq j$ we have

$$f_{jl}(e^{i\hat{H}t/\hbar},\hat{B})e^{-i\hat{H}t/\hbar} = \hat{I}. \tag{B.7}$$

For $k \geq j$ we have

$$\begin{aligned}&\mathrm{Tr}\left[\prod_{l=1}^{N} f_{jl}(e^{i\hat{H}t/\hbar},\hat{B})e^{-i\hat{H}t/\hbar}f_{kl}(e^{-\beta_N\hat{H}},\hat{A})\right]\\ &= \mathrm{Tr}\left[e^{-\beta_N(k-j)\hat{H}}\hat{A}e^{-\beta_N(N-(k-j))\hat{H}}\hat{B}(t)\right],\end{aligned} \tag{B.8}$$

where we have exploited the invariance of a trace under cyclic permutations. For $k < j$ we have

$$\begin{aligned}&\mathrm{Tr}\left[\prod_{l=1}^{N} f_{jl}(e^{i\hat{H}t/\hbar},\hat{B})e^{-i\hat{H}t/\hbar}f_{kl}(e^{-\beta_N\hat{H}},\hat{A})\right]\\ &= \mathrm{Tr}\left[e^{-\beta_N(N-(j-k))\hat{H}}\hat{A}e^{-\beta_N(j-k)\hat{H}}\hat{B}(t)\right].\end{aligned} \tag{B.9}$$

Therefore,

$$\begin{aligned}&\sum_{j=1}^{N}\sum_{k=1}^{N}\mathrm{Tr}\left[\prod_{l=1}^{N} f_{jl}(e^{i\hat{H}t/\hbar},\hat{B})e^{-i\hat{H}t/\hbar}f_{kl}(e^{-\beta_N\hat{H}},\hat{A})\right]\\ &= N\sum_{j=1}^{N}\mathrm{Tr}\left[e^{-\beta_N(N-k)\hat{H}}\hat{A}e^{-\beta_N k\hat{H}}\hat{B}(t)\right].\end{aligned} \tag{B.10}$$

To reach this last result we have exploited the following relation,

$$\sum_{j=a}^{b} g(j) = \sum_{j=a}^{b} g(b+a-j). \tag{B.11}$$

So, as was to be proved,

$$\begin{aligned}&\lim_{N\to\infty}\frac{1}{N^2}\sum_{j=1}^{N}\sum_{k=1}^{N}\mathrm{Tr}\left[\prod_{l=1}^{N} f_{jl}(e^{i\hat{H}t/\hbar},\hat{B})e^{-i\hat{H}t/\hbar}f_{kl}(e^{-\beta_N\hat{H}},\hat{A})\right]\\ &= \frac{1}{\beta}\int_0^{\beta}\mathrm{d}\lambda\,\mathrm{Tr}\left[e^{-(\beta-\lambda)\hat{H}}\hat{A}e^{-\lambda\hat{H}}\hat{B}(t)\right].\end{aligned} \tag{B.12}$$

B.2 Derivation of the Matsubara dynamics time-correlation function

To obtain the Matsubara dynamics time-correlation function (3.46), we note that $e^{\overline{\mathcal{L}}_M t}B(\mathbf{Q})$ is independent of the non-Matsubara $\mathbf{P}$ modes. They can therefore be integrated out of (3.45), giving a product of Dirac delta functions in the non-Matsubara $\mathbf{D}$ modes ($\mathbf{D} = T^T\boldsymbol{\Delta}$). As a result, the generalised Wigner transform $\left[e^{-\beta\hat{H}}\hat{A}\right]_{\overline{N}}(\mathbf{Q},\mathbf{P})$ in (3.45) reduces to

$$\left[e^{-\beta\hat{H}}\hat{A}\right]_{\overline{N}}(\mathbf{Q},\mathbf{P}_M) = (2\pi\hbar)^{N-M}A(\mathbf{Q})\int \mathrm{d}\mathbf{D}_M \prod_{k=-\overline{M}}^{\overline{M}} e^{iP_kD_k/\hbar} \times \prod_{l=1}^{N}\left\langle \eta_{l-1}^{-}(\mathbf{Q},\mathbf{D}_M)\right| e^{-\beta_N\hat{H}}\left|\eta_l^{+}(\mathbf{Q},\mathbf{D}_M)\right\rangle, \tag{B.13}$$

where $\mathbf{P}_M$ and $\mathbf{D}_M$ include only the Matsubara modes (and $\mathbf{Q}$ includes all N normal modes), and

$$\eta_l^{\pm}(\mathbf{Q},\mathbf{D}_M) = \sum_{k=-\overline{N}}^{\overline{N}} T_{lk}Q_k \pm \sum_{k=-\overline{M}}^{\overline{M}} T_{lk}D_k/2. \tag{B.14}$$

Using the Trotter factorisation of $e^{-\beta_N\hat{H}}$, the position-space matrix elements of the free-particle Boltzmann operator and trigonometric identities, we may write the following for (B.13),

$$\begin{aligned}
&\left[e^{-\beta\hat{H}}\hat{A}\right]_{\overline{N}}(\mathbf{Q},\mathbf{P}_M)\\
&= (2\pi\hbar)^{N-M}\left(\frac{m}{2\pi\beta_N\hbar^2}\right)^{N/2} A(\mathbf{Q})\int \mathrm{d}\mathbf{D}_M \prod_{k=-\overline{M}}^{\overline{M}} e^{iP_kD_k/\hbar}\\
&\times \exp\left[-\beta_N\frac{1}{2}m\sum_{k=\overline{M}+1}^{\overline{N}}\omega_k^2(Q_k^2+Q_{-k}^2)\right]\\
&\times \exp\left[-2\beta_N\frac{m}{(\beta_N\hbar)^2}\sum_{k=-\overline{M}}^{\overline{M}}\left(Q_k\sin\left(\frac{k\pi}{N}\right)+\frac{D_{-k}}{2}\cos\left(\frac{k\pi}{N}\right)\right)^2\right]\\
&\times \exp\left[-\beta_N\frac{1}{2}\left[\sum_{l=1}^{N}V(\eta_l^{-}(\mathbf{Q},\mathbf{D}_M))+V(\eta_l^{+}(\mathbf{Q},\mathbf{D}_M))\right]\right],
\end{aligned} \tag{B.15}$$

where we have used

$$\sum_{l=1}^{N}\left[\eta_l^-(\mathbf{Q},\mathbf{D}_M)-\eta_l^+(\mathbf{Q},\mathbf{D}_M)\right]^2 \tag{B.16}$$
$$=4\sum_{k=-\overline{M}}^{\overline{M}}\left(Q_k\sin\left(\frac{k\pi}{N}\right)+\frac{D_{-k}}{2}\cos\left(\frac{k\pi}{N}\right)\right)^2+\sum_{k=\overline{M}+1}^{\overline{N}}\left(\beta\hbar\omega_k\right)^2\left(Q_k^2+Q_{-k}^2\right).$$

On converting the $\mathbf{D}_M$ normal modes to their normalised counterparts $D_k/\sqrt{N}\to D_k$, we find that the Gaussians involving D_M in (B.15) are nascent Dirac delta functions. i.e. For k satisfying $-\overline{M}\leq k\leq\overline{M}$ they have the form

$$\exp\left(-\frac{mN^2D_k^2}{2\beta\hbar^2}\right)\sim\sqrt{\frac{2\pi\beta\hbar^2}{mN^2}}\,\delta(D_k). \tag{B.17}$$

Anticipating this limit, we make the replacement (B.17) and integrate out the $\mathbf{D}_M$ Matsubara modes to give

$$\begin{aligned}&\left[e^{-\beta\hat{H}}\hat{A}\right]_{\overline{N}}(\mathbf{Q},\mathbf{P}_M)\\&=\left(\frac{2\pi m}{\beta_N}\right)^{\frac{N-M}{2}}A(\mathbf{Q})\prod_{k=-\overline{M}}^{\overline{M}}e^{-\beta_N\frac{P_k^2}{2m}}\,e^{iP_kQ_{-k}\frac{2\tan(n\pi/N)}{\hbar}}\\&\times\exp\left[-\beta_N\frac{1}{2}m\sum_{k=\overline{M}+1}^{\overline{N}}\omega_k^2(Q_k^2+Q_{-k}^2)\right]\\&\times\exp\left[-\beta_N\sum_{l=1}^{N}V\left(\sum_{k=-\overline{N}}^{\overline{N}}T_{lk}Q_k\right)\right].\end{aligned} \tag{B.18}$$

Now we replace the position and momentum normal modes with their normalised counterparts, $Q_k/\sqrt{N}\to Q_k$ and $P_k/\sqrt{N}\to P_k$. This leads to

$$\begin{aligned}&\left[e^{-\beta\hat{H}}\hat{A}\right]_{\overline{N}}(\mathbf{Q},\mathbf{P}_M)\\&=\left(\frac{2\pi m}{\beta_N}\right)^{\frac{N-M}{2}}A(\mathbf{Q})\prod_{k=-\overline{M}}^{\overline{M}}e^{-\beta\frac{P_k^2}{2m}}\,e^{iP_kQ_{-k}\frac{2N\tan(k\pi/N)}{\hbar}}\\&\times\exp\left[-\beta\frac{1}{2}m\sum_{k=\overline{M}+1}^{\overline{N}}\omega_k^2(Q_k^2+Q_{-k}^2)\right]\\&\times\exp\left[-\beta\frac{1}{N}\sum_{l=1}^{N}V\left(\sum_{k=-\overline{N}}^{\overline{N}}T_{lk}\sqrt{N}Q_k\right)\right].\end{aligned} \tag{B.19}$$

If we now substitute this expression into the integral (3.45), we find

$$C_{AB}^{[M]}(t) = \lim_{N\to\infty} \frac{N^{\frac{N+M}{2}}}{(2\pi\hbar)^N} \int \mathrm{d}\mathbf{Q} \int \mathrm{d}\mathbf{P}_M \left[e^{-\beta\hat{H}}\hat{A}\right]_{\overline{N}} (\mathbf{Q}, \mathbf{P}_M)\, e^{\overline{\mathcal{L}}_M t}\, B(\mathbf{Q}). \tag{B.20}$$

We recognise the non-Matsubara position mode Gaussians in $\left[e^{-\beta\hat{H}}\hat{A}\right]_{\overline{N}} (\mathbf{Q}, \mathbf{P}_M)$ as nascent Dirac delta functions. i.e. They have the form

$$\exp\left(-\frac{2mN^2 \sin^2(\pi k/N) Q_k^2}{\beta\hbar^2}\right) \sim \sqrt{\frac{2\pi}{m\beta\omega_k^2}}\, \delta(Q_k), \tag{B.21}$$

and become Dirac delta functions in the Matsubara limit. Therefore, integrating out the non-Matsubara position modes has the following effect on the rest of the integrand in (B.20),

$$\exp\left[-\beta \frac{1}{N} \sum_{l=1}^{N} V\left(\sum_{k=-\overline{N}}^{\overline{N}} T_{lk}\sqrt{N} Q_k\right)\right] \to \exp\left[-\beta U_M(\mathbf{Q}_M)\right], \tag{B.22}$$

and

$$A(\mathbf{Q}) e^{\overline{\mathcal{L}}_M t} B(\mathbf{Q}) \to A(\mathbf{Q}_M) e^{\mathcal{L}_M t} B(\mathbf{Q}_M), \tag{B.23}$$

where $U_M(\mathbf{Q}_M)$ is the Matsubara potential (3.50) with $A(\mathbf{Q}_M)$ and $B(\mathbf{Q}_M)$ defined equivalently, and $\mathcal{L}_M$ is the Matsubara Liouvillian (3.52). Use of $2N \tan(k\pi/N) \to 2\pi k$ in the $N \to \infty$ limit leads to the Matsubara phase, and the α_M prefactor derives from a well-known formula for a product of sines,[a]

$$\prod_{k=1}^{N-1} \sin(k\pi/N) = \frac{N}{2^{N-1}}. \tag{B.24}$$

Bringing everything together gives

$$C_{AB}^{[M]}(t) = \frac{\alpha_M}{2\pi\hbar} \int \mathrm{d}\mathbf{Q} \int \mathrm{d}\mathbf{P}\; e^{-\beta H(\mathbf{Q},\mathbf{P})} e^{i\beta\theta(\mathbf{Q},\mathbf{P})}\, A(\mathbf{Q})\, e^{\mathcal{L}_M t}\, B(\mathbf{Q}), \tag{B.25}$$

as stated in Chapter 3. Note that we have dropped the M subscripts from the Matsubara positions and momenta since there is no longer a need to distinguish between the Matsubara and non-Matsubara modes. Only the Matsubara modes remain.

[a] This is easily proved by writing the left-hand side in terms of the real parts of the N^{th} roots of unity.

B.3 The error Liouvillian and the harmonic limit

The error Liouvillian can be written as follows without approximation,

$$\hat{L}_{\text{error}}(N,M) = \sum_{k=\overline{M}+1}^{\overline{N}} \frac{P_{-k}}{m}\frac{\partial}{\partial Q_{-k}} + \frac{P_k}{m}\frac{\partial}{\partial Q_k} - \frac{4}{\hbar}U_N(\mathbf{Q})\,\sin(\hat{X}/2)\cos(\hat{Y}+\hat{X}/2), \tag{B.26}$$

where

$$\hat{X} = \frac{\hbar}{2}\sum_{k=\overline{M}+1}^{\overline{N}} \frac{\overleftarrow{\partial}}{\partial Q_{-k}}\frac{\overrightarrow{\partial}}{\partial P_{-k}} + \frac{\overleftarrow{\partial}}{\partial Q_k}\frac{\overrightarrow{\partial}}{\partial P_k}, \tag{B.27}$$

and

$$\hat{Y} = \frac{\hbar}{2}\sum_{k=-\overline{M}}^{\overline{M}} \frac{\overleftarrow{\partial}}{\partial Q_k}\frac{\overrightarrow{\partial}}{\partial P_k}. \tag{B.28}$$

Note that for a harmonic potential all the normal modes are uncoupled and the error Liouvillian becomes

$$\hat{L}_{\text{error}}(N,M) = \sum_{k=\overline{M}+1}^{\overline{N}} \frac{P_{-k}}{m}\frac{\partial}{\partial Q_{-k}} - \frac{\partial U_N(\mathbf{Q})}{\partial Q_{-k}}\frac{\partial}{\partial P_{-k}} + \frac{P_k}{m}\frac{\partial}{\partial Q_k} - \frac{\partial U_N(\mathbf{Q})}{\partial Q_k}\frac{\partial}{\partial P_k}, \tag{B.29}$$

which does not feature the Matsubara modes. In other words, the part of the quantum Liouvillian that remains in Matsubara dynamics is the exact quantum Liouvillian for the Matsubara modes, provided the potential is harmonic.

B.4 The Matsubara limit for polynomial potentials

To improve computational efficiency in the Matsubara dynamics calculations, we calculated the Matsubara potential,

$$U_M(\mathbf{Q}) = \lim_{N\to\infty}\frac{1}{N}\sum_{l=1}^{N} V\left(\sum_{k=-\overline{M}}^{\overline{M}} T_{lk}\sqrt{N}Q_k\right), \tag{B.30}$$

explicitly in the $N \to \infty$ limit. The right-hand side of (B.30) can be evaluated for finite N with an N-dimensional fast Fourier transform and zero-padding of $N - M$ of the vector entries. However, this becomes increasingly time-consuming for large N. However, the right-hand side of (B.30) can be evaluated without the fast Fourier transform in the $N \to \infty$ limit for potentials that can be written in powers of q,

$$V(q) = a_0 + a_1 q + a_2 q^2 + \cdots + a_n q^n. \tag{B.31}$$

Inserting (B.31) into (B.30) gives, for the cubic term,

$$a_3 \sum_{i,\,l,\,k=-\overline{M}}^{\overline{M}} Q_i Q_l Q_k \frac{1}{N} \sum_{j=1}^{N} A_{ilk}(j/N), \tag{B.32}$$

where $A_{ilk}(j/N) = N^{3/2} T_{ji} T_{jl} T_{jk}$. Defining $x_j = j/N$ with $\Delta x = 1/N$ we have, in the $N \to \infty$ limit, an integral over products of sines and cosines (c.f. (3.55)),

$$\lim_{N\to\infty} \frac{1}{N} \sum_{j=1}^{N} A_{ilk}(j/N) = \int_0^1 \mathrm{d}x \; A_{ilk}(x). \tag{B.33}$$

Analogous expressions result from the other powers of q in (B.31). If the integrals (B.33) are worked out in advance then the calculation can remain in Matsubara position space in the $N \to \infty$ limit. This makes potential evaluation less time-consuming.

B.5 Noether's theorem and Matsubara phase conservation

As discussed in Section 3.3, the effect of imaginary-time translation is a two-dimensional rotation of the Matsubara position modes,

$$\begin{bmatrix} Q_k(\tau) \\ Q_{-k}(\tau) \end{bmatrix} = \begin{bmatrix} \cos(\omega_k \tau) & -\sin(\omega_k \tau) \\ \sin(\omega_k \tau) & \cos(\omega_k \tau) \end{bmatrix} \begin{bmatrix} Q_k \\ Q_{-k} \end{bmatrix}, \tag{B.34}$$

and likewise for the Matsubara momentum modes. Clearly the Lagrangian is insensitive to the imaginary-time translation since it has no effect on the kinetic and potential energies. In other words, the transformation (B.34) is a continuous symmetry of the Lagrangian,

$$\frac{\partial L(\mathbf{Q}(\tau),\dot{\mathbf{Q}}(\tau))}{\partial \tau} = 0. \tag{B.35}$$

From Noether's theorem, for every such symmetry there is a corresponding conserved quantity that is given by

$$\sum_{k=-\overline{M}}^{\overline{M}} \frac{\partial L(\mathbf{Q}(\tau),\dot{\mathbf{Q}}(\tau))}{\partial \dot{Q}_k(\tau)} \frac{\partial Q_k(\tau)}{\partial \tau}\bigg|_{\tau=0}. \tag{B.36}$$

Obviously,

$$\frac{\partial L(\mathbf{Q}(\tau),\dot{\mathbf{Q}}(\tau))}{\partial \dot{Q}_k(\tau)} = P_k(\tau), \tag{B.37}$$

and it is straightforward to show through differentiation of (B.34) that

$$\frac{\partial Q_k(\tau)}{\partial \tau} = \omega_k Q_{-k}(\tau). \tag{B.38}$$

The conserved quantity is therefore

$$\sum_{k=-\overline{M}}^{\overline{M}} \omega_k Q_{-k} P_k = \theta(\mathbf{Q},\mathbf{P}), \tag{B.39}$$

which is the Matsubara phase.

B.6 The thermal kinetic energy

Consider the thermal expectation value of the kinetic energy in Matsubara dynamics,

$$\langle T\rangle = \frac{1}{Z}\frac{\alpha_M}{2\pi\hbar}\int \mathrm{d}\mathbf{Q}\int \mathrm{d}\mathbf{P}\; e^{-\beta H(\mathbf{Q},\mathbf{P})} e^{i\beta\theta(\mathbf{Q},\mathbf{P})}\,\frac{1}{2m}\sum_{k=-\overline{M}}^{\overline{M}} P_k^2 \tag{B.40}$$

$$= \frac{1}{2m}\sum_{k=-\overline{M}}^{\overline{M}} \left\langle P_k^2\right\rangle^{RP} - \left\langle m^2\omega_k^2 Q_{-k}^2\right\rangle^{RP}, \tag{B.41}$$

where we have used the contour integration trick to reach the last line (see (3.107)) and the quantum canonical partition function is given by

$$Z = \frac{\alpha_M}{2\pi\hbar}\int \mathrm{d}\mathbf{Q}\int \mathrm{d}\mathbf{P}\; e^{-\beta R(\mathbf{Q},\mathbf{P})}. \tag{B.42}$$

The thermal expectation value $\langle\cdot\rangle^{RP}$ is taken over the ring-polymer distribution in the space of M Matsubara modes. The first part in (B.41) gives

$$\frac{1}{2m}\sum_{k=-\overline{M}}^{\overline{M}}\left\langle P_k^2\right\rangle^{RP}=\frac{M}{2\beta}. \tag{B.43}$$

The second part gives

$$-\frac{1}{2m}\sum_{k=-\overline{M}}^{\overline{M}}\left\langle m^2\omega_k^2 Q_{-k}^2\right\rangle^{RP}=-\frac{\overline{M}}{\beta}+\frac{1}{2}\sum_{k\neq 0}\left\langle Q_k\frac{\partial U_M(\mathbf{Q})}{\partial Q_k}\right\rangle^{RP}, \tag{B.44}$$

which results from integration by parts. Combining the two gives

$$\langle T\rangle=\frac{1}{2\beta}+\frac{1}{2}\sum_{k\neq 0}\left\langle Q_k\frac{\partial U_M(\mathbf{Q})}{\partial Q_k}\right\rangle^{RP}, \tag{B.45}$$

in agreement with the virial estimator for the thermal expectation value of the kinetic energy.[129] This is in contrast to RPMD, where the expectation value does not converge with respect to the number of beads,

$$\langle T\rangle=\frac{N}{2\beta}, \tag{B.46}$$

and also in contrast to CMD, where the expectation value is the same as the classical result,

$$\langle T\rangle=\frac{1}{2\beta}, \tag{B.47}$$

since it is simply the thermal expectation value of the kinetic energy of the centroid.

Appendix C

The Planetary Model Appendix

C.1 Identities involving sums of Matsubara frequencies

For $-\frac{\beta\hbar}{2} \leq x \leq +\frac{\beta\hbar}{2}$, we may represent $\cosh(\Omega x)$ as the Fourier series

$$\cosh(\Omega x) = a_0 + \sum_{k=1}^{\infty} a_k \cos(\omega_k x) + b_k \sin(\omega_k x), \tag{C.1}$$

where ω_k are the Matsubara frequencies. The zero frequency component is

$$a_0 = \frac{2\sinh\left(\frac{\beta\hbar\Omega}{2}\right)}{\beta\hbar\Omega}, \tag{C.2}$$

the cosine components are

$$a_k = \frac{4\Omega(-1)^k \sinh\left(\frac{\beta\hbar\Omega}{2}\right)}{\beta\hbar\left(\Omega^2 + \omega_k^2\right)}, \tag{C.3}$$

and sine components are

$$b_k = 0. \tag{C.4}$$

Therefore,

$$\cosh(\Omega x) = \frac{4\Omega\sinh\left(\frac{\beta\hbar\Omega}{2}\right)}{\beta\hbar}\left[\frac{1}{2\Omega^2} + \sum_{k=1}^{\infty}\frac{(-1)^k\cos(\omega_k x)}{\Omega^2+\omega_k^2}\right]. \tag{C.5}$$

Setting $\tau = x + \frac{\beta\hbar}{2}$, we have for $0 \leq \tau \leq \beta\hbar$

$$\cosh\left(\frac{\beta\hbar\Omega}{2} - \Omega\tau\right) = \frac{4\Omega\sinh\left(\frac{\beta\hbar\Omega}{2}\right)}{\beta\hbar}\left[\frac{1}{2\Omega^2} + \sum_{k=1}^{\infty}\frac{\cos(\omega_k\tau)}{\Omega^2+\omega_k^2}\right]. \tag{C.6}$$

Therefore

$$\frac{2}{m\beta}\sum_{k=1}^{\infty}\frac{1}{\Omega^2+\omega_k^2}=\frac{\beta\hbar\Omega\coth\left(\frac{\beta\hbar\Omega}{2}\right)-2}{2\beta m\Omega^2}, \tag{C.7}$$

and

$$\frac{2}{m\beta}\sum_{k=1}^{\infty}\frac{\cos\left(\omega_k\tau\right)}{\Omega^2+\omega_k^2}=\frac{2}{m\beta}\left(\frac{\beta\hbar}{4\Omega}\frac{\cosh\left(\beta\hbar\Omega/2-\Omega\tau\right)}{\sinh\left(\beta\hbar\Omega/2\right)}-\frac{1}{2\Omega^2}\right). \tag{C.8}$$

These expressions agree with those stated in Gradshteyn and Ryzhik.[130]

C.2 The Matsubara dynamics two-point time-correlation function distribution

The Matsubara dynamics two-point TCF within the Feynman-Kleinert approximation is

$$\begin{aligned}C_{AB}^{[M]}(t;\tau)=&\frac{\alpha_M}{2\pi\hbar}\int\mathrm{d}\mathbf{Q}\int\mathrm{d}\mathbf{P}\;e^{-\beta\frac{P_0^2}{2m}-\beta L(Q_0)-\beta\sum_{k\neq0}\frac{P_k^2}{2m}+\frac{1}{2}m\Omega^2Q_k^2}\\&\times\;e^{i\beta\theta(\mathbf{Q},\mathbf{P})}\,A(q(\tau))\,e^{\mathcal{L}_Mt}\,B(q(0)),\end{aligned} \tag{C.9}$$

where the Liouvillian is given by

$$\begin{aligned}\mathcal{L}_M=&\frac{P_0}{m}\frac{\partial}{\partial Q_0}-W'(Q_0)\frac{\partial}{\partial P_0}\\&+\frac{\tilde{p}(0)}{m}\frac{\partial}{\partial\tilde{q}(0)}-m\Omega^2\tilde{q}(0)\frac{\partial}{\partial\tilde{p}(0)}.\end{aligned} \tag{C.10}$$

By inserting Dirac delta functions for each of the four fluctuation variables $\overline{\mathbf{x}}^T=(\tilde{q}(\tau),\tilde{p}(\tau),\tilde{q}(0),\tilde{p}(0))$, we find

$$\begin{aligned}C_{AB}^{[M]}(t;\tau)=&\frac{\alpha_M}{2\pi\hbar}\int\mathrm{d}\mathbf{x}\int\mathrm{d}\mathbf{Q}\int\mathrm{d}\mathbf{P}\;e^{-\beta\frac{P_0^2}{2m}-\beta L(Q_0)-\beta\sum_{k\neq0}\frac{P_k^2}{2m}+\frac{1}{2}m\Omega^2Q_k^2}\\&\times\delta\left(\tilde{q}_2-\tilde{q}(\tau)\right)\,\delta\left(\tilde{p}_2-\tilde{p}(\tau)\right)\,\delta\left(\tilde{q}_1-\tilde{q}(0)\right)\,\delta\left(\tilde{p}_1-\tilde{p}(0)\right)\\&\times\;e^{i\beta\theta(\mathbf{Q},\mathbf{P})}\,A(q_2)\,e^{\mathcal{L}t}\,B(q_1),\end{aligned} \tag{C.11}$$

where $\mathbf{x}^T=(\tilde{q}_2,\tilde{p}_2,\tilde{q}_1,\tilde{p}_1)$ and we have made the replacment $\mathcal{L}_M\rightarrow\mathcal{L}$,

$$\mathcal{L}=\frac{P_0}{m}\frac{\partial}{\partial Q_0}-W'(Q_0)\frac{\partial}{\partial P_0}+\frac{\tilde{p}_1}{m}\frac{\partial}{\partial\tilde{q}_1}-m\Omega^2\tilde{q}_1\frac{\partial}{\partial\tilde{p}_1}. \tag{C.12}$$

Using the Fourier representation of the Dirac delta function,

$$\frac{1}{2\pi}\int_{-\infty}^{\infty} \mathrm{d}\omega\ e^{-i\omega(x-y)} = \delta(x-y), \tag{C.13}$$

we may rewrite (C.11) as follows,

$$\begin{aligned} C_{AB}^{[M]}(t;\tau) = \frac{\alpha_M}{2\pi\hbar}\frac{1}{(2\pi)^4}\int \mathrm{d}\mathbf{x}\int \mathrm{d}\boldsymbol{\xi}\int \mathrm{d}\mathbf{Q}\int \mathrm{d}\mathbf{P}\ e^{-i\boldsymbol{\xi}^T(\mathbf{x}-\overline{\mathbf{x}})} \\ \times\ e^{-\beta H(\mathbf{Q},\mathbf{P})}e^{i\beta\theta(\mathbf{Q},\mathbf{P})}\,A(q_2)\,e^{\mathcal{L}t}\,B(q_1), \end{aligned} \tag{C.14}$$

where $\boldsymbol{\xi}^T = (\psi_2, \phi_2, \psi_1, \phi_1)$. We complete the square in each fluctuation momentum mode P_k $(k \neq 0)$,

$$\begin{aligned} &\sum_{k\neq 0}\ \beta\frac{P_k^2}{2m} - i\beta\omega_k Q_{-k}P_k - i\phi_2 a_k P_k - i\phi_1 b_k P_k \\ &= \frac{\beta}{2m}\sum_{k\neq 0}\left[P_k - \frac{im}{\beta}\left(\beta\omega_k Q_{-k} + \phi_2 a_k + \phi_1 b_k\right)\right]^2 \\ &\quad + \frac{m}{2\beta}\sum_{k\neq 0}\left(\beta\omega_k Q_{-k} + \phi_2 a_k + \phi_1 b_k\right)^2, \end{aligned} \tag{C.15}$$

where

$$a_k = \begin{cases} \sqrt{2}\cos\left(\omega_k\tau\right) & k<0 \\ \sqrt{2}\sin\left(\omega_k\tau\right) & k>0 \end{cases}, \tag{C.16}$$

and

$$b_k = \begin{cases} \sqrt{2} & k<0 \\ 0 & k>0 \end{cases}. \tag{C.17}$$

Now we make the following change of variables,

$$\overline{P}_k = P_k - \frac{im}{\beta}\left(\beta\omega_k Q_{-k} + \phi_2 a_k + \phi_1 b_k\right), \tag{C.18}$$

and integrate over these coordinates using the contour integration trick described in Chapter 3 to move each $\overline{P}_k$ onto the real axis. This procedure is then repeated with the fluctuation position modes Q_k $(k \neq 0)$. Having done so we find

$$\begin{aligned} C_{AB}^{[M]}(t;\tau) = \frac{1}{2\pi\hbar}\frac{1}{(2\pi)^4}\int \mathrm{d}\mathbf{x}\int \mathrm{d}\boldsymbol{\xi}\int \mathrm{d}Q_0\int \mathrm{d}P_0\ e^{-i\boldsymbol{\xi}^T\mathbf{x}} \\ \times\ e^{-\beta\frac{P_0^2}{2m}-\beta W(Q_0)}\,e^{-\frac{1}{2}\boldsymbol{\xi}^T G\boldsymbol{\xi}}\,A(q_2)\,e^{\mathcal{L}t}\,B(q_1). \end{aligned} \tag{C.19}$$

The 4×4 symmetric matrix G is defined by

$$G = \begin{bmatrix} a^2 & 0 & b^2(\tau) & ic^2(\tau) \\ 0 & m^2\Omega^2 a^2 & -ic^2(\tau) & m^2\Omega^2 b^2(\tau) \\ b^2(\tau) & -ic^2(\tau) & a^2 & 0 \\ ic^2(\tau) & m^2\Omega^2 b^2(\tau) & 0 & m^2\Omega^2 a^2. \end{bmatrix}, \tag{C.20}$$

where a^2 is

$$a^2 = \frac{2}{m\beta} \sum_{k=1}^{\overline{M}} \frac{1}{\Omega^2 + \omega_k^2}, \tag{C.21}$$

$b^2(\tau)$ is

$$b^2(\tau) = \frac{2}{m\beta} \sum_{k=1}^{\overline{M}} \frac{\cos(\omega_k \tau)}{\Omega^2 + \omega_k^2} \tag{C.22}$$

and $c^2(\tau)$ is

$$c^2(\tau) = \frac{2}{\beta} \sum_{k=1}^{\overline{M}} \frac{\omega_k \, \sin(\omega_k \tau)}{\Omega^2 + \omega_k^2}, \tag{C.23}$$

with $\overline{M} = (M-1)/2$. The $M \to \infty$ limit is now taken which allows us to collapse the series (C.21), (C.22) and (C.23) into hyperbolic functions (see Appendix C.1) and leads to the G matrix presented in Chapter 4. Now, using the following well-known result for the Fourier transform of an F-dimensional Gaussian,

$$\frac{\sqrt{\det(G)}}{(2\pi)^{F/2}} \int \mathrm{d}\boldsymbol{\xi} \; e^{-i\boldsymbol{\xi}^T \mathbf{x}} \, e^{-\frac{1}{2}\boldsymbol{\xi}^T G \boldsymbol{\xi}} = e^{-\frac{1}{2}\mathbf{x}^T G^{-1} \mathbf{x}}, \tag{C.24}$$

we reach the following expression for the approximate Matsubara dynamics two-point TCF,

$$\begin{aligned} C_{AB}(t;\tau) = & \frac{1}{2\pi\hbar} \int \mathrm{d}Q_0 \int \mathrm{d}P_0 \; e^{-\beta \frac{P_0^2}{2m} - \beta W(Q_0)} \\ & \times \frac{1}{(2\pi)^2 \sqrt{\det(G)}} \int \mathrm{d}\mathbf{x} \; e^{-\frac{1}{2}\mathbf{x}^T G^{-1} \mathbf{x}} A(q_2) \, e^{\mathcal{L}t} \, B(q_1), \end{aligned} \tag{C.25}$$

which is the same as (4.58).

C.3 Convergence of the path integral frequency estimator

It is natural to question whether there may be a more efficient way to calculate the path integral frequency (4.123) in practice. For example, it is clear that

$$m\overline{\Omega}^2 = \sum_{l=1}^{N} a_l \left\langle V''(q_l)\, \delta\left(x - \frac{1}{N}\sum_{j=1}^{N} q_j\right)\right\rangle, \tag{C.26}$$

where $\sum_{l=1}^{N} a_l = 1$ will converge to (4.118) since the ring-polymer average is invariant under permutation of the beads. For example, we could pick $a_l = T_{lk}^2$, where T is the orthonormal matrix that corresponds to the real discrete Fourier transform (2.62), which would give the following as an alternative estimator,

$$m\Omega^2 = \left\langle \frac{\partial^2 U(\mathbf{Q})}{\partial Q_k^2}\, \delta\left(x - \frac{Q_0}{\sqrt{N}}\right)\right\rangle. \tag{C.27}$$

The question is, what choice of the set of coefficients $\{a_l\}$ will lead to the fastest convergence of (C.26) under Monte Carlo sampling? We can answer this question by rewriting (C.26) in terms of a set of N independent, identically distributed random variables Z_j,

$$m\overline{\Omega}^2 = \sum_{l=1}^{N} a_l Z_l. \tag{C.28}$$

Provided the samples are independently distributed, the variance of the provisional estimator is

$$V\left[m\overline{\Omega}^2\right] = V\left[Z\right] \sum_{l=1}^{N} a_l^2, \tag{C.29}$$

which is minimised when $a_l = \frac{1}{N}$ (subject to the constraint $\sum_{l=1}^{N} a_l = 1$). This corresponds to (4.118) and justifies this original choice.

C.4 The path integral frequency in the $T \to 0$ limit

Consider the following diagonal elements of a normalised centroid-constrained Boltzmann operator,

$$\rho_f(x, Q_0) = \frac{1}{Z_f} \langle x| \, e^{-\beta\hat{H} - \beta f\hat{x}} \, |x\rangle \, (Q_0), \tag{C.30}$$

where

$$Z_f = \mathrm{Tr}\left[e^{-\beta\hat{H} - \beta f\hat{x}}\right]. \tag{C.31}$$

By definition, integration over Q_0 gives the diagonal elements of the exact normalised density matrix for a system with Hamiltonian $\hat{H} + f\hat{x}$. Of course, in the $T \to 0$ limit, this density matrix becomes the probability density of the ground state,

$$\lim_{T\to 0} \int \mathrm{d}Q_0 \; \rho_f(x, Q_0) = |\Psi_0^f(x)|^2. \tag{C.32}$$

In Ref. 66, Ramirez and López-Ciudad show that since all the moments of Q_0 besides the first become vanishingly small in the $T \to 0$ limit, this equation becomes

$$\lim_{T\to 0} \rho_0 \left(x, \langle x\rangle_f\right) = |\Psi_0^f(x)|^2, \tag{C.33}$$

where $\langle x\rangle_f = \langle\Psi_0^f| \, \hat{x} \, |\Psi_0^f\rangle$.[66] Now, it is straightforward to show that the state $|\Psi_0^f\rangle$ also satisfies the variational minimum of the following energy,

$$E = \langle\Psi| \, \hat{H} \, |\Psi\rangle \,, \tag{C.34}$$

for all normalised trial states $|\Psi\rangle$ (we follow Ramirez and López-Ciudad in referring to these trial states as wavepackets) that satisfy the constraint

$$\langle\Psi| \, \hat{x} \, |\Psi\rangle = \langle x\rangle_f \,. \tag{C.35}$$

Using this result, we may write

$$\lim_{T\to 0} \rho_0 \, (x, Q_0) = |\Psi(x, Q_0)|^2, \tag{C.36}$$

where $|\Psi(x, Q_0)|^2$ is the probability density of the minimum energy wavepacket, subject to the constraint (C.35) with $\langle x\rangle_f$ replaced with Q_0. Multiplying both sides of the last equation by $V''(x)$ and integrating over x gives

$$\lim_{T\to 0} m\Omega^2 = \int \mathrm{d}x \; |\Psi(x, Q_0)|^2 \, V''(x) \tag{C.37}$$

$$= \langle\Psi(Q_0)| \, V''(\hat{x}) \, |\Psi(Q_0)\rangle \,, \tag{C.38}$$

where Ω^2 is the square of the path integral frequency (4.118) and $\langle x|\Psi(Q_0)\rangle = \Psi(x, Q_0)$. In other words, $m\Omega^2$ is, in the $T \to 0$ limit, the (pure state) expectation value of $V''(\hat{x})$ taken over the mininum energy wavepacket whose average position is Q_0.

On the other hand, the corresponding quantity within the Feynman-Kleinert approximation is, in the $T \to 0$ limit, the expectation value of $V''(\hat{x})$ taken over the minimum energy Gaussian wavepacket whose centre is Q_0. i.e.

$$\lim_{T\to 0} m\Omega^2 = \langle\Psi(Q_0)|\, V''(\hat{x})\, |\Psi(Q_0)\rangle\,, \tag{C.39}$$

where $|\Psi(Q_0)\rangle$ is constrained to have the following form,

$$\langle x|\Psi(Q_0)\rangle = \frac{1}{(2\pi a^2)^{1/4}}\; e^{-\frac{1}{4a^2}(x-Q_0)^2}, \tag{C.40}$$

and the parameter a^2 minimises the energy (C.34). To demonstrate this, we recognise that the Feynman-Kleinert centroid potential of mean force is, in the $T \to 0$ limit, the minimum of the following with respect to a^2,[56]

$$\lim_{T\to 0} W(Q_0) = V_{a^2}(Q_0) + \frac{\hbar^2}{8ma^2} \tag{C.41}$$

$$= \langle\Psi(Q_0)|\, \hat{H}\, |\Psi(Q_0)\rangle\,. \tag{C.42}$$

Now, using the definition of the Feynman-Kleinert frequency,

$$\lim_{T\to 0} m\Omega^2 = \frac{1}{\sqrt{2\pi}a}\int \mathrm{d}\tilde{q}\; e^{-\frac{1}{2a^2}\tilde{q}^2}\, V''(Q_0+\tilde{q}) \tag{C.43}$$

$$= \langle\Psi(Q_0)|\, V''(\hat{x})\, |\Psi(Q_0)\rangle\,, \tag{C.44}$$

as claimed.

Appendix D

Infrared Absorption Spectroscopy of Water Appendix

D.1 The effect of modifying the planetary model on the infrared absorption spectrum of the q-TIP4P/F water molecule

As detailed in Chapter 4, the first change we propose for the planetary model is the replacement of the Feynman-Kleinert centroid distribution and CMD dynamics with the exact centroid distribution and TRPMD dynamics. The second change we propose is the use of the path integral frequency (4.118) instead of the Feynman-Kleinert frequency. To further assess the effect of these modifications on planetary model infrared absorption spectra for water, we repeated our simulations of the single q-TIP4P/F water molecule at 150K, 300K and 600K using the original formulation of the planetary model as presented in Ref. 45 and Ref. 46 under the name FK-QCW(1).

To calculate the Feynman-Kleinert frequency matrix we used the exact mass-weighted Hessian of the q-TIP4P/F intramolecular potential. We iterated the simultaneous equations five times to converge the Feynman-Kleinert frequency and radius of gyration matrices with a total of 4096 samples for Monte Carlo integration. The converged radius of gyration matrix was then used to calculate the Feynman-Kleinert centroid force using 16384 samples for Monte Carlo integration. We found that this many Monte Carlo samples were required to converge the Feynman-Kleinert CMD infrared absorption spectra but an underconverged centroid force could be used to converge the planetary part of the autocorrelation function in (5.12) with no visible loss in accuracy. We used a total of 64 independent initial planet phase space points

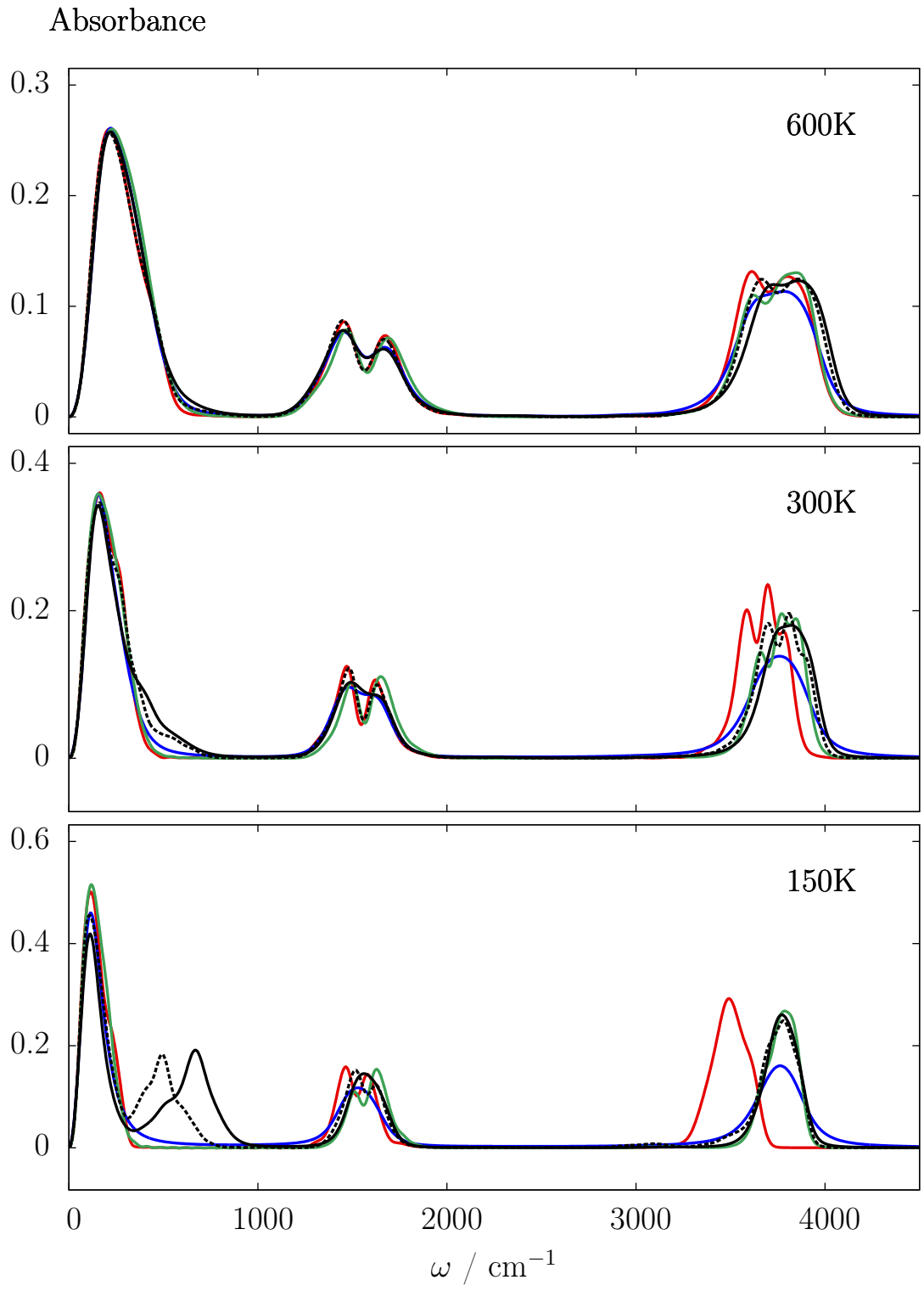

Figure D.1: Comparison of infrared absorption spectra for a single q-TIP4P/F water molecule. The lines are the same as in Figure 5.2 but for the red lines which represent the Feynman-Kleinert CMD spectra (the classical results are omitted). The dotted black lines show the planetary model results that were calculated using the original formulation of Poulsen *et al.*

to converge the integrals over the distribution of the planets. At each temperature, we calculated the dipole moment autocorrelation over a total of 10^4 independent centroid trajectories of length 2 ps (one for each of the 64 initial positions and momenta of the planets). Prior to taking its Fourier transform, we damped the dipole moment autocorrelation function with the same Hann window as described in Chapter 5. We used the same procedure with the centroid part of the autocorrelation function to produce the Feynman-Kleinert CMD result.

The results of these simulations are shown in Figure D.1. The first point to note is that the Feynman-Kleinert CMD stretch band is significantly redshifted relative to the other results at 150K. This is the result of the well-known curvature problem for CMD which, while mitigated by use of the Feynman-Kleinert approximation, is pronounced nevertheless. However, the stretch bands of the two planetary model results are in good agreement despite the incorrect Feynman-Kleinert CMD description of the stretch vibrations. Of course, this can be rationalised using the motional narrowing analysis of Chapter 5: while the high-frequency spectral properties of the Feynman-Kleinert CMD centroid dynamics are clearly incorrect, the correlation times and standard deviations of the Feynman-Kleinert stretch frequencies are likely to be very close to the (TRPMD) correlation times and standard deviations of the path integral stretch frequencies. The incorrect Feynman-Kleinert CMD stretch band does, however, contaminate the planetary model result with a shoulder on the low frequency side of the stretch band. This is simply the low-absorbance centroid contribution to the band. Such a shoulder is not present with our modified planetary model infrared absorption spectrum at this temperature since the TRPMD stretch band overlaps with the spectrum of the planetary part of the dipole moment autocorrelation function in (5.12).

As mentioned in Chapter 5, our proposed modifications lead to less rotational structure in the infrared absorption spectra at these temperatures. In particular, the bend band shows a bifurcated structure when calculated using the original formulation of the planetary model that is absent when our proposed modifications are made. However, the original formulation at 150K also presents a spurious combination band at approximately 3100 cm^{-1} which is the result of coupling of the planetary model rotation frequencies to the centroid motion. To determine this, we repeated our calculations with the lowest six eigenvalues of the Feynman-Kleinert frequency matrix set equal to zero and found that the peak disappeared. This spurious peak is washed out by the use of TRPMD rather than Feynman-Kleinert CMD for the centroid dynamics (at the expense of less rotational structure in the spectrum).

To investigate the origin of the discrepancy in Figure D.1 between the rotation

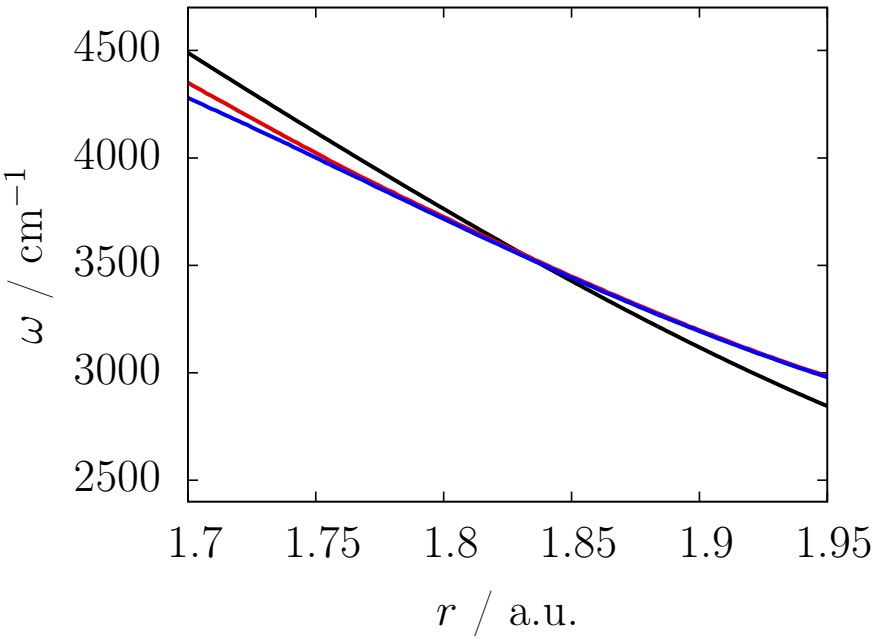

Figure D.2: Comparison of the asymmetric stretch frequency for a single q-TIP4P/F water molecule at 300K. The lines represent the Feynman-Kleinert frequency (red), the path integral frequency (blue) and the classical frequency (black).

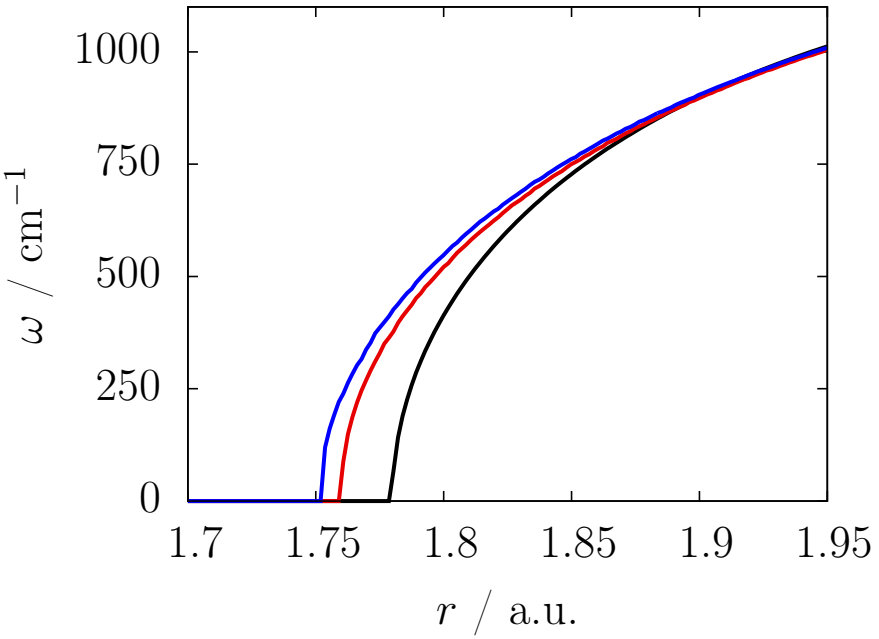

Figure D.3: Comparison of the highest rotation frequency for a single q-TIP4P/F water molecule at 300K. The lines represent the Feynman-Kleinert frequency (red), the path integral frequency (blue) and the classical frequency (black).

bands before and after application of our proposed modifications, we calculated the eigenvalues of the Feynman-Kleinert frequency and path integral frequency matrices as functions of the centroid symmetric stretch coordinate. The highest eigenfrequency (the asymmetric stretch) is plotted in Figure D.2 and the fourth highest eigenfrequency (the highest-frequency rotation) is plotted in Figure D.3. These are compared with the eigenfrequencies of the following 'classical' frequency matrix,

$$\Omega^2 = \overline{H}(\mathbf{Q}_0), \tag{D.1}$$

where $\overline{H}(\mathbf{Q}_0)$ is the mass-weighted Hessian of the q-TIP4P/F intramolecular potential. As is apparent in Figure D.2, the agreement between the Feynman-Kleinert and path integral asymmetric stretch frequencies is good over the range of thermally accessible centroid configurations. However, the agreement between the Feynman-Kleinert and path integral frequency is poorer for the rotation. At the equilibrium configuration ($r = 1.78$ a.u.), the two frequencies disagree by approximately $100\,\mathrm{cm}^{-1}$, with the path integral frequency lying above the Feynman-Kleinert rotation frequency. This discrepancy obviously manifests itself in the difference between the planetary model rotation bands in Figure D.1. Of course, since the planetary model fails to adequately describe rotations regardless of the choice of frequency matrix, this difference is interesting but ultimately unimportant.

D.2 Spectroscopic data for the condensed-phase q-TIP4P/F water simulations

	Mean	Median	Mode	FWHM
150K	779	781	765	203
300K	623	642	663	407
600K	461	456	480	659
150K	1663	1668	1673	89
300K	1589	1634	1644	114
600K	1561	1604	1628	118
150K	3496	3500	3485	142
300K	3576	3576	3554	228
600K	3679	3684	3672	305

Table D.1: Spectroscopic data for the condensed-phase classical infrared absorption spectra. Moving down the table, each panel concerns the libration, bend and stretch bands respectively. FWHM is the full width at half maximum of each band. The mode is equivalent to the position of maximum absorbance. All values besides the temperatures are in cm^{-1}.

	Mean	Median	Mode	FWHM	Mean	Median	Mode	FWHM
150K	856	886	928	166	909	932	981	264
300K	647	676	736	419	837	857	895	394
600K	470	468	504	635	815	830	895	451
150K	1637	1632	1632	97	1643	1642	1649	175
300K	1556	1594	1608	109	1616	1614	1616	195
600K	1534	1565	1583	138	1584	1582	1583	232
150K	3436	3444	3448	146	3460	3456	3428	647
300K	3531	3540	3526	232	3558	3551	3465	814
600K	3636	3643	3632	305	3683	3675	3652	1099

Table D.2: Spectroscopic data for the condensed-phase planetary model results with a time-dependent path integral frequency matrix (left) and without (right). Moving down the table, each panel concerns the libration, bend and stretch bands respectively. FWHM is the full width at half maximum of each band. The mode is equivalent to the position of maximum absorbance. All values besides the temperatures are in cm^{-1}.

	Mean	Median	Mode	FWHM	Mean	Median	Mode	FWHM
150K	762	761	745	223	776	773	765	145
300K	615	632	643	427	620	634	615	440
600K	468	462	468	655	475	468	515	640
150K	1648	1633	1636	114	1633	1629	1625	80
300K	1573	1602	1616	126	1567	1606	1615	100
600K	1547	1583	1604	130	1541	1587	1605	105
150K	3416	3420	3436	228	3257	3257	3285	225
300K	3489	3489	3481	293	3437	3444	3440	210
600K	3605	3604	3587	313	3599	3606	3620	285

Table D.3: Spectroscopic data for the condensed-phase TRPMD (left) and CMD (right) results. Moving down the table, each panel concerns the libration, bend and stretch bands respectively. FWHM is the full width at half maximum of each band. The mode is equivalent to the position of maximum absorbance. All values besides the temperatures are in cm^{-1}.

References

[1] D. Frenkel and B. Smit, *Understanding molecular simulation: from algorithms to applications*, Academic Press, 2001.

[2] W. H. Miller, J. Chem. Phys. **125**, 132305 (2006).

[3] D. C. Clary, Science **321**, 789 (2008).

[4] M. Ceriotti et al., Chem. Rev. **116**, 7529 (2016).

[5] J. C. Light and T. Carrington Jr, Adv. Chem. Phys. **114**, 263 (2000).

[6] J. Tennyson et al., Comput. Phys. Commun. **163**, 85 (2004).

[7] C. Lanczos, *An iteration method for the solution of the eigenvalue problem of linear differential and integral operators*, United States Governm. Press Office Los Angeles, CA, 1950.

[8] R. P. Feynman, A. R. Hibbs, and D. F. Styer, *Quantum mechanics and path integrals*, Dover, 2010.

[9] D. Chandler and P. G. Wolynes, J. Chem. Phys. **74**, 4078 (1981).

[10] M. Parrinello and A. Rahman, J. Chem. Phys. **80**, 860 (1984).

[11] M. Ceriotti, J. Cuny, M. Parrinello, and D. E. Manolopoulos, Proc. Natl. Acad. Sci. **110**, 15591 (2013).

[12] T. E. Markland and D. E. Manolopoulos, J. Chem. Phys. **129**, 024105 (2008).

[13] T. E. Markland and D. E. Manolopoulos, Chem. Phys. Lett. **464**, 256 (2008).

[14] M. Ceriotti, M. Parrinello, T. E. Markland, and D. E. Manolopoulos, J. Chem. Phys. **133**, 124104 (2010).

[15] M. Ceriotti, D. E. Manolopoulos, and M. Parrinello, J. Chem. Phys. **134**, 084104 (2011).

[16] M. Ceriotti and D. E. Manolopoulos, Phys. Rev. Lett. **109**, 100604 (2012).

[17] E. J. Heller, Acc. Chem. Res. **14**, 368 (1981).

[18] R. Zwanzig, Annu. Rev. Phys. Chem. **16**, 67 (1965).

[19] R. Kubo, J. Phys. Soc. Japan **12**, 570 (1957).

[20] D. T. Colbert and W. H. Miller, J. Chem. Phys. **96**, 1982 (1992).

[21] H.-D. Meyer, U. Manthe, and L. Cederbaum, Chem. Phys. Lett. **165**, 73 (1990).

[22] M. H. Beck, A. Jäckle, G. Worth, and H.-D. Meyer, Phys. Rep. **324**, 1 (2000).

[23] E. J. Heller, Acc. Chem. Res. **39**, 127 (2006).

[24] E. J. Heller, J. Chem. Phys. **75**, 2923 (1981).

[25] D. V. Shalashilin and I. Burghardt, J. Chem. Phys. **129**, 084104 (2008).

[26] S. Habershon, J. Chem. Phys. **136**, 014109 (2012).

[27] M. Ben-Nun, J. Quenneville, and T. J. Martínez, J. Phys. Chem. A **104**, 5161 (2000).

[28] W. H. Miller, J. Phys. Chem. A **105**, 2942 (2001).

[29] N. Makri and K. Thompson, Chem. Phys. Lett. **291**, 101 (1998).

[30] A. Raab, G. A. Worth, H.-D. Meyer, and L. S. Cederbaum, J. Chem. Phys. **110**, 936 (1999).

[31] M. A. C. Saller and S. Habershon, J. Chem. Theory Comput. **11**, 8 (2015).

[32] E. Wigner, Phys. Rev. **40**, 749 (1932).

[33] W. B. Case, Am. J. Phys. **76**, 937 (2008).

[34] J. E. Moyal and M. S. Bartlett, Math. Proc. Cambridge Philos. Soc. **45**, 99 (1949).

[35] J. Liu, Int. J. Quantum Chem. **115**, 657 (2015).

[36] S. Nielsen, R. Kapral, and G. Ciccotti, J. Chem. Phys. **115**, 5805 (2001).

[37] S. Habershon and D. E. Manolopoulos, J. Chem. Phys. **131**, 244518 (2009).

[38] G. A. Voth, Adv. Chem. Phys. **93**, 135 (1996).

[39] S. Habershon, D. E. Manolopoulos, T. E. Markland, and T. F. Miller, Annu. Rev. Phys. Chem. **64**, 387 (2013).

[40] S. Jang, A. V. Sinitskiy, and G. A. Voth, J. Chem. Phys. **140**, 154103 (2014).

[41] B. J. Braams and D. E. Manolopoulos, J. Chem. Phys. **125**, 124105 (2006).

[42] A. Horikoshi and K. Kinugawa, J. Chem. Phys. **122**, 174104 (2005).

[43] T. J. H. Hele, M. J. Willatt, A. Muolo, and S. C. Althorpe, J. Chem. Phys. **142**, 134103 (2015).

[44] T. J. H. Hele, M. J. Willatt, A. Muolo, and S. C. Althorpe, J. Chem. Phys. **142**, 191101 (2015).

[45] K. K. G. Smith, J. A. Poulsen, G. Nyman, and P. J. Rossky, J. Chem. Phys. **142**, 244112 (2015).

[46] K. K. G. Smith, J. A. Poulsen, G. Nyman, A. Cunsolo, and P. J. Rossky, J. Chem. Phys. **142**, 244113 (2015).

[47] M. Rossi, M. Ceriotti, and D. E. Manolopoulos, J. Chem. Phys. **140**, 234116 (2014).

[48] R. Kubo, Adv. Chem. Phys.: Stochastic Processes in Chemical Physics **15**, 101 (1969).

[49] E. Schrödinger, *Statistical thermodynamics*, Dover, 1989.

[50] H. F. Trotter, Proc. Am. Math. Soc. **10**, 545 (1959).

[51] M. E. Tuckerman, B. J. Berne, G. J. Martyna, and M. L. Klein, J. Chem. Phys. **99**, 2796 (1993).

[52] D. Thirumalai and B. Berne, J. Chem. Phys. **79**, 5029 (1983).

[53] B. J. Berne and D. Thirumalai, Annu. Rev. Phys. Chem. **37**, 401 (1986).

[54] R. Kubo, Rep. Prog. Phys. **29**, 255 (1966).

[55] I. R. Craig and D. E. Manolopoulos, J. Chem. Phys. **121**, 3368 (2004).

[56] R. P. Feynman and H. Kleinert, Phys. Rev. A **34**, 5080 (1986).

[57] R. Giachetti and V. Tognetti, Phys. Rev. Lett. **55**, 912 (1985).

[58] R. Giachetti and V. Tognetti, Phys. Rev. B **33**, 7647 (1986).

[59] T. D. Hone, P. J. Rossky, and G. A. Voth, J. Chem. Phys. **124**, 154103 (2006).

[60] O. Marsalek and T. E. Markland, J. Phys. Chem. Lett. **8**, 1545 (2017).

[61] G. R. Medders and F. Paesani, J. Chem. Theory Comput. **11**, 1145 (2015).

[62] T. D. Hone and G. A. Voth, J. Chem. Phys. **121**, 6412 (2004).

[63] E. Geva, Q. Shi, and G. A. Voth, J. Chem. Phys. **115**, 9209 (2001).

[64] A. Witt, S. D. Ivanov, M. Shiga, H. Forbert, and D. Marx, J. Chem. Phys. **130**, 194510 (2009).

[65] S. D. Ivanov, A. Witt, M. Shiga, and D. Marx, J. Chem. Phys. **132**, 031101 (2010).

[66] R. Ramirez and T. López-Ciudad, J. Chem. Phys. **111**, 3339 (1999).

[67] J. Cao and G. A. Voth, J. Chem. Phys. **101**, 6168 (1994).

[68] T. F. Miller and D. E. Manolopoulos, J. Chem. Phys. **122**, 184503 (2005).

[69] S. Habershon, G. S. Fanourgakis, and D. E. Manolopoulos, J. Chem. Phys. **129**, 074501 (2008).

[70] Y. V. Suleimanov et al., Phys. Chem. Chem. Phys. **15**, 3655 (2013).

[71] R. Pérez de Tudela, F. J. Aoiz, Y. V. Suleimanov, and D. E. Manolopoulos, J. Phys. Chem. Lett. **3**, 493 (2012).

[72] Y. V. Suleimanov, R. Collepardo-Guevara, and D. E. Manolopoulos, J. Chem. Phys. **134**, 044131 (2011).

[73] T. E. Markland, S. Habershon, and D. E. Manolopoulos, J. Chem. Phys. **128**, 194506 (2008).

[74] I. R. Craig and D. E. Manolopoulos, J. Chem. Phys. **122**, 084106 (2005).

[75] I. R. Craig and D. E. Manolopoulos, J. Chem. Phys. **123**, 34102 (2005).

[76] J. O. Richardson and S. C. Althorpe, J. Chem. Phys. **131**, 214106 (2009).

[77] T. J. H. Hele and S. C. Althorpe, J. Chem. Phys. **138**, 084108 (2013).

[78] S. C. Althorpe and T. J. H. Hele, J. Chem. Phys. **139**, 084115 (2013).

[79] T. J. H. Hele and S. C. Althorpe, J. Chem. Phys. **139**, 084116 (2013).

[80] T. J. H. Hele and S. C. Althorpe, J. Chem. Phys. **144**, 174107 (2016).

[81] N. Ananth, J. Chem. Phys. **139**, 124102 (2013).

[82] A. R. Menzeleev, F. Bell, and T. F. Miller, J. Chem. Phys. **140**, 064103 (2014).

[83] R. Welsch, K. Song, Q. Shi, S. C. Althorpe, and T. F. Miller, J. Chem. Phys. **145**, 204118 (2016).

[84] W. H. Press, B. P. Flannery, S. A. Teukolsky, and W. T. Vetterling, *Numerical recipes in Fortran 77: the art of scientific computing*, Cambridge University Press, 1986.

[85] T. J. H. Hele, Mol. Phys. **114**, 1461 (2016).

[86] M. Hillery, R. F. O'Connell, M. O. Scully, and E. P. Wigner, Phys. Rep. **106**, 121 (1984).

[87] E. J. Heller, J. Chem. Phys. **65**, 1289 (1976).

[88] J. Liu and W. H. Miller, J. Chem. Phys. **125**, 224104 (2006).

[89] J. Liu and W. H. Miller, J. Chem. Phys. **131**, 074113 (2009).

[90] J. A. Poulsen, G. Nyman, and P. J. Rossky, J. Chem. Phys. **119**, 12179 (2003).

[91] J. A. Poulsen, G. Nyman, and P. J. Rossky, J. Chem. Theory Comput. **2**, 1482 (2006).

[92] X. Sun, H. Wang, and W. H. Miller, J. Chem. Phys. **109**, 7064 (1998).

[93] J. Liu, W. H. Miller, F. Paesani, W. Zhang, and D. A. Case, J. Chem. Phys. **131**, 164509 (2009).

[94] J. A. Poulsen, G. Nyman, and P. J. Rossky, J. Phys. Chem. A **108**, 8743 (2004).

[95] J. Liu et al., J. Chem. Phys. **135**, 244503 (2011).

[96] J. Liu and W. H. Miller, J. Chem. Phys. **134**, 104101 (2011).

[97] J. Liu and W. H. Miller, J. Chem. Phys. **134**, 104102 (2011).

[98] J. Liu, J. Chem. Phys. **134**, 194110 (2011).

[99] J. H. Van Vleck, Proc. Natl. Acad. Sci. **14**, 178 (1928).

[100] H. Wang, X. Sun, and W. H. Miller, J. Chem. Phys. **108**, 9726 (1998).

[101] Q. Shi and E. Geva, J. Chem. Phys. **118**, 8173 (2003).

[102] T. Matsubara, Prog. Theor. Phys. **14**, 351 (1955).

[103] A. Royer, J. Math. Phys. **25**, 2873 (1984).

[104] R. D. Coalson, J. Chem. Phys. **85**, 926 (1986).

[105] R. Shankar, *Principles of quantum mechanics*, Springer, 1994.

[106] C. Chakravarty, M. C. Gordillo, and D. M. Ceperley, J. Chem. Phys. **109**, 2123 (1998).

[107] C. M. Bender, D. C. Brody, and D. W. Hook, J. Phys. A Math. Theor. **41**, 352003 (2008).

[108] A. Cuccoli, R. Giachetti, V. Tognetti, R. Vaia, and P. Verrucchi, J. Phys. Condens. Matter **7**, 7891 (1995).

[109] S. Habershon, T. E. Markland, and D. E. Manolopoulos, J. Chem. Phys. **131**, 024501 (2009).

[110] G. S. Fanourgakis and S. S. Xantheas, J. Chem. Phys. **128**, 074506 (2008).

[111] H. Partridge and D. Schwenke, J. Chem. Phys. **106**, 4618 (1997).

[112] V. Babin, C. Leforestier, and F. Paesani, J. Chem. Theory Comput. **9**, 5395 (2013).

[113] V. Babin, G. R. Medders, and F. Paesani, J. Chem. Theory Comput. **10**, 1599 (2014).

[114] G. R. Medders, V. Babin, and F. Paesani, J. Chem. Theory Comput. **10**, 2906 (2014).

[115] F. Paesani, W. Zhang, D. A. Case, T. E. Cheatham, and G. A. Voth, J. Chem. Phys. **125**, 184507 (2006).

[116] J. L. Abascal and C. Vega, J. Chem. Phys. **123**, 234505 (2005).

[117] M. P. Allen and D. J. Tildesley, *Computer simulation of liquids*, Clarendon Press, 1989.

[118] A. Y. Toukmaji and J. A. Board, Comput. Phys. Commun. **95**, 73 (1996).

[119] F. Harris, Proc. IEEE **66**, 51 (1978).

[120] H. C. Andersen, J. Chem. Phys. **72**, 2384 (1980).

[121] H. H. Nielsen, Phys. Rev. **59**, 565 (1941).

[122] H. H. Nielsen, Phys. Rev. **62**, 422 (1942).

[123] M. Ceriotti, J. More, and D. E. Manolopoulos, Comput. Phys. Commun. **185**, 1019 (2014).

[124] M. Rossi, H. Liu, F. Paesani, J. Bowman, and M. Ceriotti, J. Chem. Phys. **141**, 181101 (2014).

[125] V. Buch, P. Sandler, and J. Sadlej, J. Phys. Chem. B **102**, 8641 (1998).

[126] J. D. Bernal and R. H. Fowler, J. Chem. Phys. **1**, 515 (1933).

[127] F. Paesani, S. S. Xantheas, and G. A. Voth, J. Phys. Chem. B **113**, 13118 (2009).

[128] I. R. Craig and D. E. Manolopoulos, Chem. Phys. **322**, 236 (2006).

[129] D. M. Ceperley, Rev. Mod. Phys. **67**, 279 (1995).

[130] I. S. Gradshteyn and I. M. Ryzhik, *Table of integrals, series, and products*, Academic Press, 2014.